NTNU – Trondheim
Norwegian University of
Science and Technology

Analysis of beam ends with copes

Bartosz Siedziako

Civil and Environmental Engineering (2 year)
Submission date: June 2014
Supervisor: Arne Aalberg, KT
Co-supervisor: Bohdan Michalak, Lodz University of Technology

Norwegian University of Science and Technology
Department of Structural Engineering

NTNU - NORGES TEKNISK-NATURVITENSKAPELIGE UNIVERSITET
INSTITUTT FOR KONSTRUKSJONSTEKNIKK
FAKULTET FOR INGENIØRVITSKAP OG TEKNOLOGI

NTNU – Trondheim
Norwegian University of
Science and Technology

Master thesis

Topic: Analysis of beam ends with copes

Temat: Analiza belek dwuteowych o pasach podciętych w strefach podporowych

Author: Bartosz Siedziako

Supervisor: prof. Arne Aalberg, KT

Co-supervisor: prof. dr hab. inż. Bohdan Michalak, prof. PŁ

Submission date: June 2014

Norwegian University of Science and Technology

Department of Structural Engineering

Contents

List of figures

List of tables

NTNU
Norges teknisk-naturvitenskapelige universitet

Fakultet for ingeniørvitenskap og teknologi

Institutt for konstruksjonsteknikk

MASTEROPPGAVE VÅREN 2013
Master Thesis Spring Semester 2014

Bartosz Siedziako

Prosjektering av bjelkeender med utkapp

Analysis of beam ends with copes

The work includes

- Statement of the problem – comparison with the end patch loading formulas in Eurocode.
- Short summary of previous work (student works).
- Literature search. Description of some of the most relevant papers.
- Establish a numerical model in ABAQUS. Simulation and comparison with laboratory tests performed at NTNU – with focus on tests performed on an aluminium beam, and with the beams end supported on its bottom flange.
- Investigate numerically the effect of introducing stiffeners on the beam web; how the web buckle modes and extent are affected by the stiffeners, and to which extent the reaction force capacity is increased when stiffeners are introduced.
- Investigate the effect of restraints provided by connection devices as web plates, angle cleats, or welded end plates.
- And especially for the aluminium beams; investigate if softening (HAZ) due to welding of stiffeners or connection plates causes strength reduction of the beam end.

The work is to be reported as a standard technical report (master thesis) at the Department of Structural Engineering, at NTNU. It should have a summary, and delivered electronically.

The thesis report should be delivered within 10. juni 2014.

Trondheim, 14. February 2014

Arne Aalberg
Professor, NTNU

Preface and acknowledgement

This document is my project made at the end of five years of study and was created during the last semester of the master studies, when I was at NTNU - university, which in such a short time allowed me to see so many, believe in yourself and help develop my own skills. Thesis was created from a desire to create useful for industry project and to test myself in a new challenge, which certainly was writing it. I am grateful to my teaching staff from Lodz University of Technology for preparing me for this task, in which although I initially doubted was engaging, interesting and the completion of which gives me incredible satisfaction. Master's thesis was written in the Structural Department at NTNU and is translated into 30 ECTS credits.

To a large extent, in addition to the hard work this thesis was created thanks to the generosity of a large number of people who I met in Poland and Norway. I would especially like to thank my supervisor prof. Arne Aalberg for giving me the opportunity, a chance to write this paper on NTNU. Prof. Bohdan Michalak for accepting my work at the Department of Structural Mechanics and once again leading it at the Technical University of Lodz.

I am extremely grateful to all my family, which I could always count on. This is extremely lucky and it is a gift to have such loved ones. Just thinking about you managed to add me strength and motivation. Thank you that You always believed in me.

Separately, I would like to thank my parents and brother for Your continued support, love, years of care, advices, all moments spent together and for creating the best possible conditions for work and study. My thesis, I would like to dedicate just you.

Special thanks to Ewa Laskowska, my personal mentor over the last year. For inspiration to acting, for supporting a good word in moments of doubt and conversation, after which everything seemed easier. Without you, this work would never have been formed.

Bartosz Siedziako

Trondheim, 23.05.2014

Wstęp i podziękowania

Ten dokument jest moim projektem wykonanym na zakończenie pięcioletnich studiów i powstał w czasie ostatniego semestru magisterskiego, kiedy przebywałem na NTNU – uczelni, która w ciągu tak krótkiego czasu pozwoliła mi zobaczyć tak wiele, uwierzyć w siebie i pomóc rozwinąć własne umiejętności. Praca magisterska powstała z chęci stworzenia użytecznego dla przemysłu projektu i sprawdzenia siebie w nowym wyzwaniu, jakim z pewnością było pisanie jej. Jestem wdzięczny swoim prowadzącym z Politechniki Łódzkiej za przygotowanie mnie do tego zadania, w które choć początkowo wątpiłem było angażujące, interesujące i którego ukończenie daje mi niesamowitą satysfakcję. Praca magisterska napisana została w Structural Department, wydziale NTNU i przeliczana jest na 30 punktów ECTS.

W dużej mierze oprócz ciężkiej pracy praca powstała dzięki życzliwości bardzo dużej ilości osób, które spotkałem w Polsce i Norwegii. Szczególnie chciałbym podziękować swojemu promotorowi prof. Arne Aalberg za danie mi możliwości, szansy na napisanie pracy na NTNU, za wykazane zaufanie i poświęcony czas. Prof. Bohdanowi Michalakowi podziękowania składam za przyjęcie mojej pracy pod skrzydła Katedry Mechaniki Konstrukcji i po raz kolejny poprowadzenie mojej pracy na Politechnice Łódzkiej.

Jestem niesamowicie wdzięczny całej mojej rodzinie, na którą zawsze mogłem liczyć. To niezwykłe szczęście i dar mieć takich bliskich. Samo myślenie o Was potrafiło dodać mi sił i motywować. Dziękuję, że zawsze we mnie wierzyliście.

Osobno chciałbym podziękować rodzicom i bratu za ich nieustające wsparcie, miłość, lata opieki, porady, wszystkie wspólnie spędzone chwile oraz stworzenie najlepszych warunków do pracy i nauki. Swoją pracę magisterską chciałbym zadedykować właśnie Wam.

Szczególne podziękowania dla Ewy Laskowskiej, mojej osobistej mentorce w ciągu ostatniego roku. Dziękuję za inspirowanie do działania, za wsparcie dobrym słowem w chwilach zwątpienia i rozmowy, po których wszystko wydawało się łatwiejsze. Bez Ciebie ta praca by nigdy nie powstała.

Bartosz Siedziako

Trondheim, 23.05.2014

Chapter 1:
Introduction

1.1. Description of the problem

When detailing structural joints, for instance in grillage beams, coping of member ends may be necessary for the parts to fit together. For I-section beams this usually implies cutting off one or both flanges at the end of one of the beams, while leaving most of the web height intact. Fig. 1 shows three examples of a coped secondary beam; using either a connection plate welded to the main girder, an end-plate welded to the web of the secondary beam or the use of web angles. In most cases one can assume simply supported end connections when coped beam connections are used.

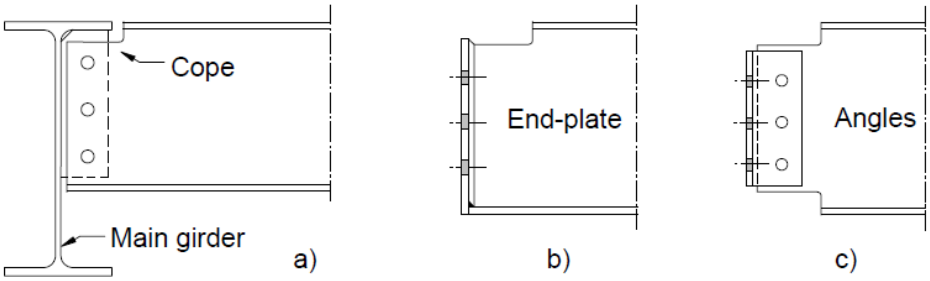

Figure 1.1 Examples of coped beams

The coping reduces both the strength and the stiffness of the beam end, leaving a reduced section either in the shape of a tee-section or a rectangular one. In addition, the cope introduces stress concentrations at the cope corner, and reduces the stability of the beam web due to the lack of transverse restraint from the flange along the horizontal edge of the cope. The reduced initial stiffness of the coped specimens is mainly due to reduced cross-section in the coped region. The topic of Coped Beams has been investigated in several student projects at NTNU in Trondheim. The focus has primarily been to develop capacity formulas for the reaction force capacity of the beams (like the formulas for end patch loading in Eurocode 3-1-5), and to validate numerical models (ABAQUS). The numerical models are used to extend the knowledge on the behavior of the coped beams, and to give insight into the behavior and the effect of varying conditions such as varying

support details, varying cope size, with and without stiffeners, aluminium or steel beams, etc.

1.2. Industrial motivation

The current problem arose during the construction of the dam. Search for a solution was initiated from an actual design problem, exactly for a gate structure in a dam. In the project this gates were constructed from several parallel I-beams. These beams were placed next to each other and connected by longitudinal tongue and groove system at the flange tips. The initial idea was to construct light-weight rectangular, planar gates, so aluminium material was used. At the beam ends large reaction force will occur, as a result of high hydrostatic pressure. Gate guides height had to be strictly limited and this caused, that the ends of the beams should be coped, leaving end of the webs laterally unsupported.

In this problem strengthening the structure by welding the stiffeners at the coped regions was impracticable due to HAZ softening when welding. This caused the need to pay special attention to investigate the capacity of the beams at the coped ends. The major design issue is the resistance against local web buckling. This buckle problem is not covered in previous investigation on typical building type connections, thus a tests program was carried out to provide the solutions relevant to the case. Moreover test program was extended to include cope dimension and connection design not previously covered.

1.3. Expected outcomes

It is expected that this student work will reveal how cope weakened the aluminium profiles of the beams. One of the aims of this work is to develop the models of seated beams, which will reflect the tests made in laboratory and provide accurate results. If they will be related to the value of ultimate reaction force, buckling shape and response curve model can be assumed as valid.

Then stiffeners as reinforcement at the end of the beam will be analyzed. In this part of studies the most important will be to investigate how HAZ effect influence on the capacity and whether they are an appropriate way of strengthening aluminum beams.

Chapter 2:

Theoretical Background

2.1. About aluminum

2.1.1. General properties/alloys

Most common aluminium is produced from bauxite ($Al_2O_3 \cdot 2H_2O$), which is one of the minerals that contains most this chemical element. Alumina, or aluminium oxide, is extracted from the bauxite through refining. Through electrolysis after Bayer method, pure aluminium is produced. The liquid aluminium is cast into extrusion ingots, sheet ingots or foundry alloys, all depending on what it will be used for. Before cooling of the melted aluminium, the alloy materials are added. Different alloys have different properties, and often have different ranges of use.

Pure aluminium does not have high material strength, with yield strength from 65 to 102 MPa. We can consider it as a quite soft material. The strength is achieved with small portions of alloying elements. Mechanical properties can also be improved by special machining. To most common alloy materials we can include copper (Cu), manganese (Mn), silicon (Si), magnesium (Mg) and zinc (Zn). In table below the main alloying elements for the European alloys used most often are listed.

AA number	Main alloying element
1***	Pure aluminium
2***	Copper (Cu)
3***	Manganese (Mn)
4***	Silicon (Si)
5***	Magnesium (Mg)
6***	Silicon/magnesium (Mg_2Si)
7***	Zinc (Zn)
8***	Other elements

Table 2.1 Main aluminium alloys

AA is the desribing system (European norm based on the American Aluminium Association). The first digit refers to the main alloy, and the next one telling about the control level of impurties. Last two digit idnicate the minium value of aluminium in percentage. For this work following alloy was used EN AW-6082 temper T6 [1]. The 6060-alloy contains mainly magnesium and silicon while other 6xxx-alloys in addition have significant amounts of some other alloying elements. This allow usually easy to extrude, have medium strength and possess good corrosion resistance.

2.1.2. Aluminium advantages

-It is not common known, that there are huge resources of aluminium. It is most abundant element in the earth's crust, after oxygen and silicon. Today, bauxite is the only commercial ore used for production of aluminium, but in the future we will have more sources for aluminium. If we consider today's production, the bauxite reserves will last more than 100 years.

-Aluminium is strong and light. Its weight is 2,7 g/cm^3 what is around one third of the weight of steel. It is obvious, that low weight means reduced energy consumption in transportation and gives advantages during assembly in buildings.

-Aluminium in buildings, construction and transport is fire-proof. It will only burn if it will has shape as very thin foil. Moreover aluminium melts at 660^{0}C without releasing any gases.

-Great advantage of this material is also the fact, that it has low melting point, is ductile, what makes it easy to form. Because it is easy to process in cold and hot condition this allows design flexibility and integration in advanced transport and building industries.

-It is very long-life material. Aluminium forms a protective coating that makes it highly corrosion resistant. This prolongs the life of aluminium in cars and buildings, reduces need for maintenance also reduces environmental impacts due to replacements.

-There are also other properties of aluminium, which makes it very special material like. It is superconductor for heat and electricity. This makes aluminium the best choice for energy-efficient systems for electrical transmission, such as transfer components. It can also reflect both heat and light. Very important is the knowledge that about 75% of all aluminium ever produced is still in use, because only five percent of the energy required to produce the primary metal initially is needed in the recycling process

2.1.3. Aluminium in industry

Aluminium as a structural material is becoming more popular in recent years because of all the interesting qualities of the material. The low weight in proportion to the strength is one of the important properties and aluminium is therefore often preferred instead of other more traditional materials. High energy efficiency in the reflectors reduces energy consumption. Today aluminium is used in many different structures like balconies, windows, roofing sheets, railings and so on. But it is also used in larger structures like framed structures and more heavy, load bearing structures such as for instance bridges and roofs. Offshore aluminium is used in helipads, staircases, railings, fire walls and entire living quarter modules on platforms. Compared to steel, aluminium needs less maintenance, and even though the material costs are higher, the total life-cycle costs are often lower. Aluminium is actually used in almost all aircrafts, and in cars it has been used for same years. The tendency is to replace almost all steel structures in cars with aluminium to obtain cars with low weight and minimized fuel consumption, in addition to a higher safety and durability.

2.1.4. Welding

Welding is used extensively in steel structures. In aluminium alloys, welding causes a reduction of the strength and ductility of the material and a direct transformation of the design rules applied for steel structures would be inappropriate. Welded components are used to a continuously larger extent in the automotive industry because of the larger stiffness these components have relative to other jointed connections and the reduction in the costs of production. 6xxx-alloys are heat treatable alloys, which means that heating and cooling will affect the material properties. When these alloys are welded, the base material close to the weld is affected by the high temperature and some aluminium properties partly be lost. For 6xxx-alloys the weld materials are often stronger than the base material and the destruction of the welded part of these alloys rarely occurs in the weld itself.

Eurocode [1] gives hints how to input effects of welding into to the model. It is suggested to use reduction factors $p_{0,haz}$ and $p_{u,haz}$. The characteristic value of the 0,2% proof strengths $f_{0,haz}$ and the ultimate strength $f_{u,haz}$ gives these coefficients:

$$p_{0,haz} = \frac{f_{0,\mathrm{haz}}}{f_0}$$

$$p_{u,haz} = \frac{f_{u,haz}}{f_u}$$

In 3.2a, 3.2b and 3.2c in tables of Eurocode 9 [1] can be found values of these strengths, which depend on type of alloy. In design, capacity of welded part should be reduced so it can be done in two ways. It is possible to use reduced area of cross-section A times $p_{0,haz}$ or reduced strength $f_{0,haz}$ and effect will be the same: f_0 A· $p_{0,haz}$ = $f_{0,haz}$ ·A. Values of these coefficients also highly depend on profile type (sheet, strip, plate, tube, bar or extruded). They may be in range of 0,28 - 0,91 for $p_{0,haz}$ and 0,47 - 0,96 for $p_{u,haz}$. Except for a few exceptions reduction of ultimate strength is lower than proof strength and in very general most values for $p_{0,haz}$ is around 0,50 and $p_{u,haz}$ around 0,65.

The same standard also gives information about area, where this reduction in the capacity should be used. For this studies obligatory will be picture from the figure 6.6 of mentioned standard, which was presented below. It is important to emphasize that if the distance *) is less than $3b_{haz}$ it should be assumed that the weakened area extends to the full width of outstand. Values b_{haz} are given in Eurocode and depend on type of welding.

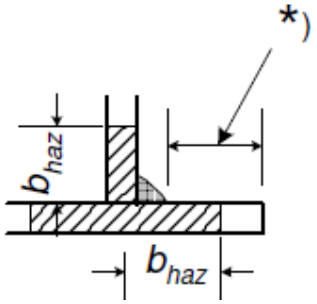

Figure 2.1 Area weakened by welding

2.2. Theory of buckling in the plates

2.2.1. Brief description

There are some structures, in which buckling phenomenon which does not occur. On the other hand plates and columns under the load causing compression are very vulnerable to buckling. Especially when compressive force meets slender structure it can deflect in a very large manner. But generally buckling expression is used somewhat imprecise about two different phenomena which are so called elastic instability and inelastic failure.

Euler's theory, i.e. the simple theory of buckling of bars can only calculate the critical force and the corresponding buckling shape. This is so called linear buckling

theory, because it uses a linear differential equation of the line deflection. It should be noted that stability problems are always non-linear and it is not allowed to apply here the principle of superposition. Should depart from the assumption that the curvature is small and take the exact formula specifying its shape. Deflections can be then arbitrarily large and the differential equation is a nonlinear. Together with buckling theory is associated critical load expression. This is the value of the force/stress, which when loaded causes that structure loses its state of equilibrium what means that becomes unstable. This is happening, because buckling occurs when the structures stiffness is dramatically and in fact the following expression drops to zero: $[K_T] = [K_m] + [K_g] = 0$ for a short period of time. K_T is resultant tangent stiffness, which is sum of composed elastic (material) stiffness K_m and the stress (geometrical) stiffness. Taking into account energy considerations, buckling occurs when the membrane (axial) strain energy is converted into bending strain energy with no change of externally applied load. This is why, how it was emphasized at the beginning, slender structures like thin plates, or columns large deformations will occur when this conversion takes places. The membrane stiffness is much greater than bending stiffness. In this student work will be considered two cases: elastic plate buckling and over-critical plate buckling behavior.

2.2.2. Eigen value plate buckling analysis and elastic plate buckling

Also known as elastic plate buckling analysis theory has characteristic assumptions like:

- Load depends on one parameter λ. $P = \lambda P^*$
- Load is conservative, what means, that does not change direction during deformation of the structure.
- System (in this case shell) is perfect, without geometrical, material or load imperfections that interfere perfect conditions before bucking.
- Load $P_{cr} = \lambda_{kr} P^*$ it is critical loading after reaching buckling occurs. P^* is the configuration load corresponding in this case to λ=1.

This analysis is used to calculate the eigen values (buckling loads) and eigen vectors of the system under consideration. The eigen value buckling analysis is based on finding the solution to the equation:

$$\left(K_0^{NM} + \lambda K_\Delta^{NM}\right)\nu^M = 0$$

K_0^{NM} represents the base state stiffness, K_Δ^{NM} represents differential (stress) stiffness, λ represents an eigen value and v^M represents the eigen vector of the system.

In elastic plate buckling the web of investigated beam (XHP 260) will act as a plate loaded with membrane actions. After exceeding the web critical force (buckling capacity) the web becomes unstable. Because web in coped region has lost its support by one or both flanges, it is particularly vulnerable for buckling. To calculate this critical stress for isotropic material there must be used differential equation given below. The critical membrane actions are determined based on the plates differential equation derived from equilibrium considerations of an infinitesimal deformed element.

$$\nabla^4\omega = \frac{1}{D}\left(N_x\frac{\partial^2\omega}{\partial x^2} + N_y\frac{\partial^2\omega}{\partial y^2} + N_{xy}\frac{\partial^2\omega}{\partial x\partial y}\right)$$

The equation can be solved after taking into consideration boundary condition like also the type of loading. The following expression for critical buckling load for plates loaded in axial compression and moment could be obtained:

$$\sigma_{x,cr} = k_\sigma\frac{\pi^2 E}{12(1-\nu^2)}\left(\frac{t}{b}\right)^2$$

k_σ parameter depends on the boundary conditions and the distribution of externally applied forces. For plate loaded in shear, the critical value is given by the following expression:

$$\tau_{xy,cr} = k_\tau\frac{\pi^2 E}{12(1-\nu^2)}\left(\frac{t}{b}\right)^2$$

k_σ parameter is the plate buckling factor for shear. To increase the plate's capacity the most common longitudinal and vertical stiffeners are used. Use of stiffeners will alter buckling pattern, which normally allows plate to buckle in a number of sinus waves.

2.2.3. Nonlinear buckling

The behavior of the beam under the reaction force load cylinder is complex. The displacement and load have a linear relationship – as the load increases, the displacement also increases and stiffness increases. However, as seen in Figure 2.2 at Point A, once a buckling begins to occur, the displacement increases more quickly with the same rate of loading until the critical buckling load is reached. At this point, the structure essentially has no stiffness. Buckling is not typically caused by overstress of a structure as it occurs while stresses are still below the yield strength of the material. Rather, buckling is caused by imperfections/instabilities in the structure. Figure 2.2 shows an example of a complex,

unstable response of a structure. The nonlinear buckling analysis should exhibit similar behavior, the best, to point B on the curve.

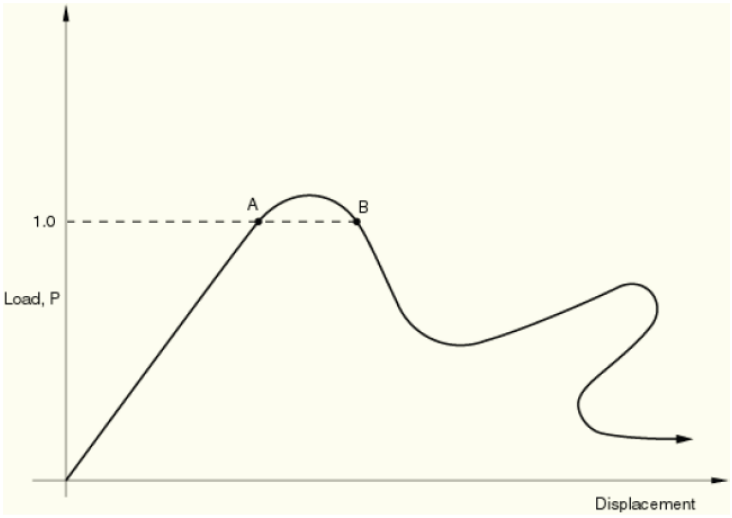

Figure 2.2 Proportional loading with unstable response

The solution for a non-linear system is usually carried out by traversing the non-linear load-displacement equilibrium curve in several increments. Each increment has a set of iterations being used to arrive at the solution of the system at that particular increment. The increment size is based on the non-linear analysis technique used. The basic equation solved for iteration in any non-linear analysis can be solved by two different non-linear methods of analysis namely Newton's method and modified RIKS algorithm.

2.2.4. Plate capacity – recommendations in design

There is a big difference between the best known and most frequently used buckling process in columns (bar elements) and plates. For the plates there is possibility to exceed the external load over the critical buckling load, due to a redistribution of the internal stresses. Columns on the other hand will collapse during buckling. This over-critical capacity can be significant and useful in design.

Design recommendations for plates are found in the Eurocode 3-1-5 [13]. The capacity is based on the plate's effective area in the compressional zone for plates loaded by axial forces and moment. This effective area is defined by the expression $A_{c,eff} = \rho A_c$, where A_c is the plates compressional area and ρ is a reduction factor. About this factor decides plate's slenderness λ_p. To calculate it expression above should be used.

$$\lambda_p = \sqrt{\frac{f_y}{\sigma_{cr}}}$$

Where σ_{cr} is the elastic critical buckling stress. Finally the plate's capacity could be found from formula:

$$N_x = f_y A_c \rho = f_y A_{c,eff}$$

The same Eurocode 3 [13] provides also the design recommendations for plates loaded with transverse force. The plate's load capacity depends on the plate's slenderness, which is the function on plate height-to-thickness ratio (h_w to t_w). Regarding the plate's slenderness, three failure modes are identified, as seen in figure 2.3.

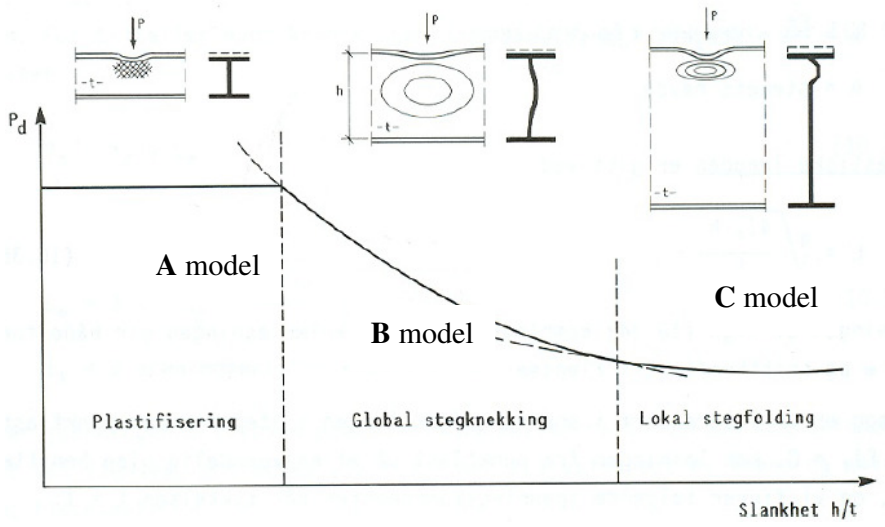

Figure 2.3 Failure modes

A model is for small values of h_w / t_w . Its result is that the web near the loaded position will be subject to plasticization.

B model is for intermediate values of h_w / t_w . Its result is that the beam fails in global buckling of the web.

C model if for high values of h_w / t_w . Its result is that web cripples directly below the loaded position, while the rest of the web stays nearly undistorted.

The design recommendations, which covered all the failure modes in figure above are based on the design model developed by Lagerqvist [15]. The capacity is determined based on the assumption that the vertical stresses in the web below the loading are distributed equally over a section with length L_{eff} , thus the beam's capacity equals:

$$F_{Rd} = \frac{f_{yw}\, L_{eff}\, t_w}{\gamma_{M1}}$$

In this approach the most difficult is to find L_{eff} value (effective length for resistance to transverse load). To find it some calculations must be done before. The reduction factor χ_F for resistance must be found as the most relevant coefficient but first plate's relative slenderness λ_F, critical force F_{cr} and critical coefficient k_F, also surrogate lengths l_y called effective loaded length and l_e and $m_{1,2}$ (two dimensionless parameters) coefficients also. The necessary formulas for these calculations are given below. F_{yw} is the characteristic value of strength of the web material and b_f is the flange width.

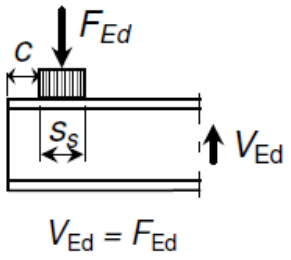

$$k_F = 2 + 6\frac{s_s + c}{b_w} \le 6$$

Figure 2.4 Load application and buckling coefficient according to Eurocode 9-1-1.

$$L_{eff} = \chi_F\, l_y$$

$$\chi_F = \frac{0{,}5}{\lambda_F} \; and \; \chi_F \le 1$$

$$\lambda_F = \sqrt{\frac{f_{yw}\, l_y\, t_w}{F_{cr}}}$$

$$F_{cr} = 0{,}9 k_F E \frac{t_w^3}{h_w}$$

$$k_F = 2 + \frac{6(s_s + c_s)}{h_w} \le 6$$

$$l_y = min \begin{cases} l_e + t_f \sqrt{\frac{m1}{2} + (\frac{l_e}{t_f})^2 + m2} \\ l_e + t_f \sqrt{m1 + m2} \end{cases}$$

$$l_e = \frac{k_F\, E\, {t_w}^2}{2 f_{yw} h_w} \le s_s + c_s$$

$$m1 = \frac{f_{yf}\, b_f}{f_{yw} t_w}$$

$$m2 = 0{,}02\,(\frac{h_w}{t_f})^2 \; if \;\; \lambda_F > 0{,}5 \qquad and \qquad m2 = 0 \; if \;\; \lambda_F \leq 0{,}5$$

2.2.5. Bracket plate analogy

Often in practice, the problem of plate buckling in joints is simplified by using column models with an effective width or series of parallel column strips. As it will be showed later this methods provides large simplifies, but it is easy in use and gives conservative results. Buckling model for the compressed zone of an unstiffened column web panel in a beam-column joint in EN 1993-1-8 could be given as a such example. On the figure 2.5 below there is illustration, which helps to explain this model.

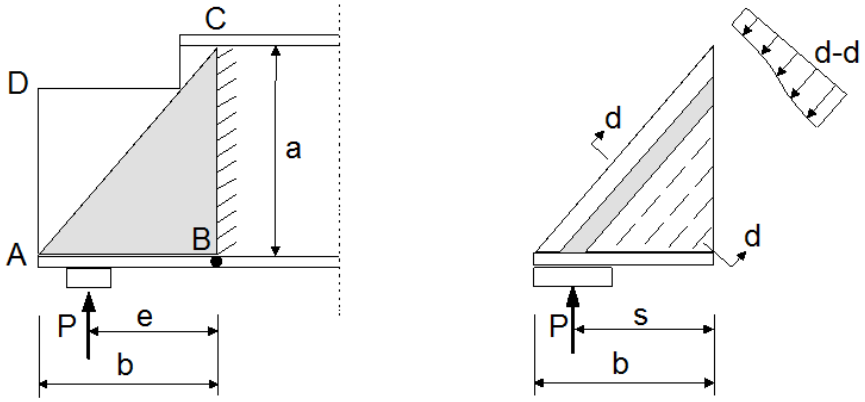

a) Bracket b) Column strips

Figure 2.5 Bracket model

On a picture a) it is showed how bracket web plate is created. The grey shaded region ABC in the beam web is assumed as rigidly connected to the bottom flange of the beam and what is far from elastic behavior also rigidly connected to the web along a vertical line BC. In this model only shaded region is taking into account, so the part of the beam outside the inclined line AC is neglected. As it was showed on the picture force P is loaded by a point at a distance e from point B.

This model was considered by many authors. Salmon [16] create an early design model for bracket plates. His work gave elastic buckling coefficient and b/t limits. The model assumes that resultant of the loading acted at a distance e=0,6b and gives very conservative results. Later this model was improved by many authors, where other load positions were considered and . Also some of the them incorporated post-critical strength

and plastic mechanisms. But here model proposed by Martin [17] was chosen to compare the results.

In Martin's work the bracket plate is assumed to act as a series of column strips parallel to the inclined edge AC. It could be said that this lines are also almost parallel to the line of buckling. The capacity of the plates is calculated as a sum of capacities of the individual column strips, assuming clamped edge. Stress distribution over the width of the bracket must be nonlinear as shown for line d-d as long as lengths of the single columns are varying. Martin determined column design stress using Rankine formula to deal with the interaction between yielding and elastic buckling. The scheme of his model if on the figure 2.5 b). There is shown also that the resultant of the applied load is located at the distance s from point B. The Martin's capacity expression given below includes also a contribution from elastic hinge in the flange:

$$R_{Martin} = \frac{\pi^2 E t^3}{24 s}\ ln\left[1 + \frac{12 f_y}{\pi^2 E t^2}\frac{b^2}{[(b/a)^2 + 1]}\right] + \frac{M_{p,fl}}{s}$$

Martin in his work emphasized that this expression includes a variable s defining the position of the resultant applied force and a term M_p which are lacking in the Salmon [16] theory. M_p is theoretically the maximum bending moment that the section can resist. When this point is reached a plastic hinge is formed and any load beyond this point will result in theoretically infinite plastic deformation. For the rectangular section can be calculated with the following formula: $M_p = \sigma_y \cdot bd^2/4$.

2.3. Most relevant papers

2.3.1. Local loss of stability by Cheng and Yura [22]

J. J. R. Cheng and J. A. Yura with have been studying for several years steel beams with cutaway . They have come forward with a proposal to equations that can be used to find the capacity of such beams. Cheng and Yura published in 1986 formulas for capacity of local loss of stability. After next four years they published a note on the fatigue strength of beams with cutaway. Results are summarized in a memorandum that Cheng released in 1993 [24]. It is important to emphasize that their papers for steel beams are not necessarily suitable for aluminium beams and should be used carefully.

For this work Cheng's and Yura's method for design of coped beams against local web buckling will be considered. In their design model the region of the web affected by

the cope is represented by a rectangular model plate with three simply supported edges and one free (figure 2.5). The loading is assumed to be linearly varying compressive stress over the height. At the coped corner due to discontinuity mainly of the web but also flange a stress concentration may occur. Regular calculations for bending and shear stresses describe real, actual stress distribution poorly at the coped region. In these researches slenderness is important issue. For not slender webs the stress concentration is very high and material can yield at the coped corner, what will cause the beam failure due to inelastic local web buckling. For slender webs failure can occur by elastic local web buckling on the other hand. The design value of the buckling stress at the top of the web is given by:

$$\sigma_{cr} = f_1 \frac{k_\sigma \pi^2 E}{12(1-\nu^2)} \left(\frac{t}{h_0}\right)^2 \; where:$$

t is the thickness of the web,

h_0- height of the coped beam, h-height of the beam

E is the Young modulus ,

ν Poisson value.

Last to numbers f_1 and k_σ deserve for some description. Generally when Chang and Yura came up with their design model, to make it simple for design purposes, they decided to start up with a regular plate buckling model described in Eurocode. Two added factors were entered to the formula to represent the more complex nature of the bucking problem in the coped beams. Factor f_1 takes into account the effect of the stress concentration at the cope corner but also presence cope depth, influence of the shear stresses and moment variations over the coped end. With increasing cope length, stresses concentration will be limited only to a small area at the cope end. This value is given as:

$$f_1 = 2 \cdot \left(\frac{c}{h}\right) \; for \; \frac{c}{h} \leq 1$$

$$f_1 = 1 + \left(\frac{c}{h}\right) \; for \; \frac{c}{h} > 1$$

The factor k_σ is the plate buckling coefficient considers the cope dimensions and derived from analytical and numerical solutions but also by curve fitting techniques. On the figure 2.6 there is showed how this factor depends on cope ratio and how was separated in the two zones with different formulas.

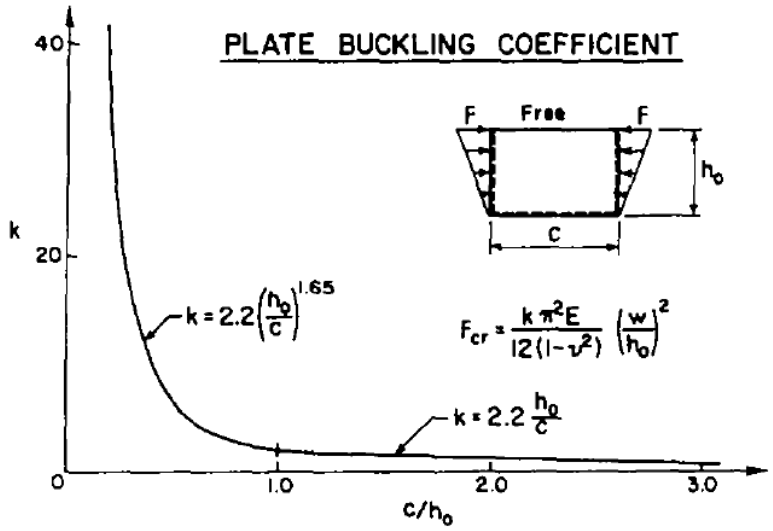

Figure 2.6 Plate buckling model

$$k_\sigma = 2{,}2 \cdot \left(\frac{h_0}{c}\right)^{\beta} \quad where \;\; \beta = 1{,}65 \; for \frac{c}{h_0} \leq 1 \; and \;\; \beta = 1{,}0 \; for \frac{c}{h_0} > 1$$

Cheng and Yura included in their studies experimental testing in the laboratory and also they did numerical simulations. Only beams with cope ratio described by $c < 2 \cdot h$ were investigated and also with $d_c < h/2$ (figure 3.2 explains this values). From practical point of view there are very small chances that in construction engineering will be used others.

2.3.2. Yam [23]

Although Chang's and Yura's model is easy to use it poorly reflect the fact that buckle phenomenon can extend far into the uncoped region of the web. Yam's studies can be considered like a continuation of the Chang's and Yura's work, because they stated that their model underestimated the capacity of the beams with small ratio d_c / h (cope depth to beam height) and more accurate formulas were needed.

Yam proposed a design modified plate model, which is showed on the figure 2.7 with geometry and applied shear stresses field, which were calculated from finite elements simulations. Yam conducted not only numerical simulations but also many laboratory tests for a wide range of beam and cope geometries, giving magnitudes and distributions varying along the edges. In his work he claimed that shear stresses will be decisive for buckling behavior for the cope ratio c/h_0 (cope length to reduced height ratio) lower than

1,5 and also that bending stresses can be neglected in this model, so moment was not considered.

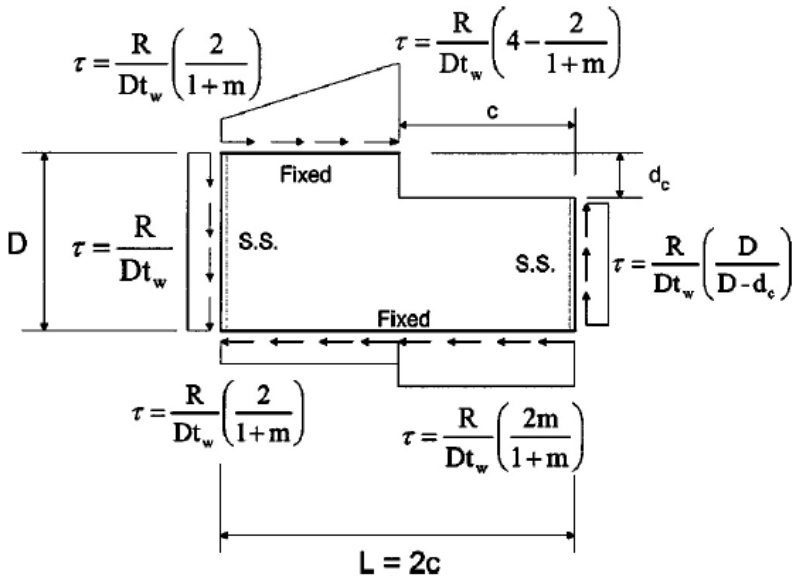

Figure 2.7 Yam's modified plate model

Yam's model still have many simplifications like for example mentioned omission of the moment, but also shear stresses at the intersection between the compressional flange and the web are larger than in theory due to remaining equilibrium. Despite this for small ratios Yam's model predicts capacities ranging from 92% to 106% of measured one, what is significant improvement compared to Cheng and Yura. Increasing the plate's model length from h_0 to 2·c allow minimizing the effect of the boundary conditions. Finally the design value for the local web buckling for I beams with cope on the top flange was developed:

$$R_d = \tau_{cr} \cdot t_w(h - d_c) = \frac{k_s \pi^2 E}{12(1-\nu^2)}\left(\frac{t_w}{h_0}\right)^2 \cdot t_w(h - d_c) \quad for \quad \tau_{cr} \le \tau_{max} = \frac{f_y}{\sqrt{3}}$$

All factors above remain the same as described in 2.3.1 except k_s, which is shear buckling coefficient found in numerical solutions and depends on a, b parameters. This parameters vary with the d_c/h ratio.

$$k_s = a\left(\frac{h_0}{c}\right)^b \; with$$

$$a = 1{,}38 - 1{,}79\frac{d_c}{h} \qquad b = 3{,}64\left(\frac{d_c}{h}\right)^2 - 3{,}36\frac{d_c}{h} + 1{,}55$$

2.4.Finite element method (FEM)

FEM is used on wide field of applications and is generally shown to give high accuracy solutions. There is vast library of finite elements which makes it the most common method used on computer programs. Despite this, trouble mesh generation for areas with complex geometry but fortunately ABAQUS gives a lot of options letting control mesh (more about this can be found in point 4.12). The solutions obtained from simulations by this method in ABAQUS can supplement or even replace real testing in the laboratory and will make it possible to produce data for a large number of specimens at a small cost. But the mistakes always can happen so it is important to provide validation of model and then extend investigations only in program.

The finite element method involves finding an approximate finite element solution for the different factors like displacements, deformations, tractions etc., on a body when subjected to a certain loading condition. It is a numerical approximation is based on an integral-differential equation called the virtual work principle given in equation which is a transformed form of partial differential equilibrium equation.

2.5. Solution methods

Except the linear, eigenvalue buckling analysis also two types of nonlinear analyses were used to solve the problem.

2.5.1. Riks method

The modified Riks method is a solution method in ABQUS used for load cases where the loading is proportional to, or governed by a single scalar parameter. In this student work, this scalar parameter is the reaction force at the end of the beam. The results is a load proportionality factor (a multiple of the applied load) and displacements. Since both loads and displacements are unknown, another quantity, called arc length, along the static equilibrium path in load-displacement space, is used to measure the progress of the solution. This allows the modeling of both stable and unstable structures. Many good papers were written about this method and information about the modified Riks method can be found in [19, 21]. For the modified Riks solution, the applied load is irrelevant because the load will be increased until collapse occurs, even if the load exceeds the applied load. The modified Riks algorithm is based on finding a load proportionality factor ψ in each increment of the analysis.

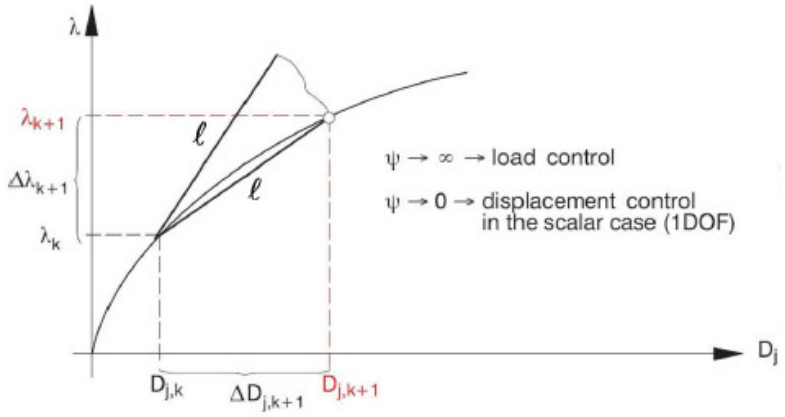

Figure 2.8 Iteration scheme for Arc-length method

2.5.2. Newton

Newton method will be used in "General static" analysis type. This method provides with a solution for a local buckling problem by introducing an automatic mechanism used to find the proper path. The incremental-iterative procedure that advances the solution while satisfying the global equilibrium equations at each iteration 'i', within each time (load) step 'n+1'. Generally method uses following equation:

$$x_{n+1} = x_n - \frac{f(x_n)}{f'(x_n)}$$

After choosing some initial point x_n tangential line to the graph is created, which intersect the horizontal axis what allows getting next x_{n+1} initial point and next line. The process is repeating to the moment when the solution will be almost equal to the real. This method can be illustrated on the figure below.

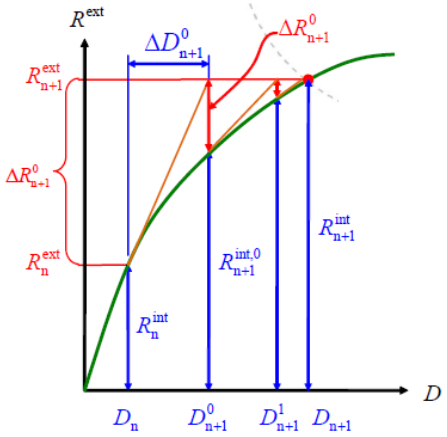

Figure 2.9 Iteration scheme fo Newton method

To get more rapid convergence modified Newton method was invented. It differ from the standard method in that the tangent stiffness K_T can be updated occasionally (but not it the every iteration). In case of standard, initial Newton method it is update only once and this is why method may result in a slow rate convergence. The difference between these varieties of Newton method can be explained the best by figure 2.10.

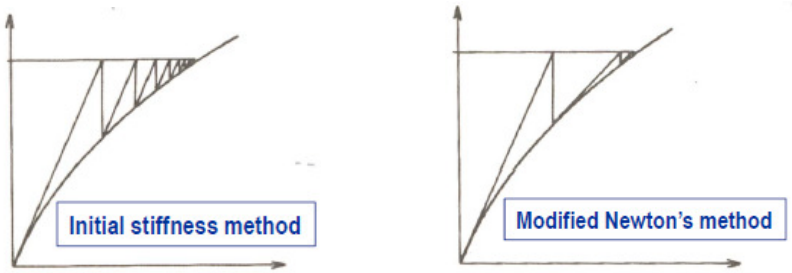

Figure 2.10 Comparison between Newton's methods.

2.6.HAZ

As it was stated in 2.1.4 6xxx-alloys are heat treatable alloys, which means that heating and cooling will affect the material properties. In this case heating from welding is taken into account and the reduction in strength properties caused by this phenomenon could be significant. Heat affected zone or HAZ is the area, where the base material is affected by the welding. Generally HAZ can be explained tht welding temperature and time of the welding cause transformation of the metal's microstructure and affects the "grain" size of the weld structure. This change is very of the visible even for the human eye and problem was showed in the figure below.

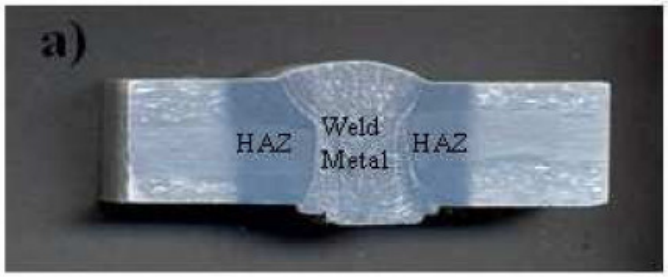

Figure 2.11 Heat affected zone of aluminium specimen

The metallurgist can often predict the changes in microstructure knowing the time-temperature history of the metallic specimen, but in this studies Eurocode 1999-1-1 was used to predict necesarry values (more in point 6.1) like reduction in strength or area, where this reduction occurs.

2.7.Previous student's works

2.7.1. Bonkerud [12]

In his work Bonkerud was checking behavior of coped steel I – beam with special attention on the buckling of the web. For his investigation many tests were done on IPE300 profile. Bonkerund stated that under some circumstances it is not necessary to check buckling capacity, because yielding will determine the beams capacity. This special conditions are ratio h/t_w (height to thickness) of the web should be below 42 and cope ratio c/h should be lower than 2. Based on the Bonkerud studies, following formula for ultimate reaction force was presented in [26]:

$$R_{\text{coped}} = R_{\text{uncoped}} \left(1 - B \cdot \frac{c}{h_0}\right) with$$

B factor in very simply equals 0,32 for steel and 0,4 for aluminium. $R_{uncoped}$ can be calculated from formula concluded in Eurocode 3.

On the figure 2.12 below it can be seen plate model designed by Bonkerud. From the beam the rectangular plate with dimensions axb was extracted. As it was emphasized by dotted lines plate is simply supported on three edges, which are in diagonal position. On the next figure 2.13 there is a comparison between deformations in Bonkerud's model and deformation in lateral direction from ABAQUS.

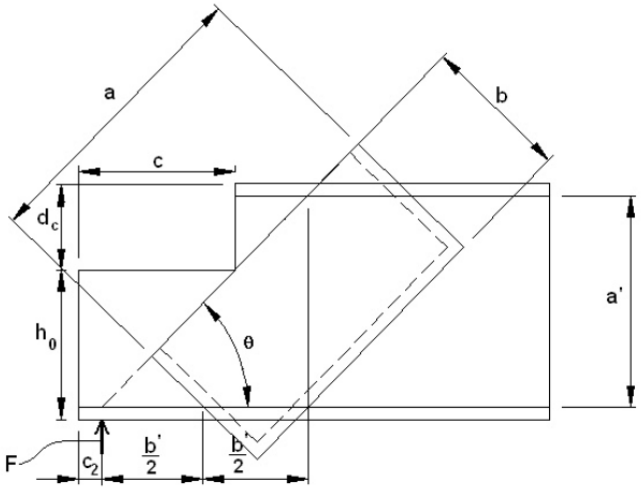

Figure 2.12 Bonkerud's plate model

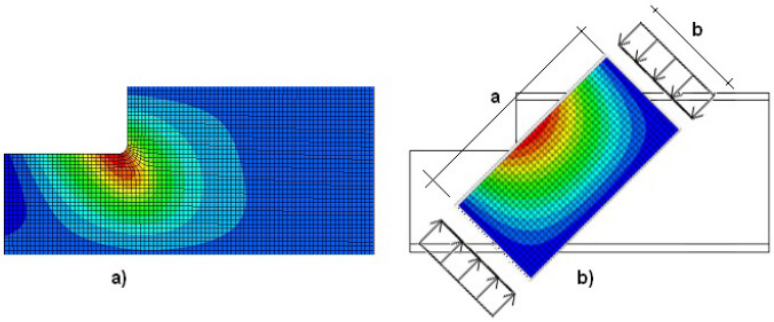

Figure 2.13 Lateral deformations in ABAQUS (a) and in Bonkerud's model (b)

2.7.2. Urseth [5]

In his work Urseth investigated different types of reinforcement of coped beams (steel IPE 300 was considered) by stiffeners. Firstly he established the model for coped beam, which can be stated for valid, because in comparison with laboratory tests, gives results ranges from 0,87 to 1,04. Then he has developed this model to check the effect of strengthening the coped beam with different reinforcing measures. Longitudinal stiffeners alone or in combination with vertical stiffeners were used in his work. The effect of reinforcement was investigated on beams with different cope ratio c/h_0 (cope length to reduced high).

It turned out that the stiffeners are not able to protect the beam's web against buckling but the can increase the capacity of these beams due to improved stability of the coped end. These statements, however, are true only for a cope ratio c/h_0 lower than 1. In other cases Urseth didn't find almost any difference in new capacity.

Regardless of thickness or width (dimensions) of the longitudinal stiffener Urseth's studies showed that capacity rose in the same pattern (model 2 differs from model 2 on the figure 2.14 the thickness of stiffener). Moreover only in the biggest cope (detail C), the length of longitudinal stiffener is important for the capacity what can be seen on the figure 2.14 below, otherwise provision of horizontal stiffeners did not improve beam's capacity. Results given on charts are divided by $P_{max,1000}$ - max support force with longest stiffener length.

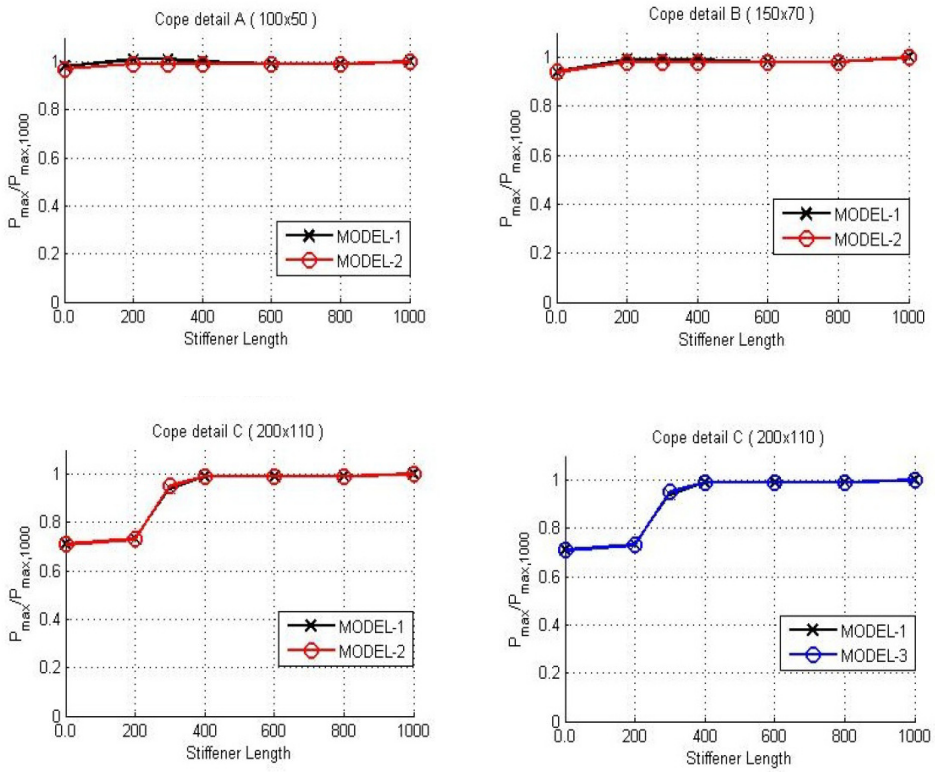

Figure 2.14 The impact of longitudinal stiffeners by Urseth

From Urseth's work it can be deducted that only connection of vertical and horizontal stiffeners can improve the capacity of the beam significantly. Vertical stiffener should be place at loaded point or both at loaded point and at the cope corner. To expand the knowledge in the subject as a future work Urseth recommended checking phenomenon of strengthening by stiffeners in a beams made from different material like aluminium. It is very important to emphasize that results from his thesis can't be used on aluminium beams or estimate ultimate force in any way. XHP 260 profile has even more slender web than IPE 300 and moreover aluminium material has much lower Young's modulus than steel what makes it even more vulnerable for buckling. What's more, additional stiffeners have to be welded to the cross-section and in aluminium welding causes always the problem, because of the HAZ effect, what reduces properties of material and again makes buckling easier to occur.

2.7.3. Gundersen [7]

Main part of Gundersen's master thesis focused on investigations of capacity of the aluminum beam ended by vertical plate, which would be welded to the web and the flange at the cope end. Mentioned plate would be used to connect the secondary coped beam to the main girder by four bolts. In conclusion of her work she made the following assumptions.

Firstly it appeared that the HAZ effect in this case does not have big impact on the ultimate capacity. Actually maximum load was only a slightly higher for the beam without HAZ. It was even taken into consideration if it is worth to take HAZ effect in further calculations. Results from mentioned researches can be found in the table below. It need to be emphasize that the HAZ zone in Gundersen's work was very small and don't affect the cope corner.

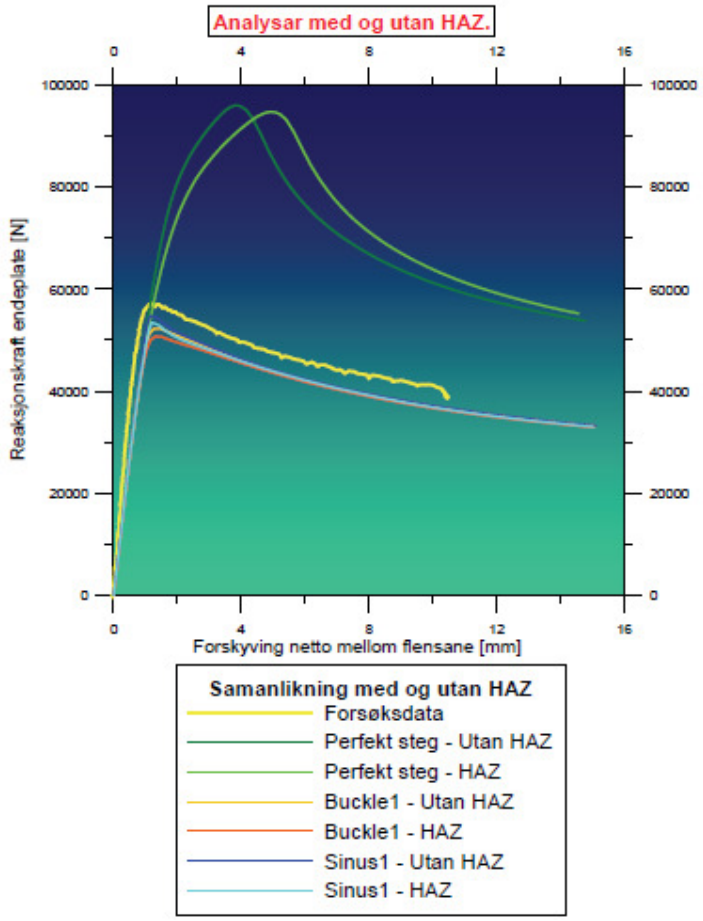

Figure 2.15 Results from Abaqus with and without HAZ effect - Gundersen

The numerical simulation of bolted end plate showed higher capacity for the beam. Many thicknesses of the plate were considered in her work. Differences between 6 , 10, 20 and 30 mm thick plates were studied and the influence of the thickness on capacity of the beam were investigated. Capacity increased when plate becomed thicker . Differences between 6 , 10 and 20 mm was very clear , while 20 and 30 mm gave about same result. This suggested that the thicker end plate than 20 mm will not provide increase in capacity.Finally also she claimed that it is important to include reduced material strength in the HAZ of bolted end plate on beam with cutaway.

Chapter 3:

Tests

3.1. Introduction and purpose

The physical tests with the coped aluminium beams were done at the NTNU lab in the Structural Department. Tests were necessary to validate the numerical model and help to solve the problems in connection with gate of the dam. Without this experiments there will be not possibility to be sure, that the models in ABAQUS reflects the reality well. To solve describing problems two types of tests were done. In the first the material properties were determined from standard tension tests. The brief description about the results can be found in 4.6 point of this project. Main part of the research was to examine the behavior of coped beams under the concentrated load. The whole process of testing included investigation of behavior: seated beam ends, stiff seated beams, coped specimens with connections, double-coped beams made from both steel and aluminium. For the steel material IPE 300 cross-section were investigated, and for the aluminium cross-section XHP 260.

3.2. Geometry of the samples.

3.2.1. Tests setup and single coped ends, seated beams

In case of seated beam ends five cope geometries were investigated. The length of the longest cope equals the height of the beam section, while deepest cope equals half the beam section height. To make the cope saw was used. They were cut and given a radius r_1 = 15mm at the corner. Beam were seated on a steel block, which was s=40mm wide and a cylindrical rotation bearing during the tests. Overhang, which is marked on figure below as “g” was 10mm. The same support conditions were used for all coped and uncoped beams. This type of geometry allowed to ensure well-define load application point and gained precise measurements.

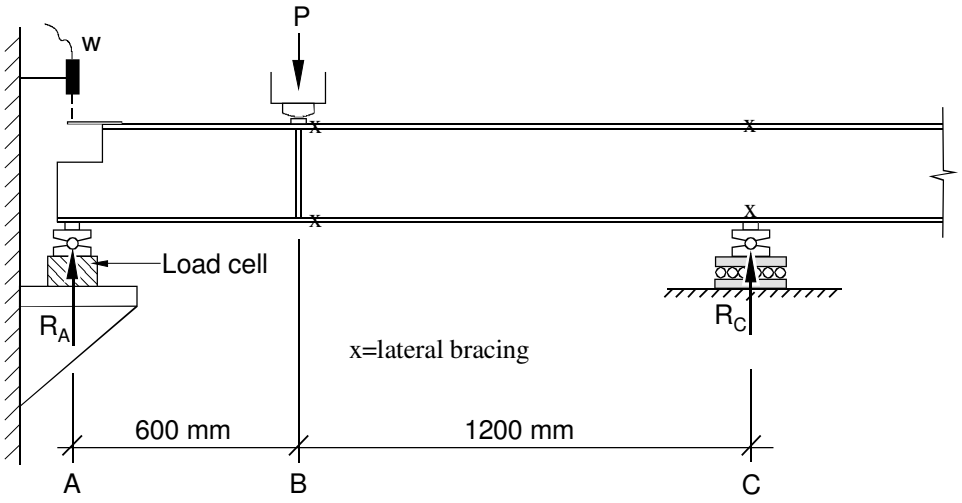

Figure 3.1 Test setup

On the figure above is test setup scheme. A and C points represent the position of the cylindrical bearings, on which beam is simply supported. P is the force applied by hydraulic actuator under displacement control at the distance of 600mm from coped end. Load cell placed below bearing measured the reaction force R_A at the cope. All vulnerable zones except at the cope were restrained against lateral displacement and rotation about the beam longitudinal axis. In the support C and at the actuator restraints were provided by vertical guides. Moreover vertical web stiffener was placed under the applied load.

During tests not only reaction force was measured but also displacement. Optical displacement transducer was mounted like was on the figure above to measure the vertical displacement w of the top flange of the beam. This was obtained by adding to the top flange small plate. The main aim of this device was to measure decreasing distance between the top and the bottom flange due to web strains and web buckling displacement. When the test was finished deformed length of the beam was cut off and remaining part of the beam could be used for the next investigation.

List of the investigated specimens for the seated beams is given below. Five specimens were tested for the uncoped aluminium A1 sample and two for A2 sample. On the figure 3.2 there are symbols in further works, also general view on the cope idea and geometry.

Specimen / dimension:	c [mm]	d_c [mm]
A1	0	0
A2	88	97
A3	175	97
A4	260	97
A5	175	70
A6	175	130

Table 3.1 Investigated samples

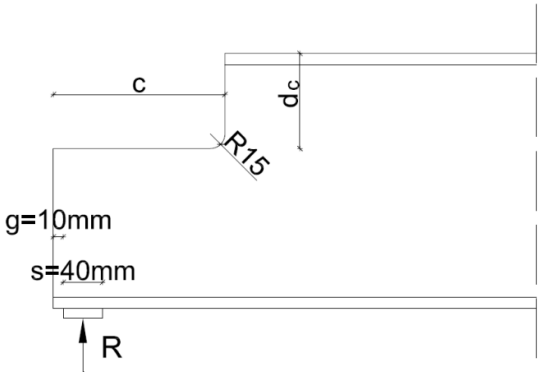

Figure 3.2 Coped ends geometry

3.2.2. Coped specimens with connections

Except the seated beams laboratory tests were done also on top coped specimens with connections. This allows extending the scope of investigation and helps in confirming the accuracy of the numerical model. Three different possibilities of connections were tested. Specimens A7, A8 and A9 represent the most common support conditions in building structures. All of them have the cope size 88mm by 97mm, so they come from A2 specimen. First one A7 had a 140mm wide and 10mm thick end-plate, which was welded to the web and the bottom flange of the beam. In this case end-plate was supported directly on the load cell with no additional restraint, allowing the beam end to rotate freely. No stiff seat was used. A8 is specimen, in which angles were used. They have equal arms, 60mm length and 6mm thick. Coped end was bolted to a stiff wall by three, 16 mm bolts with the bolts located 30mm from the edge by means of two web angles. Last, A9 specimen had the same bolts position like in the A8 sample in the web, but this time beam end was supported by two aluminium flat bar hangers, with size equals 50 x 6mm. General geometry of these samples can be seen on figure 3.5.

3.3. Tests results

3.3.1. Seated beams

It is crucial to emphasize, that every specimen with coped end failed in local out of plane buckling web. Tests lasted until measured vertical displacement „w” reached approximately 15mm. In the same time out of plane displacement of the web was from 30 to 40mm. In investigated coped specimens the buckle developed around the corner of the cope and extended into the uncut section. It was noticed, that larger cope cause smaller

area of the buckle. On the picture below there is showed shape of the beam end after

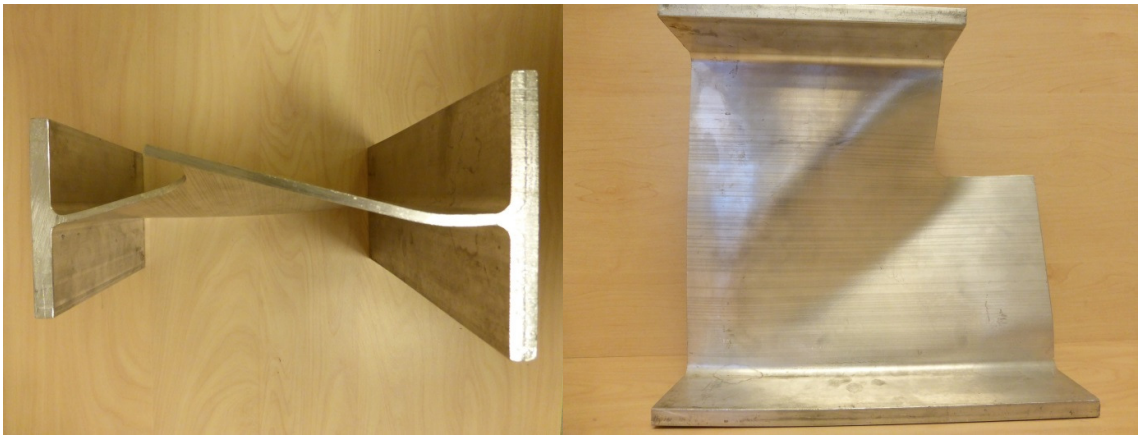

Figure 3.3 Web buckle for A2 specimen

applying buckling load. These are typical web buckle. A2 specimen has been showed.

In the uncoped specimens A1 the transverse displacements of the web were concentrated next to the bottom flange. The buckle extends about 200 mm into the beam. For the specimens with smaller cope like A2 this value is lower and is around 180 mm. On the other hand A6 specimen with the deepest cope, where only half section height remaining showed, that in this case buckle was confined only to the area near the cope corner, and did not extend beyond distance 90 mm along the horizontal edge of the cope. For A4 sample with the longest cope, buckle was also limited to the corner. It is obvious in case of these facts, that both shape and the orientation of the buckle highly depend on cope geometry. The smallest cope gives the largest buckle.

Reaction force R_A showed on the figure 3.1 is the force which is responsible for buckling. On the charts exactly this force will be compared with displacement value “w”. Ultimate/critical force decrease when cope’s dimensions grow. For the five nominally equal uncoped specimens A1, the ultimate force is from 75 kN to 87 kN. Next two equal specimens A2 with the smallest cope (88x97mm) failed for the critical force 67,8 kN and 64,6 kN. The longest coped specimens A4 (260x97mm) buckled failed down at force equals 31kN. On the other side 35,6 kN was sufficient to induce the buckle in A6 sample with the deepest cope (175x130mm). These values mean that for A2 specimens it was obtained 16% reduction compared to uncoped beam and for A4 and A6 this reduction was much larger successively 61% and 55%. Because the steel samples are not the topic of this research I will just mention that obtained reductions are very similar. A comparison

between force-displacement curves for steel and aluminium specimens showed, that this curves are similar, both with respect to the shape and the capacity reduction, caused by cope.

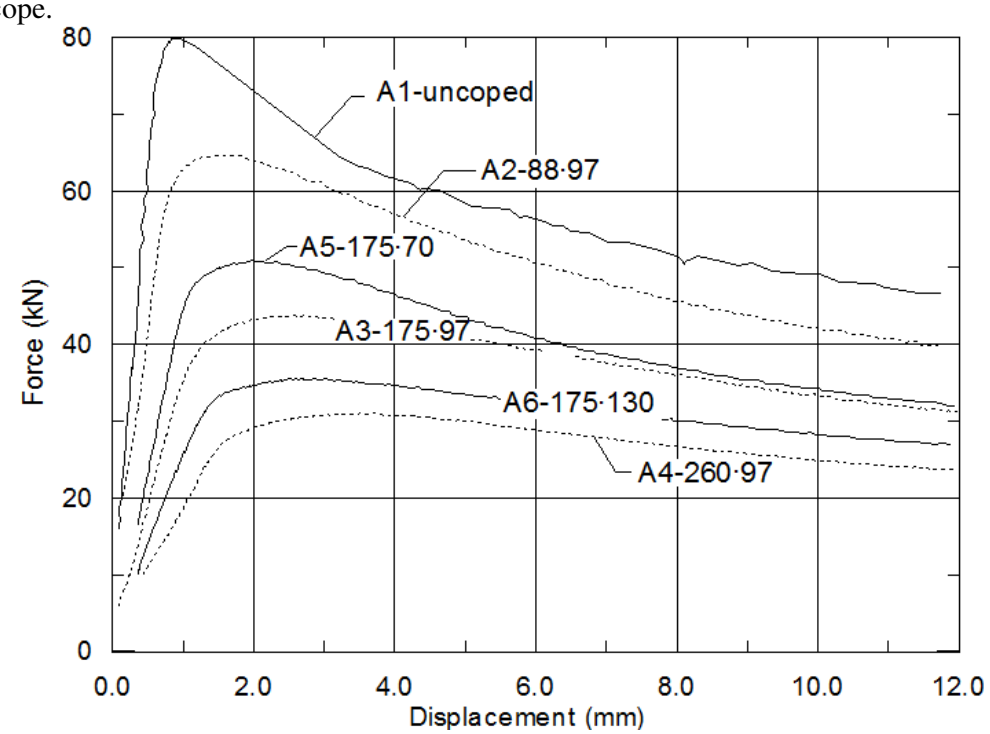

Figure 3.4 Force – displacement curves, seated beams in laboratory tests

3.3.2. Specimens with connections

In case of A7 sample it can be seen, that there was a 14% reduction in comparison to A2 sample, where there was no additional parts. The ultimate force equals 57 kN and it could be surprise, that it is lower that for A2. It can be explained by the difference in moment arm. For A7 this value is e=93mm in comparison with e=58mm for A2 specimen it gives almost twice higher moment value in coped zone. It was noticed that buckle developed more locally, near the cope corner for A7 and in A2 the largest transverse displacement occur at the end of the beam. The reason of this behavior is fact that welded-end plate prevents out-of-plane movement and rotation of the web.

For A8 specimen reported slight increase in ultimate force up to 75,8 kN and is very close to obtained value for A1 specimen (uncoped beam). This time it is really hard to estimate the real value of the moment arm. It can be only stated that distance between bolt line and the end of cope is 58mm. After tests buckle shape was investigated. From transverse web deformation it was claimed that buckle moved from the connection to the

corner of the cope. This was due to the huge restraint caused by the 60 mm wide arms of the angles.

The last investigated specimen with connection A9 gives the highest value of the ultimate force equals 77,8 kN. Also in this case web buckle moved away from connection to the cope corner. The reaction force can be consider to be placed 58 mm from the end of the cope, so it is in the center of the flat bar hangers (the same distance like in A2 specimen). If the sample will be compared with A2 the increase in capacity is significant. The reaction force tensions the web in the region of the connection and reduces the buckling tendency.

For whole specimens with connections there is same trend. Due to the restraining effect of the connections it was noticed that beyond the ultimate force the response curves for A7, A8 and A9 specimens is decreased at a slower rate than for the seated specimens A1 and A2. Whole described results are showed on the figure below.

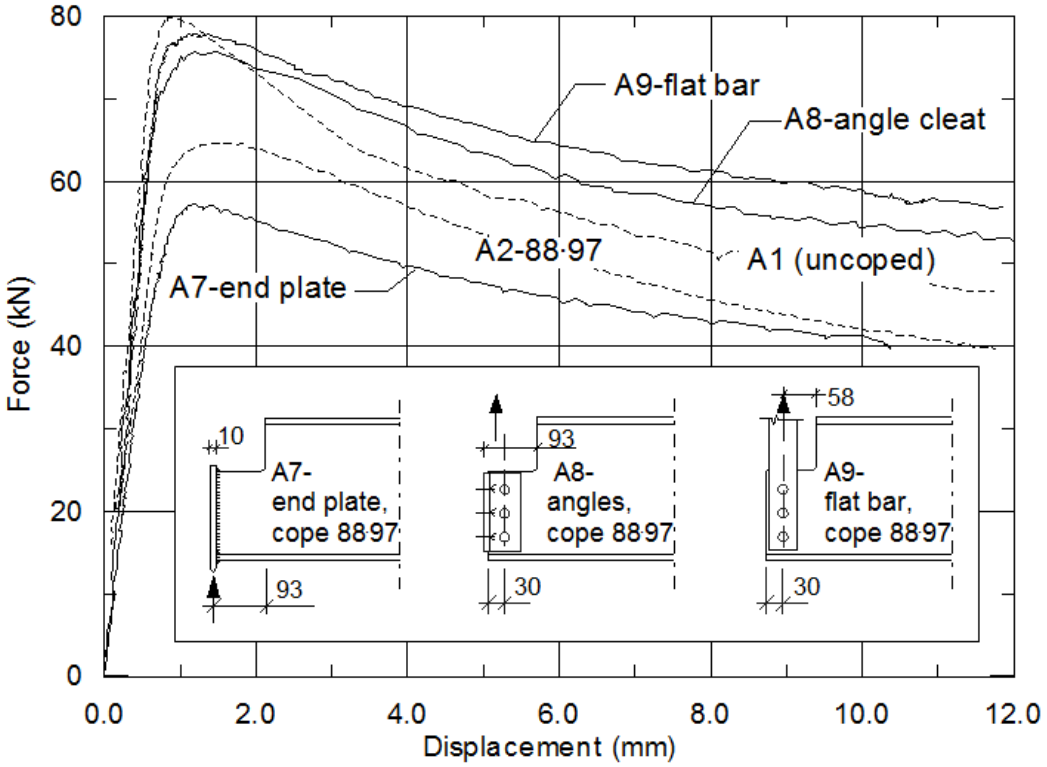

Figure 3.5 Force – displacement curves, connection design

Chapter 4:

Numerical Models

4.1. Program choice

The finite element method is used to conduct the analysis for this project. The software used is ABAQUS 6.12, a product of Dassault Systemes. Abaqus is an industry leader in the field of finite element analysis. This project requires nonlinear large displacement analysis, for which the Abaqus solver is known as best in class. In point 4.3 of this paper were included the most relevant issues arising from the use of this program.

4.2. The main objective

I devoted a lot of attention and I put a lot of work to develop a model that would reflect the reality. It is not possible due to defects in materials and geometry, and many other reasons which cannot be predicted to create a model which will allow us to maintain results like from the laboratory. But the main aim of this work was to be the closest as much as possible to reality. Although research will always lead to exacts results, they are expensive and need specialized equipment adequate space, conditions and preparations. In contrast, numerical calculations require only time and knowledge how to simulate the problem properly.

To solve the problem in this case both methods were used. A lot of tests in the laboratory were done, also I considered many different possibilities for numerical model trying to find this one, which together create best reflecting reality. This approach allows assume, that developed model is correct and expand obtained formulas on more general cases, saving time and money for next researches.

I drew special attention for simulating sources of nonlinearity. Most metals, also aluminum have a fairly linear stress/strain relationship at low strain values; but at higher strains the material yields, at which point the response becomes nonlinear and irreversible.

4.3. Brief introduction to ABAQUS analysis

4.3.1. Units

It is crucial to emphasize in the beginning, that there are no predefined system of units within ABAQUS, so the user is responsible for choosing the correct values. All input data must be specified in consistent units. During my work I used SI systems of consistent units. But because I had to operate sometimes on very small values of length I have decided to express it in millimeters and then I matched others unit.

Quantity	SI	SI (mm)
Length	m	mm
Force	N	N
Mass	kg	tonne (10^3 kg)
Time	s	s
Stress	Pa (N/m^2)	MPa (N/mm^2)
Energy	J	mJ (10^{-3} J)
Density	kg/m^3	$tonne/mm^3$

Table 4.1 Units in ABAQUS

4.3.2. Material behavior

In ABAQUS the models elastic material properties are implemented by Young's modulus (E) and Poisson's ratio (ν), while the plastic material properties are implemented as the stress-strain relation. ABAQUS uses true strain, which fulfill special criteria. Strain has to be able to predict zero strain for rigid-body motion and reduce to infinitesimal strains if nonlinear terms are neglected. Additionally the strain measures should be able to predict finite strain in a realistic manner, i.e. for full compression it should diverge to an infinite negative strain (ε → -∞ when L → 0) and for infinite elongation it should diverge to an infinite positive strain (ε → ∞ when L → ∞). It could be easily seen from the figure below that only true (logarithmic) strain ε_L fulfills these criteria.

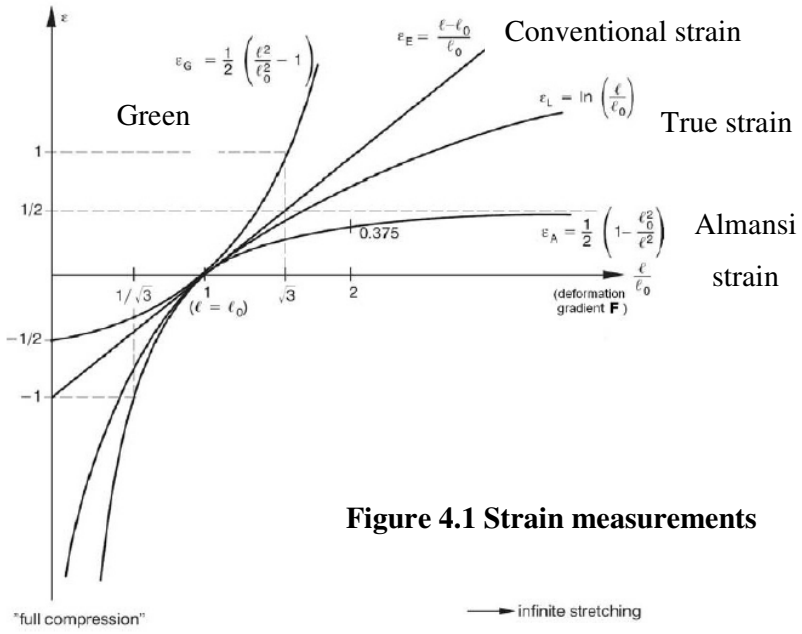

Figure 4.1 Strain measurements

Unlike conventional (engineering) strain (ε_E), true strain accounts for the geometrical changes the specimen undergoes during deformation. Thus, the strain increment is denied with respect to the current length (L): $d\epsilon_l(t) = \frac{du_L(t)}{L}$

Finally ABAQUS expects the stress – strain data to be entered as true stress and true plastic strain, hence material data which originally are given by the engineering values must be converted into such. In addition the modulus of elasticity must correspond to the slope defined by the first point (the yield point).

To convert the conventional stress to trues stress following equation should be used:

$$\sigma_{true} = \sigma_{nom}(1 + \varepsilon_{nom})$$

To convert the conventional strain to true strain following equation should be used:

$$\varepsilon_{true} = ln(1 + \varepsilon_{nom})$$

To convert the true strain to true plastic strain following equation should be used:

$$\varepsilon_{pl} = \varepsilon_{true} - \frac{\sigma_{true}}{E}$$

4.3.3. Imperfections

A brief explanation about the possibility of introducing imperfections in ABAQUS will allow to focus more on choosing the best case for nonlinear geometry in point 4.9 of this paper. It is crucial to emphasize, that ABAQUS has no tool, which just would allow for the direct introduction of imperfection. But fortunately there are possible solutions for this problem and a geometric imperfection pattern can be generally introduced into an otherwise "ideal" model for a postbuckling load-displacement analysis. Mentioned program offers four ways to define an imperfection:

- As a linear superposition of buckling eigenmodes .
- From the displacements of an ABAQUS/Standard static analysis.
- By specifying the node number and imperfection values directly on the data lines. To make this operation, it will be necessary to create a file containing the description of the project in the ABAQUS.
- It is also possible to change initial geometry before running buckling analysis, by injected into the system forces which cause small displacements of nodes. The direction of the forces allows predicting the shape of the deformations, but not controlling it fully. If the task will be divided into different steps, and in the first one

initial geometry will be changed by very small forces it the second step calculations will start on this new geometry, which would be not perfect anymore.

Using the buckling modes of the structure to define the imperfection in the model involves two analysis runs with the same model definition. ABAQUS/Standard is used with the "buckle" procedure to establish the probable collapse modes. Then ABAQUS/Explicit is used to perform the postbuckling analysis. It is possible to introduce an imperfection to the geometry in the ABAQUS/Explicit analysis by adding these buckling modes to the "perfect" geometry. It is important to consider the scaling factor for each mode. The lowest buckling modes are assumed to provide the most critical imperfections, so they are usually given the largest scaling factor. Finally the scaled deformation patterns of the buckling modes are added to the perfect geometry to create the perturbed mesh.

4.4.Elements

4.4.1. Elements choice

A wide range of elements is available in Abaqus. But this amount of option raises a problem for the selection of appropriate one. Each element is characterized by: family, degrees of freedom, number of nodes, formulation and integration. Generally the most used elements are on the figure 4.2.

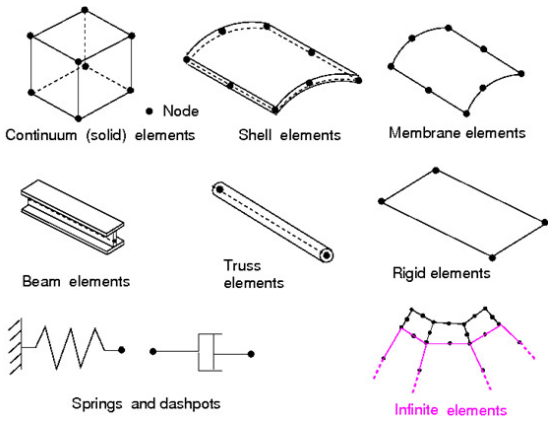

Figure 4.2 Commonly used element families

It was decided to simulate the problem with using two different element families: shell and solid. It was expected that solid elements should give the best results, but in this case the geometry of beam (we will treat it as thin plate parts) encourage trying to find the solution with shell elements.

Another issue to consider was how many nodes used element should have. Displacements, rotations, temperatures, and the other degrees of freedom (like acoustic pressure, electric potential) are calculated only at the nodes of the element. At any other point in the element, the displacements are obtained by interpolating from the nodal displacements. On the figure 4.3 you can see difference between 4 and 8-node shell.

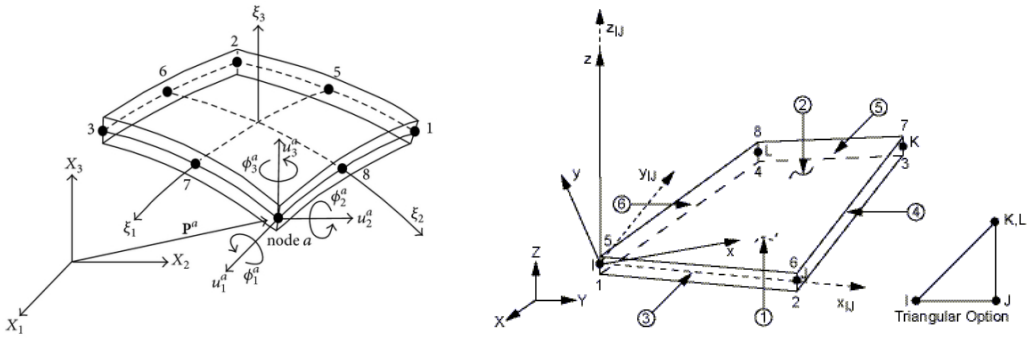

Figure 4.3 Shel elements 8-node and 4-node

Elements that have nodes only at their corners, such as the 4-node shell, use linear interpolation in each direction and are often called linear elements or first-order elements. 8-node shell use quadratic interpolation and are such elements often called quadratic elements or second-order elements.

4.4.2. Shell

Shell elements are used to model structures in which one dimension (the thickness) is significantly smaller than the other dimensions and in which the stresses in the thickness direction are negligible. A structure, whose thickness is less than 0,1 of a typical global structural dimension generally can be modeled with shell elements. This is a very general assumption, but for the web this ratio equals 0,020 and for the flange this condition is also fulfilled and equals 0,098.

At the beginning of this study linear shells (called S4 elements) were used for the mesh due to their fast computational time. However, problems were encountered using this type of element because linear shells are prone to shear locking. Shear locking can affect the performance of fully integrated, linear elements subjected to bending loads and it is the reason of underestimation of deflection. Since the edges of quadratic elements are able to curve, shear locking is not typically an issue. They may exhibit some locking if they are distorted or if the bending stress has a gradient, but typically don't have as many issues as

linear shells. Figure below, from the Abaqus 6.12 documentation [2], shows a comparison of how linear and quadratic shells behave under a bending load.

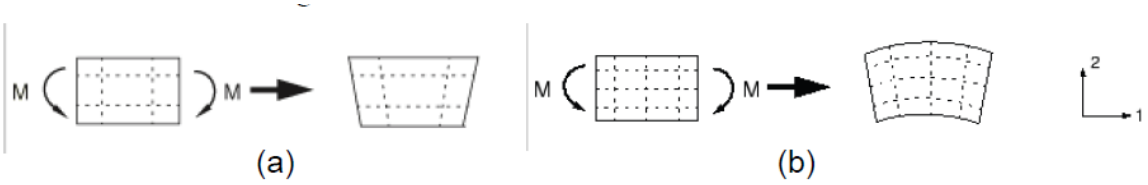

Figure 4.4 Deformation of a fully integrated, linear element (a) and a fully integrated, quadratic element – S8 (b) subjected to bending moment M

As it can be seen, shear locking causes the elements to be too stiff in bending. In reality lines parallel to the horizontal can have curvature, and lines through the thickness remain straight. The angle between the horizontal and vertical lines remains at 90°. But in fully integrated, linear elements the edges are unable to curve. So these elements function perfectly well under direct or shear loads, but are not good for this studies.

Quadratic shells (S8 elements) were then used to mesh the part. However, the solution time increased tremendously, and for an unknown reason, the beam was not undergoing to collapse in this way, how it was expected. With further reading through the Abaqus documentation, it was found that S4R5 and S4R elements, which are reduced integration linear shells with 5 degrees of freedom per node (and 6 in case of S4R), are recommended for modeling thin shell structures. These elements are used for the Abaqus benchmarking studies and example problems for use in modeling for example thin cylinders. Therefore, these elements were utilized for this study and yielded accurate results. After several results these elements were decided to be used, what confirmed [4], where it was found, that S4R are suitable for large-strain analysis and S4R5 provide for arbitrarily large rotations but only small strains.

Linear reduced-integration elements like S4R tend to be too flexible because they suffer from their own numerical problem called hourglassing.

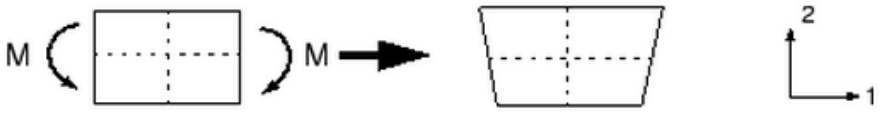

Figure 4.5 Deformation of a linear element with reduced integration subjected to bending moment M.

Neither of the dotted visualization lines on figure 4.5 has changed in length, and the angle between them is also unchanged, which means that all components of stress at the element's single integration point are zero. This bending mode of deformation is thus a zero-energy mode because no strain energy is generated by this element distortion. The element is unable to resist this type of deformation since it has no stiffness in this mode. In coarse meshes this zero-energy mode can propagate through the mesh, producing meaningless results. It is important to emphasize, that reduced-integration elements use one fewer integration point in each direction than the fully integrated elements. The locations of the integration points for reduced-integration, quadrilateral elements are shown in Figure 4.6.

Figure 4.6 Integration points in two-dimensional elements with reduced integration

Also studies on previous similar analyses done by students on NTNU confirmed, that this choice is the best according to accuracy and time of calculations. Urseth [4] in his work used S4R elements and claimed that for undistorted elements reduced integration provides more accurate results compared to full integration, because it softens the behavior of the element [6]. The same conclusion can be found in paper [7] were also S4R were used for numerical modeling.

4.4.3. Solid

In case continuum elements I used the deductions learned from the 4.4.2 point of this paper. It was wise to use similar working elements to reduce probability of inaccuracies and increase accuracy of the results. Finally C3D8R elements were used, what means an 8-node linear brick with reduced integration and hourglass control. From the same reason like in point 4.4.2 instead of quadric elements, linear elements were chosen in this model.

4.5.Geometry of cross section

4.5.1. Measurements

Before the tests in the lab started a lot of measurements were done. In this way, the actual dimensions of aluminum profile were checked, which slightly differ from nominal. Middle values of measured dimensions are showed on the figure below.

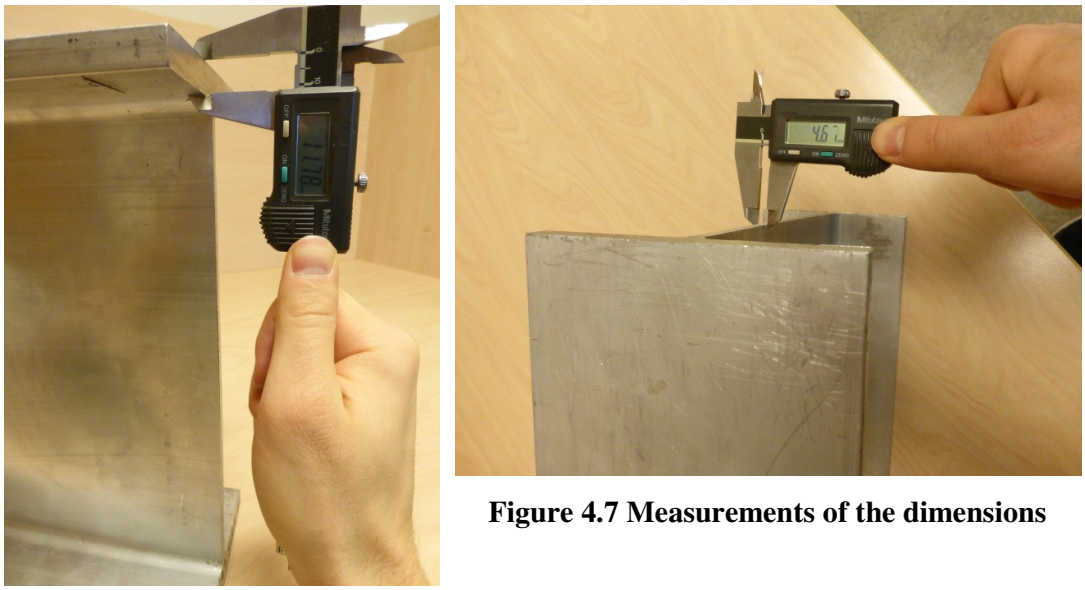

Figure 4.7 Measurements of the dimensions

There were found some differences between the declared values. For the modeling real dimensions were used, which are shown in the table 4.2.

XHP 260	h [mm]	b [mm]	t_f [mm]	t_w [mm]	r [mm]	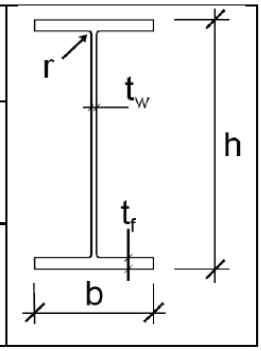
Nominal values	260	120	12	5	7	
Real values	259,2	119,4	11,7	4,65	7	

Table 4.2 Comparison between declared nominal and real dimensions

4.5.2. Shell elements

For use in the shell elements it was decided to introduce a cross-section by single lines, which will be identify the middle surface of each part of the XHP profile. This approach resulted in the problem of determining the thickness of the individual fragments. The translation the real cross-section to shell element geometry is on the figure below.

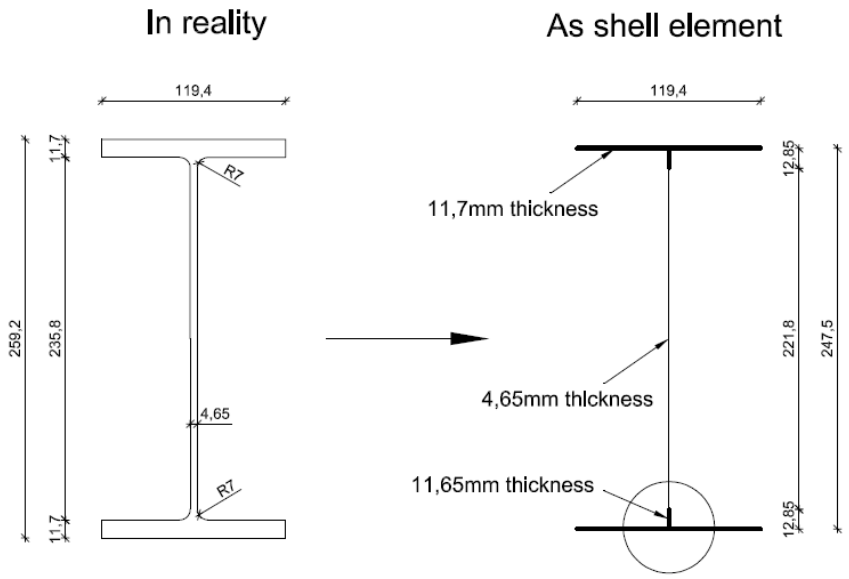

Figure 4.8 Geometry inputted to ABAQUS for shell elements

Special attention was paid to the area in the circle, where the web connects to the I-beam flange. Since shell elements do not have a volume, it is not possible to model the web's rounded shape at the intersection between the web and flanges in an exact manner. Buckling is particularly sensitive part of the web having a thickness of 4.65 mm and on the other hand, this phenomenon does not occur in the area of the fillet radius R7. It was simulated by giving the part of the web next to the flange higher thickness. The length and thickness of this part was assumed in following way:

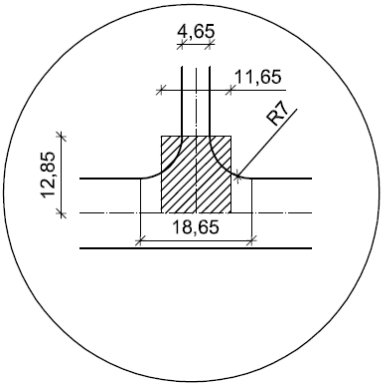

$$\text{thickness} = \frac{4{,}65+18{,}65}{2} = 11{,}65\text{mm}$$

Figure 4.9 Solution for the detail of connetion between flange and web

4.6.General geometry

To reduce time consumption for the numerical calculations only part of whole beam was modeled. It was decided to create the part of the beam from support, where is the cope to the place, where the force will be putted. This causes the need to give serious consideration to the location of the supports and the selection of theirs type in the model. More can be found in point 4.13 of this work.

4.6.1. Shell elements

In case of the shell elements 3D objects was created from single planar parts, connected in a proper way. These single parts are shown on the figure beside. After creating it they were moved to assembly part, where after geometrical operations they allow to gain final model. To each part homogeneous thickness, material properties and necessary data were assigned. For different copes only l1, h1 and h2 are changing. Their values depending of the cope dimension are given in the table below.

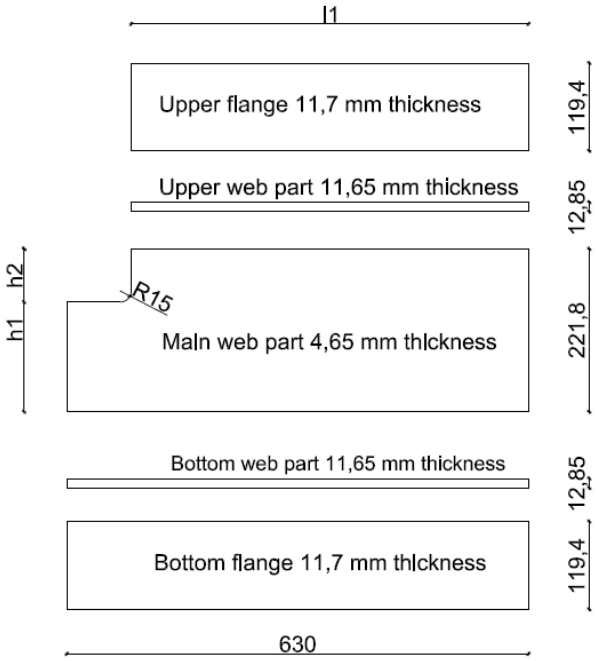

Figure 4.10 Parts creating shell model

Sample / dimension:	c [mm]	d_c [mm]	h2 [mm]	h1 [mm]	l1 [mm]
A1	0	0	0	221,8	630
A2	88	97	72,45	149,35	542
A3	175	97	72,45	149,35	455
A4	260	97	72,45	149,35	370
A5	175	70	45,45	176,35	455
A6	175	130	105,45	116,35	455

Table 4.3 Dimensions of parts creating shell model

4.6.2. Solid elements

To transform 2D solid element (cross-section) into 3D (beam) the extrusion command were used. It was necessary to create two profiles, one which will be XHP 260 profile and second, where the flange will be cut, to model the cope. After creating these two cross-sections they were extruded in length according to cope dimension. Then parts were linked and whole beam was modelled. Additionally small part was also created to model the rounded area of the web, where buckle occurs. So it was decided that this small part of model can have high influence on results.

4.7. Material

4.7.1. Elastic properties

Elastic design is carried out by assuming that at design loads structures behave in a linearly elastic manner. An elastic analysis is performed by applying the design loads and required internal forces in the structural elements (members and connections) are determined and adequate design strength is provided. Since the element forces are determined based on elastic behavior, the design is governed by elastic stiffness distribution among the system elements. It is commonly understood that most structures designed by elastic method possess considerable reserve strength beyond elastic limit until they reach their ultimate strength. In ABAQUS we set elastic behavior by determining the Young's modulus and Poisson's ratio (figure 4.11). These values were adopted according to Eurocode 1991-1-1 (it gives 0,3 value as a Poison ratio but difference does not affect on results).

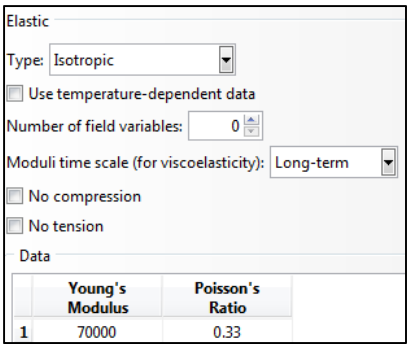

Figure 4.11 Elestic properties inputted to ABAQUS

4.7.2. Plastic properties

Plastic design offers several advantages over the traditional elastic design. With plastic analysis, a structure can be designed to form a preselected yield mechanism at ultimate load level, what leads to a known and predetermined response during extreme events. This has special significance in the context of this design, where it is essential for the structure to deform in a preselected manner to achieve similarity to the tests.

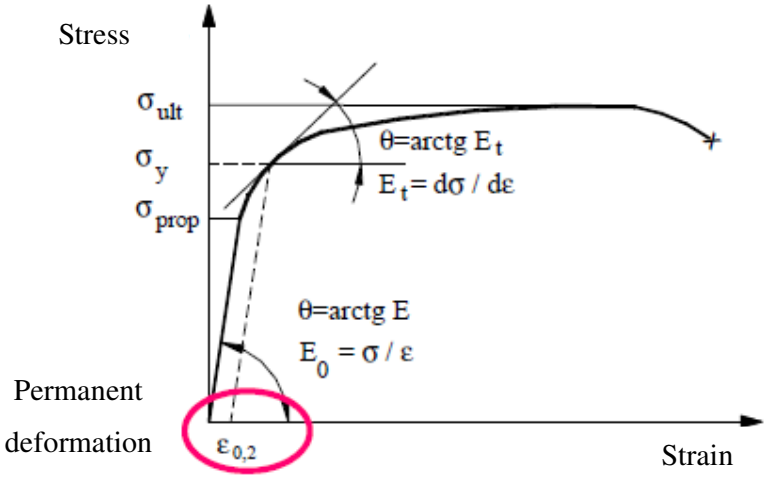

Figure 4.12 Strain-stress curve for materials without clear yielding point

Aluminium belongs to materials without clear yield strength. In that case to get its value we should use permanent deformation ratio $\varepsilon_{0,2}$. Yield strength is determined by moving elastic part of chart from zero strain to 0,2 % strain. The intersection of this line with stress-strain curve allows us to find the yield strength. This procedure is showed on the figure above.

To obtain the appropriate curves ten samples of the aluminium were investigated. The material properties were determined from standard tension tests. During choosing places of coupons was taken into account that it web can buckle and this part of the sample is exposed for the highest stresses. Secondly after tests it turned out that the geometry of buckling does not depend on a single direction. Finally it was decided to take the coupons in three different directions (horizontal, vertical and 45 degree) only from the web.

In the results a certain anisotropy was observed as illustrated by the mean values of yield strength f_{02} = 258 MPa and ultimate strength f_u = 297 MPa in the longitudinal direction, f_{02} = 244 MPa and f_u = 279 MPa in the 45-degree direction, and f_{02} = 270 MPa and f_u = 306 MPa in the transverse direction. Specimens 1 and 2 were vertical, specimens from 3 to 7 were horizontal and specimens from 8 to 10 were 45-degree samples. The figures below shows the test results for 45-degree samples.

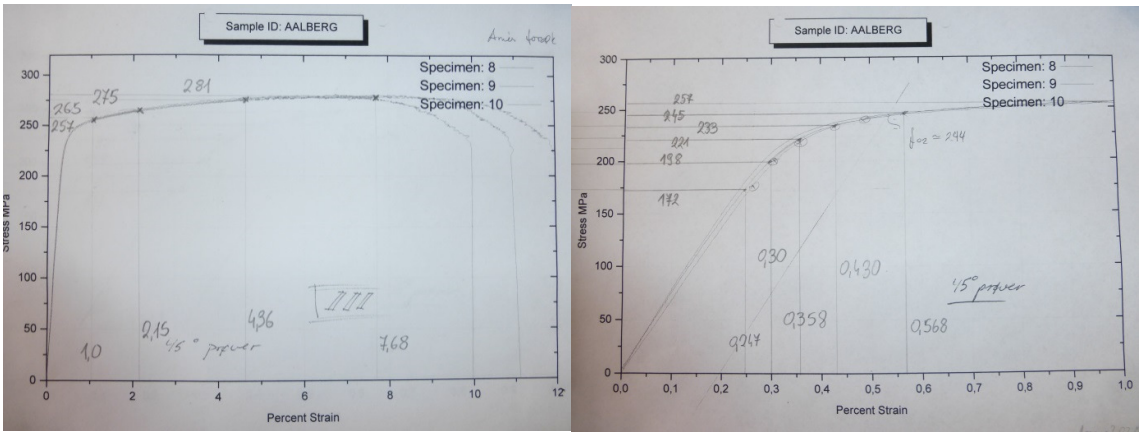

Figure 4.13 Results from standard tension tests

From each sample I have tried to create a set of curves, which will be very similar to the original graph. The middle values were chosen to characterize each type of coupons. Then final curve was created. In the table 4.4 below have been collected the results.

Vertical samples		Horizontal samples		45 degree samples		Final curve	
Stress [MPa]	Strain [%]	Stress [MPa]	Strain [%]	Stress [MPa]	Strain [%]	Stress [MPa]	Strain [%]
150	0,214	150	0,214	150	0,214	150,0	0,214
206	0,281	185	0,276	172	0,247	202,0	0,296
227	0,33	210	0,324	198	0,3	224,6	0,352
250	0,39	225	0,358	221	0,358	241,0	0,141
262	0,477	238	0,4	233	0,43	251,1	0,502
270	0,6	250	0,517	245	0,568	255,2	0,599
281	1	265	1	257	1	268,2	1,000
298	3,1	275	2,15	265	2,15	278,8	2,20
303	5,1	284	3,74	275	4,36	287,1	3,90
303	8	290	8,61	281	7,68	291,3	8,000

Table 4.4 Tension tests results for different specimens

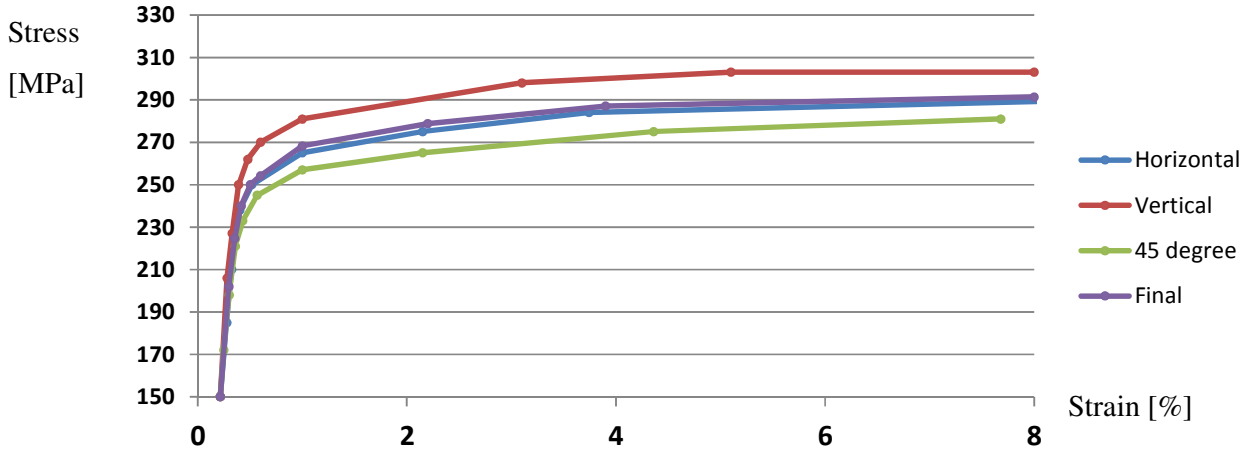

Figure 4.14 Stress-strain curves

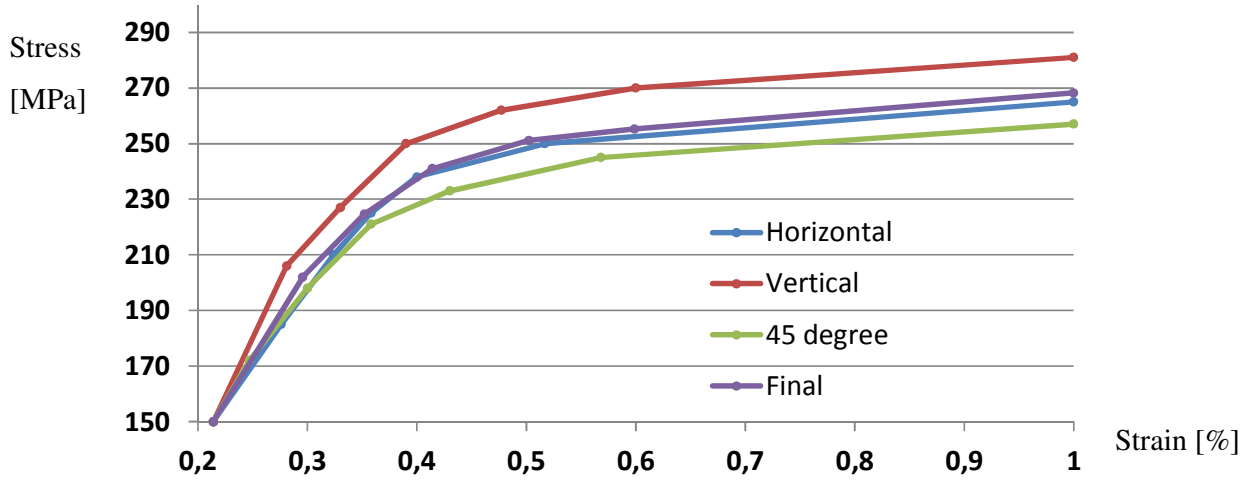

Figure 4.15 Strain-stress curves. Zoom to the interval from 0,2% to 1% strain.

Knowing the conventional strain and stress it was possible to calculate true stress and true plastic strain, which are the values expected by ABAQUS. This is described in more detail in point 3.2.2. You can also find there formulas allowing to convert conventional values to true values. In the table below can be found data(true strain and stress), which were given to ABAQUS:

Conventional Stress [MPa]	Conventional Strain [%}	True Stress [MPa]	True Strain [%]	True plastic strain [%]
150,0	0,214	**150,3**	0,214	**0,0000**
202,0	0,296	**202,6**	0,295	**0,0058**
224,6	0,352	**225,4**	0,351	**0,0294**
241,0	0,414	**242,0**	0,413	**0,0674**
251,1	0,502	**252,4**	0,501	**0,1405**
255,2	0,599	**256,7**	0,597	**0,2302**
268,2	1,000	**270,9**	0,995	**0,6081**
278,8	2,200	**284,9**	2,176	**1,7691**
287,1	3,900	**298,3**	3,826	**3,3997**
291,3	8,000	**314,6**	7,696	**7,2466**

Table 4.5 Plastic properties inputted to ABAQUS (true stress and true plastic strain)

4.8. Type of analysis

4.8.1. Linear buckling

The effect of buckling will be studied using finite element analysis. The least expensive way to study this effect would be by conducting a linear eigenvalue buckling analysis. This analysis, however, is known to be anticonservative [3,18]. The eigenvalue method predicts the buckling strength of an ideal linear structure. Since it is a linear solution, the stiffness matrix is not updated during the solution and the results predict a load carrying capability greater than the structure could actually sustain. This is the biggest disadvantage, but even with this Linear buckling analysis was used for these studies due to the several reasons. Firstly this short analysis allows getting the buckling shapes, which will be very useful in giving imperfections to the more advanced models. ABAQUS has the capability of using the results of an eigenvalue buckling analysis to impart imperfections into a part for a buckling analysis. It also very good way of checking results. It expected that real values will be lower than from this ideal linear analysis, so the

eigenvalue force can be the upper limit of the load. To choose this type of analysis in step creation panel “linear perturbation” as a procedure type must be chosen and then “Buckle”.

4.8.2. Static general and Riks

In this situation the best solution was to perform a nonlinear, large displacement static buckling analysis. Although this method is more time consuming and computationally expensive, it is typically a more accurate method for determining buckling capability of a part. The nonlinear large displacement method gradually increases the load in steps. The equilibrium equation, {F}=[K]{U}, is solved for displacement, {U}, in each step by an iterative process. As the load increases in each step, the stiffness matrix, [K], is updated to reflect the new stiffness under the current loading. The load is increased until instability occurs and the stiffness approaches zero. Once this occurs the finite element package is unable to find a solution and the job is aborted. In this moment the structure is unable to carry any more load and buckling has occurred.

For this studies, except linear eigenvalue also nonlinear buckling analysis was performed. A nonlinear buckling analysis will then be performed on the cylinder using a static Riks solution and General static solution, which can model large deflections and post-buckling behavior. By default more desirable is General static analysis. Firstly it provides very accurate results and what is also very important is much faster than Riks algorithm. In addition in point 4.10 it is described a method for the introduction to the model loading, which is suitable for General static analysis.

Results showed that the General static analysis provides better results than Riks method for considered problem especially in case of force-displacement curve. The exemplary results from all analyses (linear buckling, general static and general riks) for A1, A2 and A3 specimens are given in the table below.

Specimen	Linear buckling (eigenvalue) [kN]	Nonlinear analysis, General Static [kN]	Nonlinear analysis, Riks Static [kN]
A1	96,4	76,00	75,80
A2	68,99	64,41	x
A3	43,71	43,60	x

Table 4.6 Comparison of different methods

The symbol in the table 4.6 x means that program from some reason gave very strange results, which can't be compared or calculations were aborted. When the shape of force-displacement curves were considered it turned out that that only General Static method can be used for further analyses. To gain results above as imperfection first buckle shape was used with 0,2mm maximum displacement.

4.9.Load

In nonlinear analysis it is not obvious, that simply applying the load allow us to obtain the right results. This is because incremental load control methods, they can only work effectively if nonlinearity spreads gradually. Commonly used methods cannot predict a sudden change in the stiffness and it is not able to trace the equilibrium path beyond limit and turning points, respectively. From the previous researches the expected shape of strain-stress curve is known [5], [7]. This allows me to claim that it is better to replace the load, by applying a displacement as a factor causing the deformation of the beam. The benefits of such an approach results from the figures below.

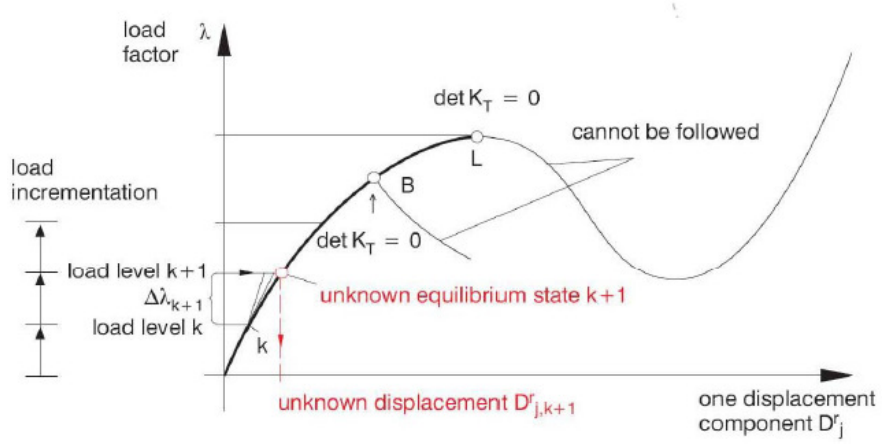

Figure 4.16 Load control

At limit (L) and bifurcation (B) points the tangent stiffness K_T becomes singular and the solution of the nonlinear equilibrium equations is not unique at this point. This knowledge was crucial while choosing displacement as applying factor to ABAQUS. In the buckling analysis we must take into account also part of the path after L – point.

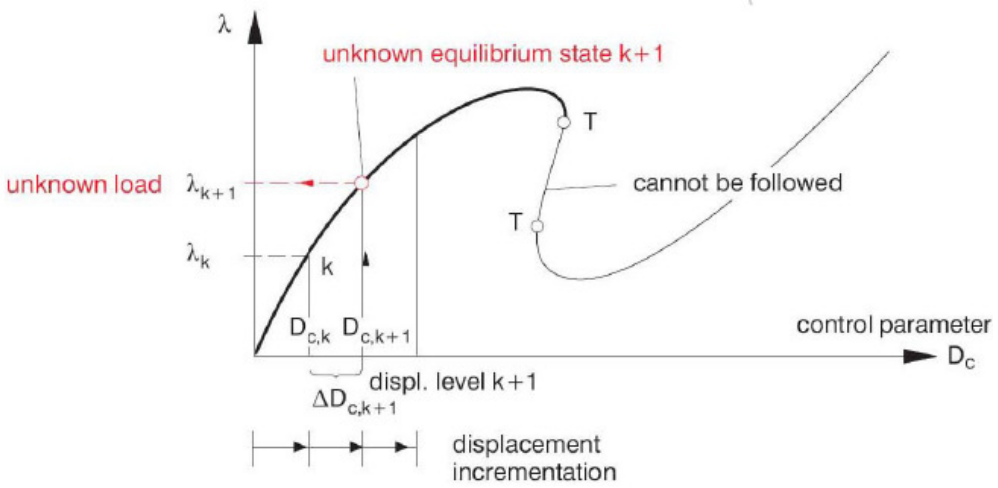

Figure 4.17 Displacement control

This type of incrementation has also weaknesses. The problem occurs in this case, when the limit point is exceeded. Then we cannot go beyond turning (T) points. Because then it would be necessary to prescribe negative displacement increments, what is impossible. But from the previous student's works it was assumed that it won't happened.

4.10. Imperfections

4.10.1. Idea of imperfections

In designing thin shells, it is typically assumed, that they are perfectly flat plates and the imperfections resulting from manufacturing processes are not captured. It is typically found that results obtained from experiment are significantly different from the theoretical solution. The discrepancy is thought to be due to imperfections in an actual manufactured part that are not accounted for in theory. Because I wanted to avoid such situation, this study will examine how imperfections in designing beam can affect its buckling load capacity. The postbuckling behavior of some structures, such as thin cylindrical shells (and thin elements generally), depends strongly on the imperfections in the original geometry so it is important to choose it wisely.

Investigated XHP 260 aluminium cross-section had some initial imperfections at the beam ends. They were consisted in general of small flange misalignment and a small sideway bow of the web between flanges, with amplitude less than 0,5mm.

4.10.2. Imperfection shapes

During calculations it turned out that initial imperfections have huge influence on post buckling behavior. Moreover without them, created model may give very wrong

results. The predicted deformation shape could be quite different from the buckle modes observed in experiment. It was decided to investigate initial imperfections in many ways and choose the best one, which will provide the most accurate results compared to tests. A2 and A3 specimens were chosen for these investigations, because their buckling shapes differ a lot. Imperfections were introduced to the model in following methods:

- The easiest way for providing imperfections was to create an initial shape by putting a small, transverse force, which can change geometry of the beam in very small level. Disadvantages of this method are facts that the shape of imperfections can't be controlled in any way and also impossible to determine the value of preload. It was only known that measured imperfections of the specimens ranged from 0,1 to 0,5mm. After a few steps the value of the preload was set at 20N, which resulted in the transversal displacement of 0,272mm (A3) and 0,185mm (A2). Because cope shape and position creating high risk that beam will be accidentally hit at the end of free end, just this place was chosen for the application of the preload in perpendicular direction to the web surface.

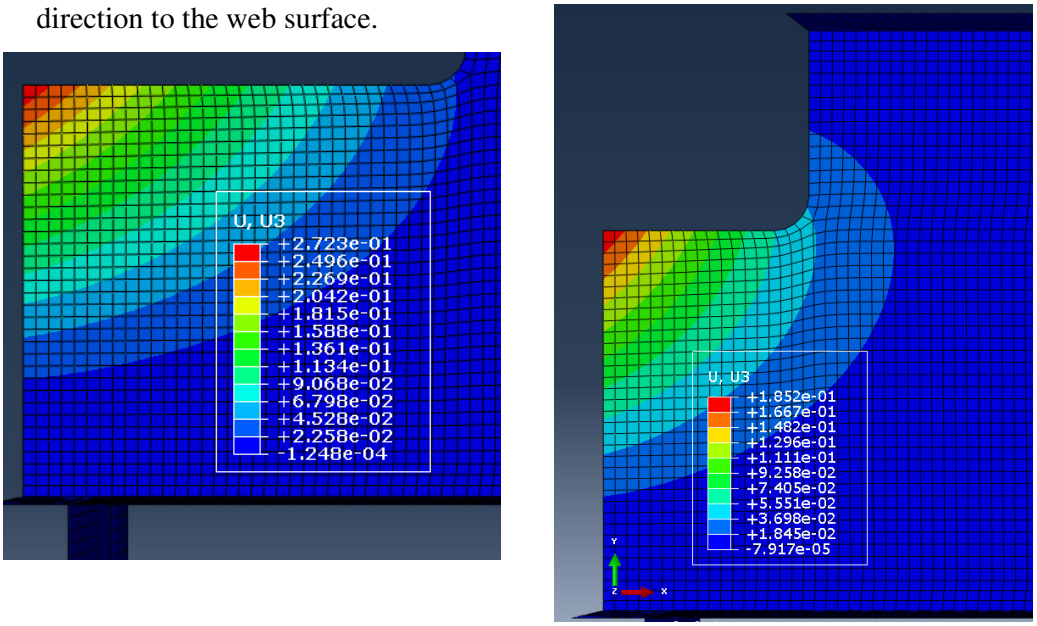

Figure 4.18 Imperfection shapes caused by preload.

- Next idea for providing imperfections to the model was based on the use of buckling shapes. This time it was necessary first to save nodal characteristic about displacement after eigenvalue analysis to the file and later assign them to the step in console of the program by using imperfection command. Also the amplitude should be chosen, because initial imperfections should be reduced. 0.1, 0.2 and 0.3 factors

have been chosen for this task. For this work following mixture of buckling shape was used:

Buckle imperfections	First mode shape	Second mode shape	Third mode shape	Fourth mode shape	Fifth mode shape
A	0.3	0	0	0	0
B	0.2	0.1	0.05	0.05	0.05
C	0	0	0	0.1	0.2
D	0.1	0.1	0.1	0.1	0.1

Table 4.7 Investigated imperfections caused by buckle modes

Last method by which imperfections were introduced to the model was to manual change of coordinates, which define position of the nodes. The whole model with all necessary for calculation data was transformed into the text file, where node's coordinates can be found. Then for matrix with geometry algorithm was created, which changed the initial coordinates and gave beam sin/cosine wave shape. Because of the large amount of nodes this task can't be done by manual changing the coordinates. Only transversal, perpendicular to the web surfaces imperfections have big influence on the postbuckling behavior so only "z" position of nodes in this case was changed by formula:

$$z_{new} = z_{old} + 0{,}3 \cdot sin\left(\frac{m\pi x}{L}\right) cos\left(\frac{n\pi y}{H}\right)$$

L and H are the length and height of the beam, x and y are coordinates of every single node along the axis. Value 0,3 was chosen as a amplitude of the imperfection and m and n allow expressing how many sin/cosine wave will be created along axis. In case of the height the most reasonable was to create only one sinus wave from bottom to upper flange, so n=1 and m value was tried as 1, 2 and 3. That means that specimens got free shapes from sinus contribution:

- Sinus1 with one sinus half wave in longitudinal direction and 1 sinus half wave in vertical direction,
- Sinus 2 with two sinus half wave in longitudinal direction and 1 sinus half wave in vertical direction,
- Sinus 3 with three sinus half wave in longitudinal direction and 1 sinus half wave in vertical direction.

Formula given above had to be modified, because point in the middle of the high at the fixed end was chosen as a starting point with coordinates 3318,4 on x axis, 110,9 on y axis and 0 on z axis.

$$z_{new} = z_{old} + 0{,}3 \cdot sin\left(\frac{m\pi(x - 2688{,}4)}{630}\right) cos\left(\frac{\pi(y - 110{,}9)}{247{,}5}\right)$$

4.10.3. Choice of imperfection shape

In the charts below the results obtained on A2 sample are presented. In case of A3 they were exactly the same and every statement regarding to A2 will be true in A3 results. Generally it turned out that the vast majority of the used shapes can be used as initial imperfections. In some cases the incrimination was to fast but even with it generally the differences between the curves are very small and each one of them is similar in shape to the received one from laboratory tests. Ultimate forces obtained in nonlinear analysis are given in the table below. In laboratory tests 66,2 kN ultimate reaction force was obtained as a middle value.

Imperfection type	Buckle A	Buckle B	Buckle C	Buckle D	Sin 1	Sin 2	Sin 3	Load
Ultimate force [kN]	64,02	64,22	66,26	64,63	64,80	63,68	62,43	64,09

Table 4.8 Ultimate forces with different buckle shapes for A sample

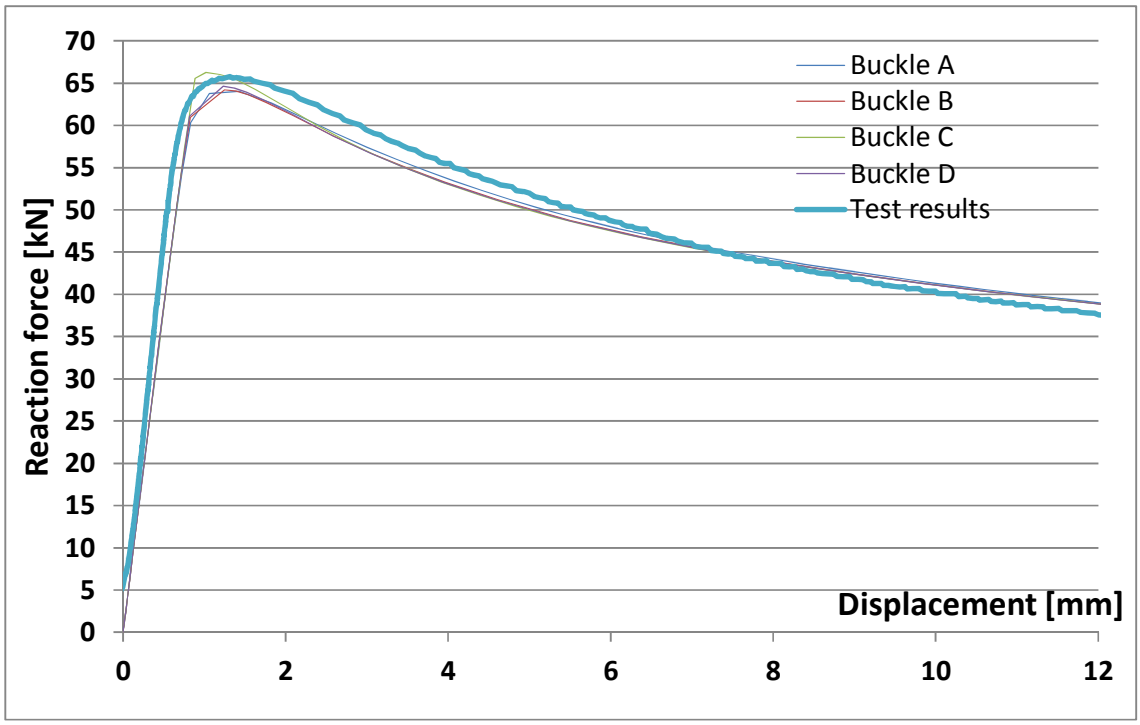

Figure 4.19 Buckle's imperfection tests

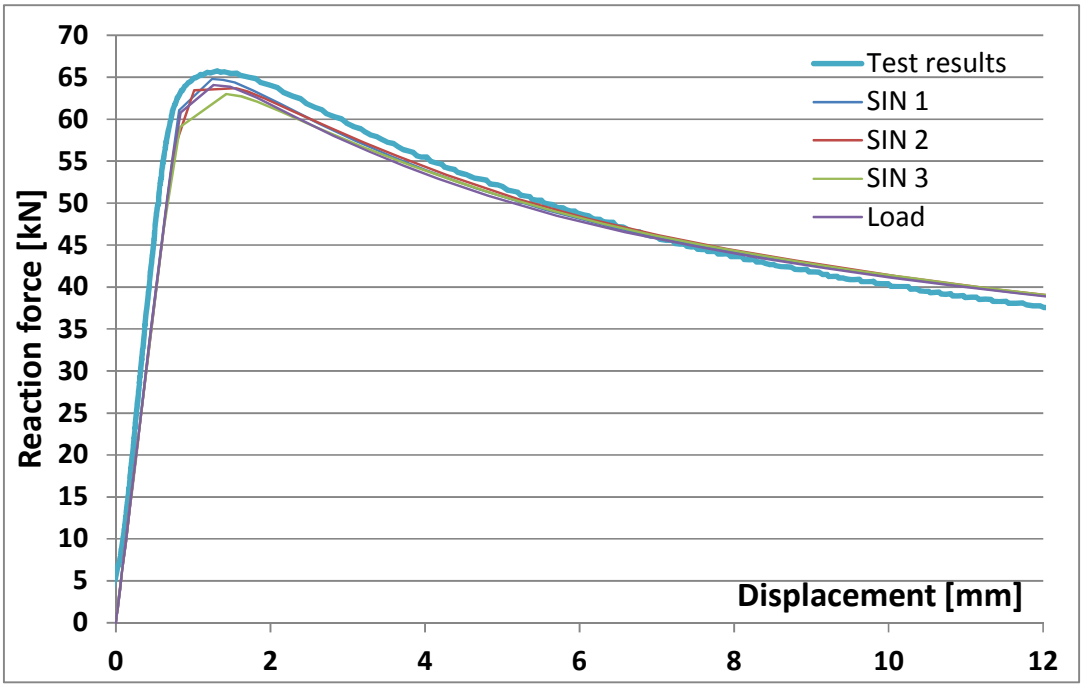

Figure 4.20 Sinus and load imperfection tests

As a final choice of initial imperfection Buckle A shape was used. Firstly it provides very accurate results both in shape and in ultimate reaction force value. Also the deformation pattern corresponds to this one, which can be observed on specimens after laboratory tests. Finally the method, which allows inputting the buckle imperfections like this to the model, is much easier to use than changing the nodes position in separate program (like in the sinus waves case). Moreover by using this method always additional linear analysis will be provided, which helps to control the results and buckle shapes. Summarizing, each specimen in further calculation will get its own imperfection shape based on first buckling with amplitude equals 0,3 mm. By deciding on Buckle A shape is also preserved some degree of security because it gives lower capacity than tests.

4.10.4. Reference to the measurements

The initial imperfections (size of the bow between flanges) were measured before running tests. Results are given in the table below.

Specimen	A1	A2	A3	A4	A5	A6
Imperfection size [mm]	0,5 / 0,5 / 0,5 / 0,1 / 0,4	0,2 / 0,3	0,3	0,3	0,2	0,2

Table 4.9 Measured web imperfections

4.10.5. Reference to the Eurocode standard

Eurocode [13] gives clues for implementing the imperfections into the model in the finite element method analysis. They can be found in annex of NS-EN 1993-1-5. According to table C.1 they should be taken into account when buckling resistance is investigated. In the next table C.2 there could be found proposed equivalent geometric imperfections.

Table C.2: Equivalent geometric imperfections

Type of imperfection	Component	Shape	Magnitude
global	member with length ℓ	bow	see EN 1993-1-1, Table 5.1
global	longitudinal stiffener with length a	bow	min (a/400, b/400)
local	panel or subpanel with short span a or b	buckling shape	min (a/200, b/200)
local	stiffener or flange subject to twist	bow twist	1 / 50

Table 4.10 Proposed by Eurocode imperfections in FEM

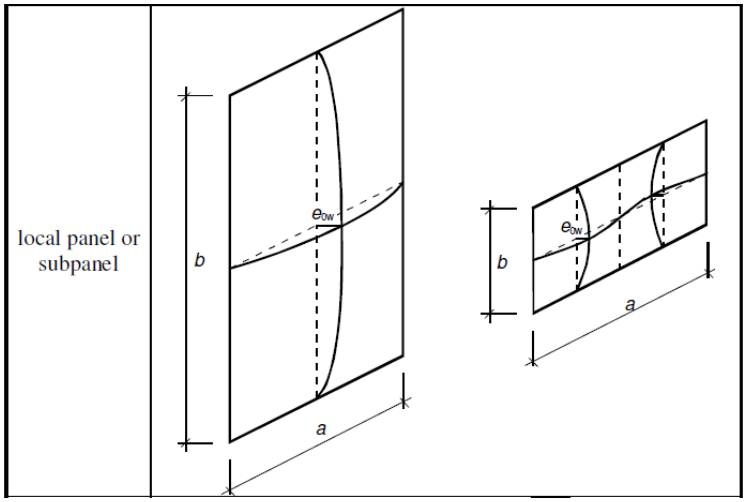

Here the most important component according to imperfections is web of the beam, which could be treated as panel with a height and b length. Eurocode recommend in this case buckling shape as a imperfection what agreed with obtained results. Only the suggested magnitude is different from 0,3 mm used. Eurocode gives higher value: 221,8 / 200 = 1,1 mm what is very conservative. Because this misalignemnt was measured 0,3 mm value was left.

4.11. Incrementation

In case of nonlinear analysis of buckling general static gradually increases the load (this time it is displacement) in steps. From this reason calculation time is much longer, because stiffness matrix must be updated in each step, because of changes in geometry .The number of this steps depends on defined incrementation. Smaller steps gives more accurate results but can forced much more time request. On the other hand, by using to big increments point of buckling could be missed, but a lot of time could be saved. To deal with this problem the following steps have been taken. Maximum value of

increment size was set as 0,04. That means that at least 25 times stiffness matrix should be updated what is satisfactory number. But nevertheless this increment size could be to big especially when buckling or plastic deformations will starts. From this reason ABAQUS selects the appropriate values from the interval from max to min increment size (Newton method has algorithm which can choose value of increment). To deal with buckling minimum value was very low and equaled $1 \cdot 10^{-8}$. Also in the beginning of analysis, to prevent very fast changes and "catch" up the proper buckling value increment size has been established as 0,001. The most common calculations were carried out in more than 40 steps and smallest increment size was, when buckling occurs but it never dropped below $1 \cdot 10^{-4}$. Nevertheless to gain final results maximum value of increment was reduced to 0,02.

4.12. Meshing

4.12.1. Mesh Type

In this type analysis shell elements were chosen as a "family" in ABAQUS. Linear geometric order of quad with reduced integration was assumed. That produces a S4R elements as a mesh element type. Point 4.4 gives more information about choosing this type.

Not less important was also to find the way of meshing, which will provide the most aligned finite element mesh. Because even if the element size and type will be good, bad shapes of these elements could provide inaccuracy of results. Many techniques have been used and the best results give structured technique for quad-dominated element shape. The results of meshing can be seen on the figure below.

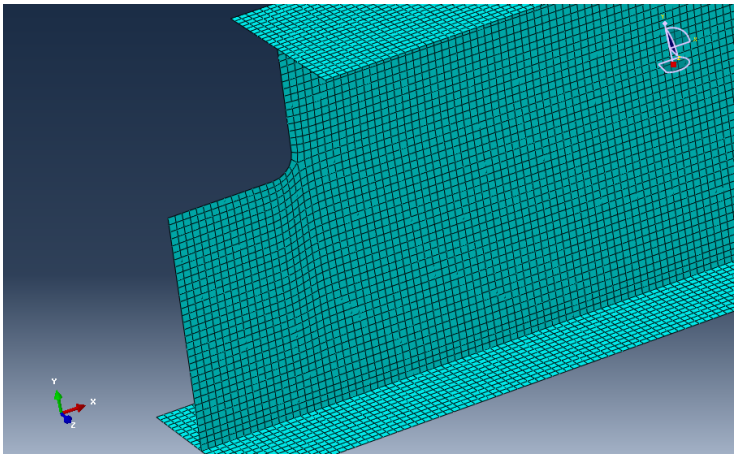

Figure 4.21 Structures meshing technique

4.12.2. Mesh Size

The element size is one of the most important factor influencing on the element models accuracy. Generally the results will improve along with the increasing density of the finite elements. Next advantage, which encourages the use of small elements is also the fact, that refined mesh also lowers the appearance of hourglass modes in the model. But while choosing the size of elements must be taken into account that the gain in accuracy comes with the cost of severely increased computational time.

For this work experience from previous studies was used. Also a lot of tests in ABAQUS were done to estimate the best size of mesh. In his work Bonkerud [12] investigated the effect of reduced element size on his model's accuracy. Finally, he concluded that a element size of 10 mm or less provided accurate results, hence for further studies he chose a mesh size of 7 mm. Urseth [5] in his thesis suggested the research of Bonkerud, and he also claimed that 7mm mesh size gives satisfactory results. But both of them were working on IPE 300 specimens, profile, which is slightly bigger than XHP 260. Gundersen [7], who also studied on aluminium profile, estimated that the size of elements should goes in line with Bonkerud, who concludes that an element 7x7 mm gives satisfactory results, both in terms of capacity and analysis time. Then since XHP 260 is a somewhat smaller cross section than the IPE 300 as Bonkerud used, the elements size was reduced from 7x7 mm to 6x6 mm in her thesis. This change gave approximately the same number of elements over the height of both beams.

It was decided to run own calculations, which helps to find the proper mesh size, which allows gaining results as soon as possible without losing accuracy. For this problem A2 specimen was used. Following mesh size was tested: 3mm, 4mm, 5mm, 6mm, 8mm, 10mm,12mm, 15mm and 20mm. The assumption was that the sample with 3mm mesh size gives the real results.

Analysis focused on the elastic buckling value, and also non-linear buckling problem was taken into account. As imperfection all samples got a buckle shape with 0.2mm amplitude. In the table below besides the force data there is also given a number of equation, which program had to solve in case of buckling analysis. For the static general analysis these equations had to be solved in each step, what means that lower incrementation results much longer time consumption. Time factor was estimated as a percentage value of number of equation in comparison with exact solution (for 3x3mm).

Mesh Size	Number of equation	Eigenvalue [kN]	Inaccuracy [%]	Time factor [%]
3x3mm	201570	**68,74**	0,0	**100**
4x4mm	113496	**68,85**	0,160	**56,3**
5x5mm	73134	**68,99**	0,364	**36,3**
6x6mm	50382	**69,22**	0,698	**25,0**
8x8mm	28164	**69,52**	1,135	**14,0**
10x10mm	18078	**70,06**	1,920	**9,0**
12x12mm	12636	**70,57**	2,262	**6,3**
15x15mm	8520	**71,14**	3,491	**4,2**
20x20mm	5020	**72,81**	5,921	**2,5**

Table 4.11 Influence of the mesh size on results (linear buckling)

It is clearly showed that the size of the mesh should not be very small. The largest investigated size of elements 20x20mm is almost seven times bigger than the lowest, but the differences in results given from these analyses is only 5,92%. Moreover it could be assumed that the inaccuracy is linear function of mesh size and during the same time factor increases, with making mesh denser, exponentially. It could be more clearly seen at the figures 4.22 and 4.23.

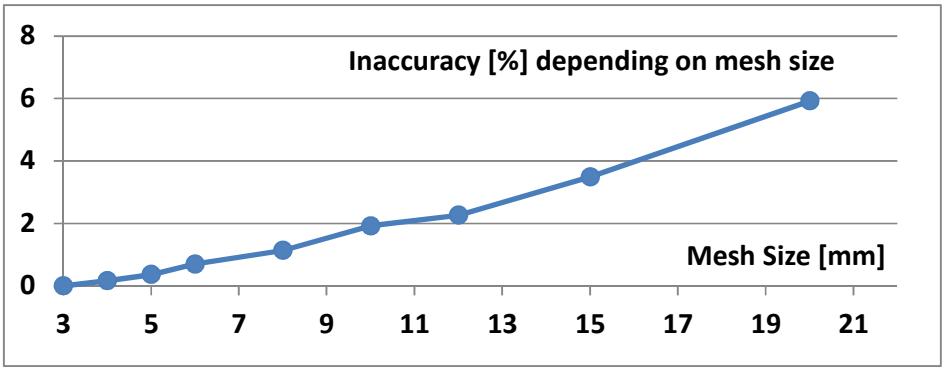

Figure 4.22 Mesh size – inaccuracy (linear buckling)

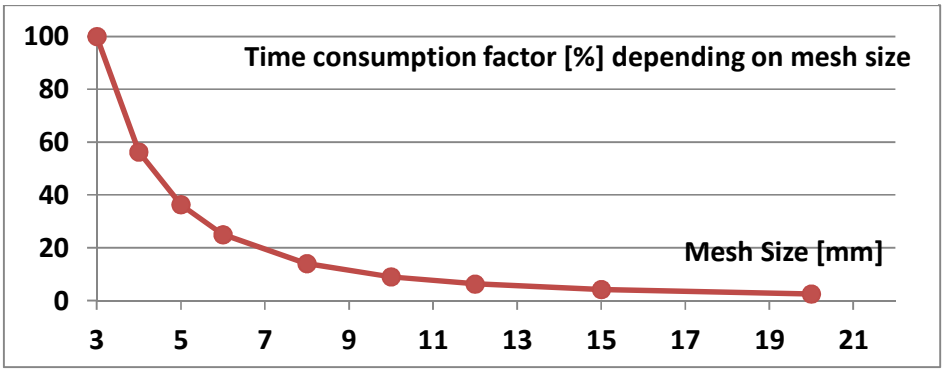

Figure 4.23 Mesh size – time of calculations (linear buckling)

From this charts it seems, that there is no sense to use smaller S4R elements (see 4.4.2), than 12x12mm. For this mesh size inaccuracy is slightly higher than 2% but from the other hand calculations can be done almost 16 times faster. It is a great advantage. Time consumption is relevant and its savings can be used for more researches. Even the buckle shape remains very close to exact, what can be seen on figure below.

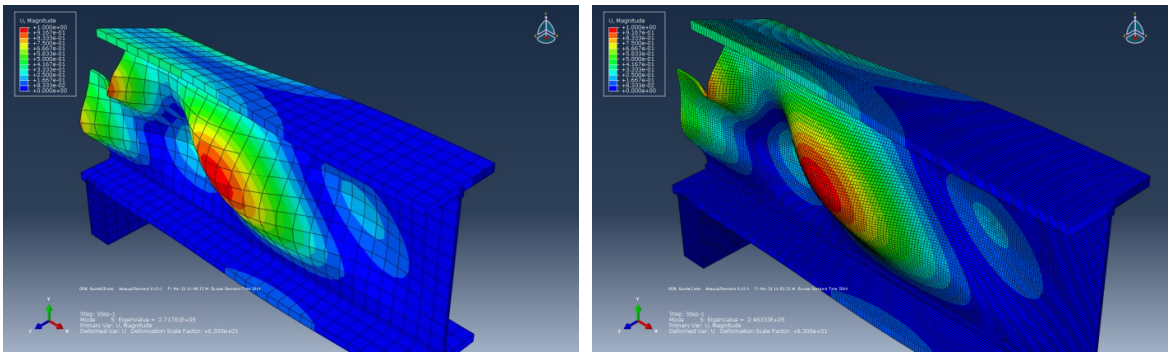

Figure 4.24 Comparison between buckle shape with 20x20 and 3x3 mesh size. S4R elements

But linear analysis in this case is not decisive and the same operations were done for nonlinear analysis to see what the influence of mesh size is in this case. Here, very quickly it was noticed the vast difference in the demand for time between beams with high and low dense mesh. The reason for this is the process of performing calculations. This time they are made in small time steps and the important factor are increments, whose number exceeds 40. This mean, that when the time difference between two sizes of mesh was 2 seconds in linear analysis, here it will be larger than 80 seconds in theory.

Because to perform calculations implicit method was used time costs are not easy to predict. Using the implicit method, experience shows that for many problems the computational cost is roughly proportional to the square of the number of degrees of freedom. If we consider the same example of a three-dimensional model with uniform, square elements refining the mesh by a factor of two in all three directions increases the number of degrees of freedom by approximately 2^3, causing the computational cost to increase by a factor of roughly $(2^3)^2$, or 64. The disk space and memory requirements increase in the same manner, although the actual increase is difficult to predict [2]. Below final results from nonlinear analysis are given.

Mesh Size	Number of equation	Max reaction force [kN]	Inaccuracy [%]	Time factor [%]
3x3mm	201570	**64,23**	0,0	**100**
4x4mm	113496	**64,30**	0,109	**56,3**
5x5mm	73134	**64,41**	0,280	**36,3**
6x6mm	50382	**64,53**	0,467	**25,0**
8x8mm	28164	**64,74**	0,794	**14,0**
10x10mm	18078	**64,95**	1,121	**9,0**
12x12mm	12636	**65,28**	1,635	**6,3**
15x15mm	8520	**65,64**	2,195	**4,2**
20x20mm	5020	**68,72**	6,700	**2,5**

Table 4.12 Influence of the mesh size on results (nonlinear buckling)

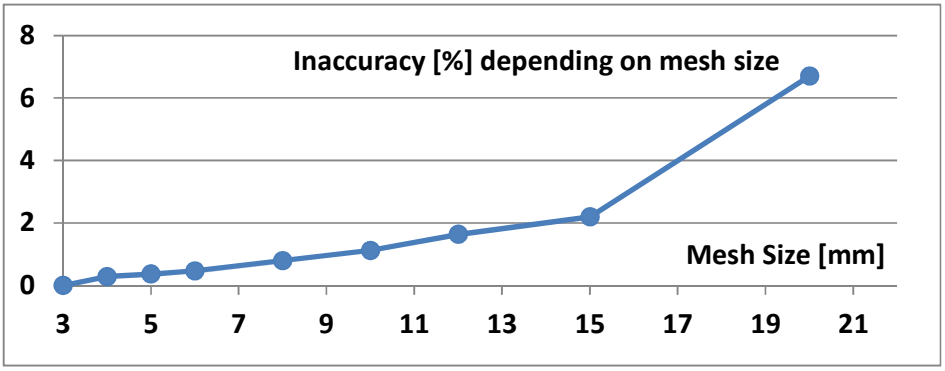

Figure 4.25 Mesh size – inaccuracy (nonlinear buckling)

All these results confirmed Bonkerud [12] theory that an element size of 10 mm or less provided accurate results. But it was decided with respect to others papers [5], [7] to use 5x5mm mesh. Another reason for this choice is fact that it allows to get very good results of meshing in rounded part of the beam (figure 4.21). Also in this way it was obtained satisfactory enough smooth curve, because the differences between then for different mesh size could be large, what can be seen on the figure below.

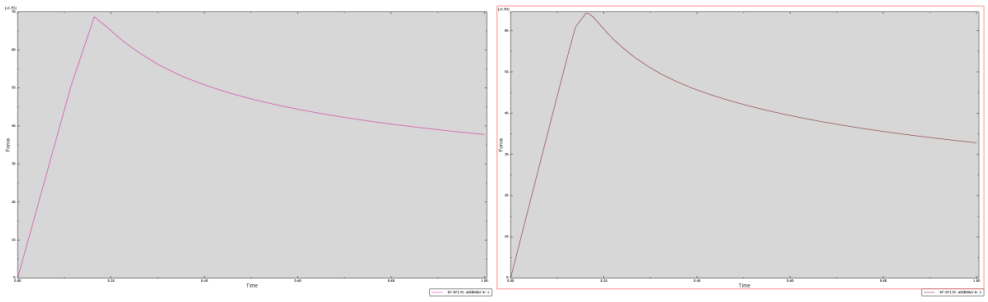

Figure 4.26 Force curve view, low (left) and high (right) density of mesh

4.13. Support / load properties

4.13.1. Supports

The original intention of this point was to reduce the size of the problem. Simulating whole beam with all additional stiffeners, supports could actually create more problems and longer time consumption than gives more accurate results or other profits. For these reasons, the focus was on the maximum simplification necessary geometry, which had to be modeled in ABAQUS. Always simpler models are easier to be controlled and to investigate influence of separate elements. As a result of this considerations following assumptions were done:

- 600 mm beam will be consider, buckle never extends after this area.
- All vulnerable/sensitive zones except at the cope were restrained against lateral displacement and rotation about the beam longitudinal axis. This is why it can be assumed that in place where vertical stiffener was added under the applied force fixed support can be placed.
- Instead the force imposed to the beam, reaction force from support at the coped bam will be considered as a load causing the buckling.
- Cope end was secured in the tests against lateral movement at the bottom flange, what will be modeled by adding support blocking displacement in perpendicular to the web surface direction.

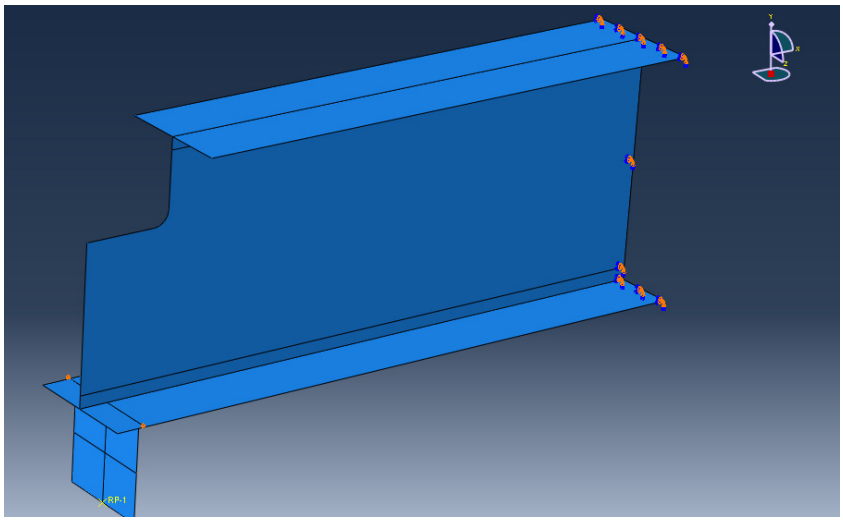

Figure 4.27 Supports: encastre at the one end and lateral supports near the cope

4.13.2. Load

3 different methods inputting the load to the model were examined:

- By a single concentrated load (displacement) in y direction.
- By simulating the 40 mm wide plate.
- By shell element.

It turned out that first method will not provide the accurate results. High concentrated stresses interfere results and moreover sometimes make impossible to obtain them. Even after distributing load on the whole flange, results wasn't satisfactory.

To model the plate which is infinitive stiff, "constraints" formula was used. Generally this technique is to select the type of connection between master and node slaves. As a master node reference point was created in the middle of the flange. Then every nodes at distant from the line presented position of the inputted force of 20 mm were selected as a slave nodes. As a method linked this two node types Equation type was used and data are presented below. As a result of this equation all nodes will have the same displacement in y direction (second degree of freedom).

Click mouse button 3 for table options.

	Coefficient	Set Name	DOF	CSYS ID
1	1	slave	2	(global)
2	-1	RF	2	(global)

Table 4.13 Constrain equation inputted to the model

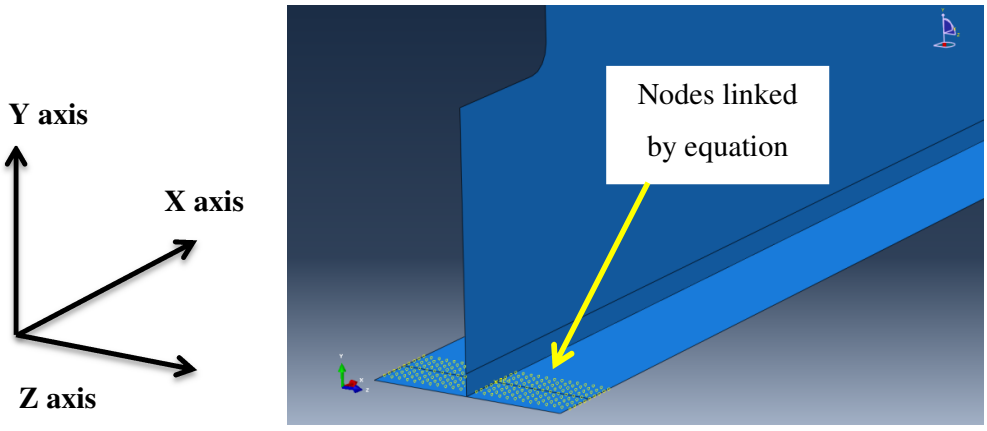

Figure 4.28 Slave nodes simulating plate and main axis location

The results given from this analysis were not conservative. Force causing buckling was 86,00 kN, what means almost 25% higher capacity than it valid results. Moreover shape of deformation was little different from this one, obtained in the tests. The reason of this behavior was very stiff type of support. The beam starts to act almost like it was fixed. Equals displacement of nodes blocked a possibility of rotation at the end of the beam. During tests this option existed. It was decided thus to abandon this type of imposing the load.

Finally model with shell element was investigated. It provides very accurate results and didn't cause any problems with calculations. To avoid problem with high concentration of stresses at the bottom of the shell load was distributed on the whole surface also by "constraints" formula.

Chapter 5:

Numerical analysis – beams ends with cope

5.1. Geometry in ABAQUS

5.1.1. Shell

Before obtaining the final geometry of beam, single planar parts had to merged. To make sure that all parts have been given the correct thickness ABAQUS was asked to render the shell thickness. On the figure 5.1 below there is a created geometry for A6 specimen.

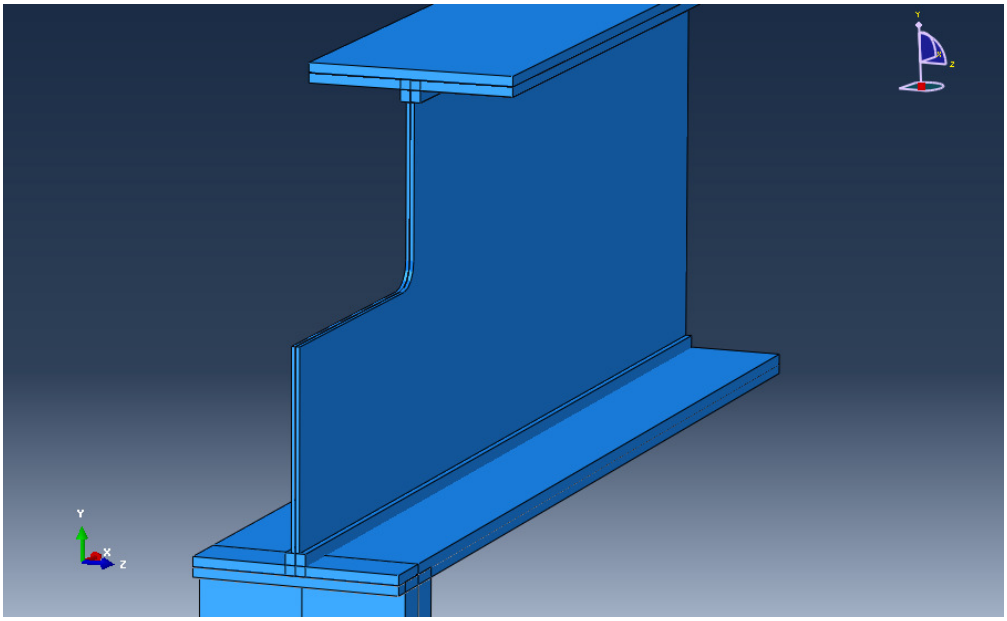

Figure 5.1 View on geometry created in Abaqus – A6 sample

It could be easily seen that because of using shell elements there always will be some doubling the material near the areas, where different planar parts meets.

Each planar part was done according to Table 4.3. In this case only the web has more complicated geometry. During the creating this part of the beam every dimensions were checked. Figure 5.2 shows dimensioned web part of A3 specimen.

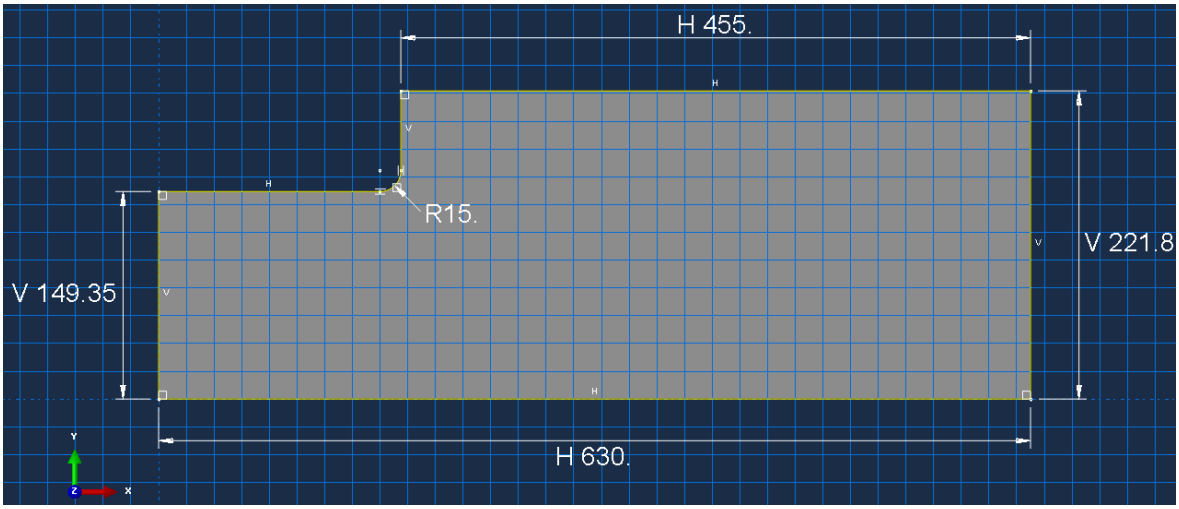

Figure 5.2 Sample dimensions of the web (A3 specimen)

5.1.2. Solid

Complete beam consists of 3 parts. Cutted part, where cope was made has the length 88mm in case of A2 specimen. The longer part with full cross-section is 542mm long. Last and the smallest part was created to simulate the rounded part of the beam in the corner of the cope. Dimensions of described elements can be seen on figure below.

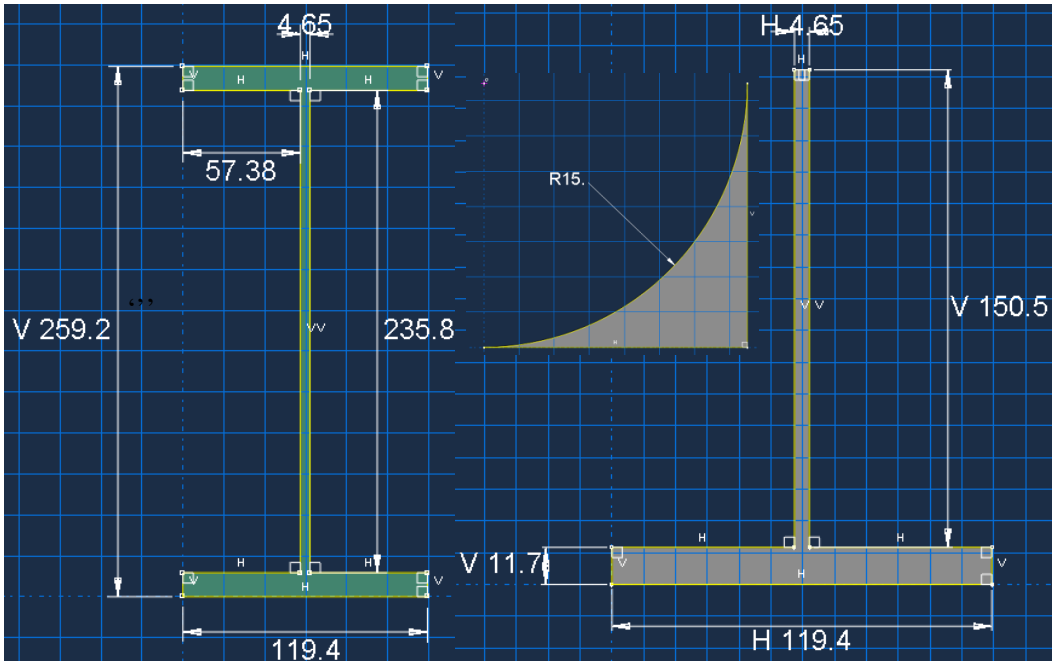

Figure 5.3 Dimensions of parts inputted into ABAQUS (A2 solid specimen)

The beam, which was composed of these parts has the exact shape as in reality. What is more, this time as opposed to shell elements there is no assumptions and mass doubling.

5.2. Buckling shapes

Beam's deformations illustrated below belongs to A2 specimens. Figures from 5.4 to 5.8 are showing first five buckle shapes of the investigated beam.

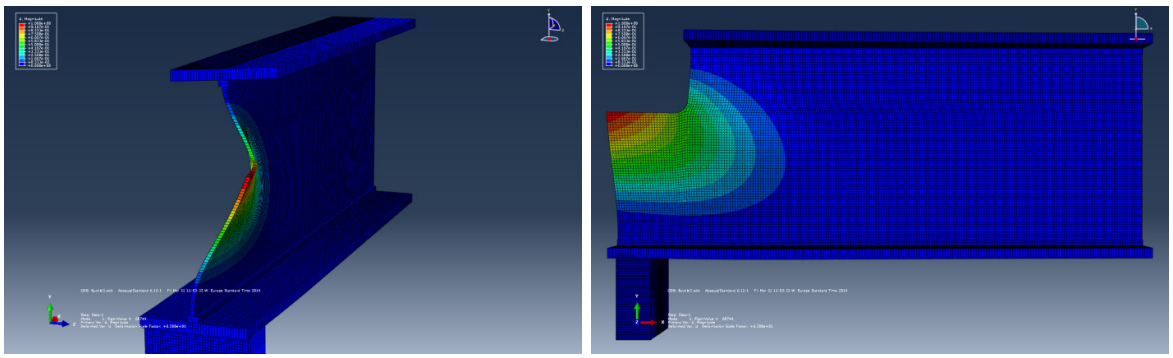

Figure 5.4 First buckling shape of A2 specimen

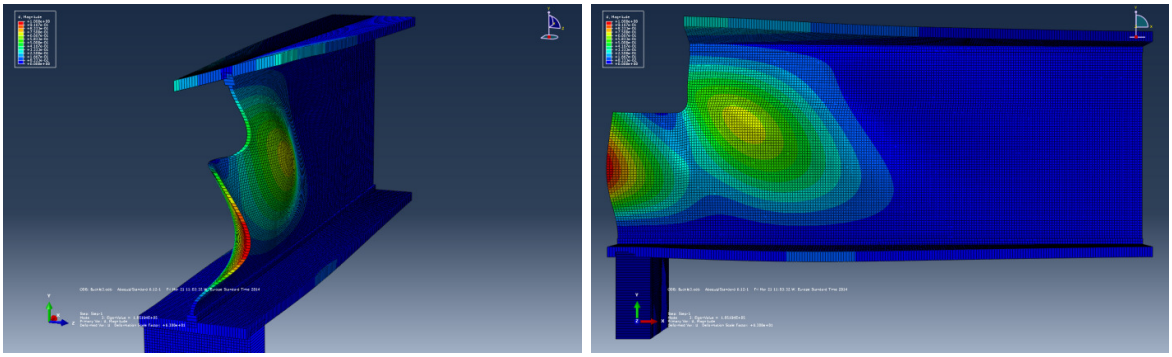

Figure 5.5 Third buckling shape of A2 specimen

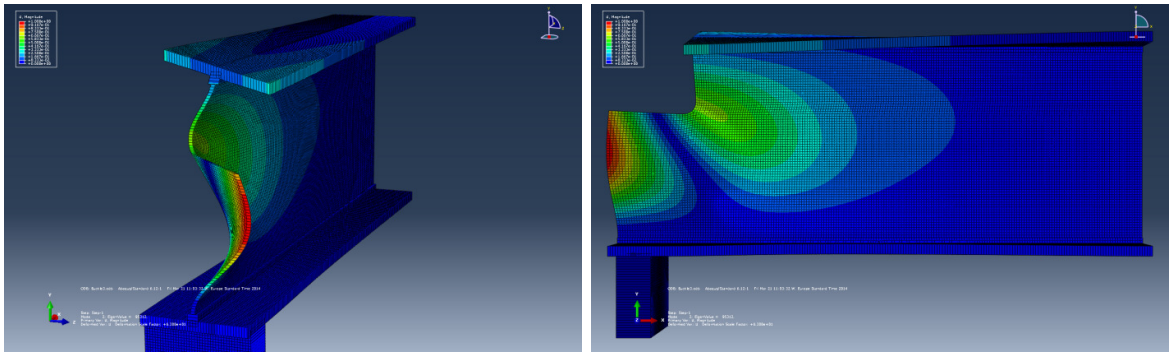

Figure 5.6 Second buckling shape of A2 specimen

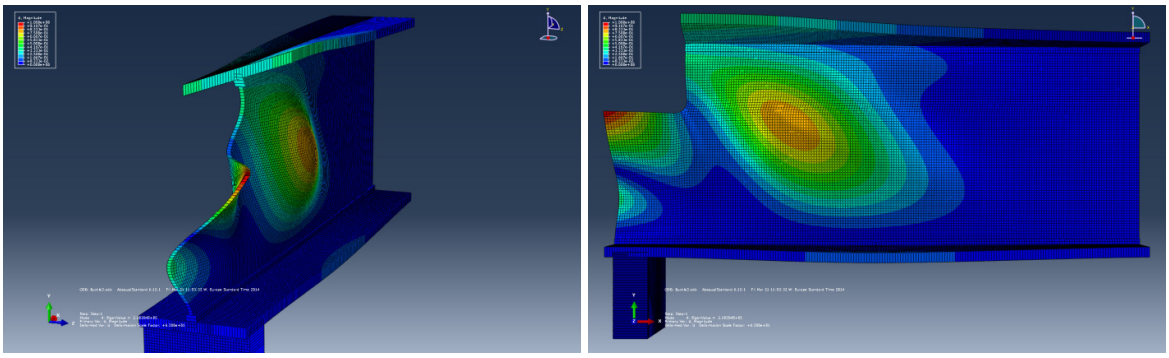

Figure 5.7 Fourth buckling shape of A2 specimen

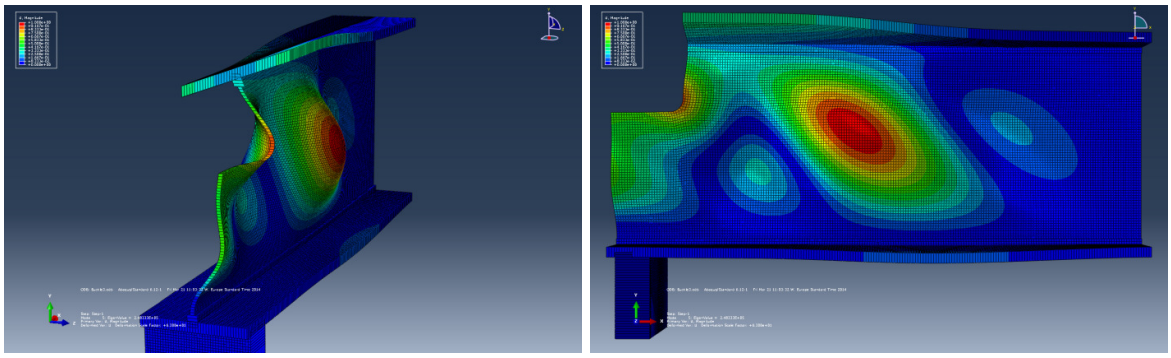

Figure 5.8 Fifth buckling shape of A2 specimen

5.3. Solid and shell comparison

For the meshing solid elements procedures described in 4.13.2 and 4.4.2 were used. Final results can be seen on the figure 5.9. Worth emphasizing is the fact that calculations in this case lasted about twenty times longer if we consider the same incrementation and same mesh size (5x5mm). It was huge disadvantage, because it has been considered very difficult to check more possibilities and large amount of specimens on solid model.

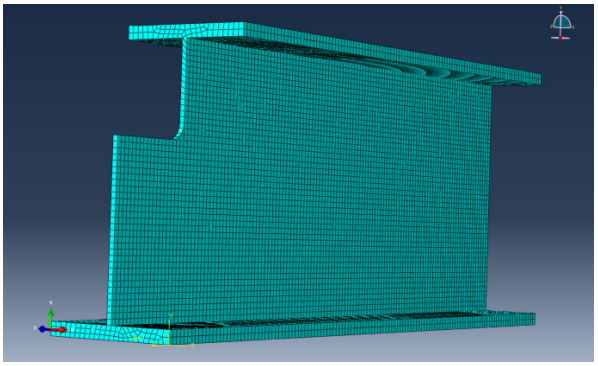

Figure 5.9 Meshing with solid elements

Unfortunately calculations from undefined reason turned out totally wrong. It was decided then to use more advanced elements for meshing. C3D20R: a 20-node quadratic brick with reduced integration handled with the task much better and approve the model version designed with shell elements (point 5.5). Unfortunately they sharply increased the number of equations, which had to solved and time consumption. Even after reducing mesh size to 10 mm it took a lot of time to get results. Results are presented below.

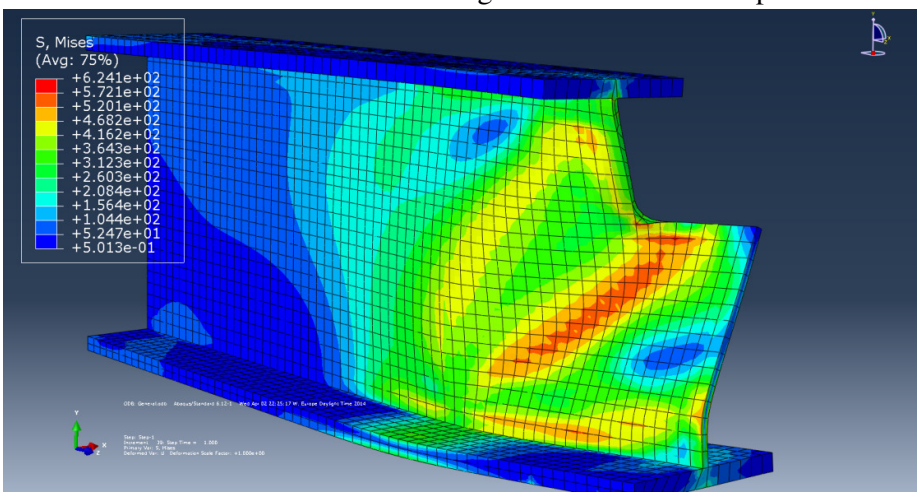

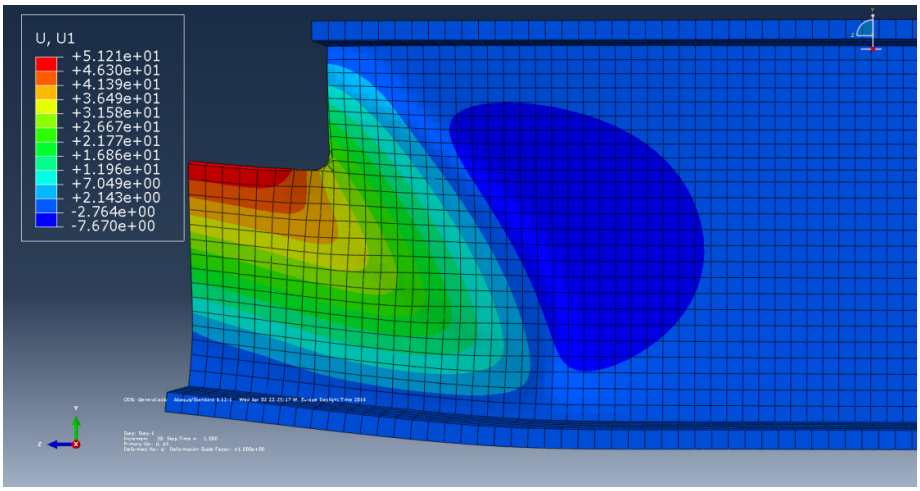

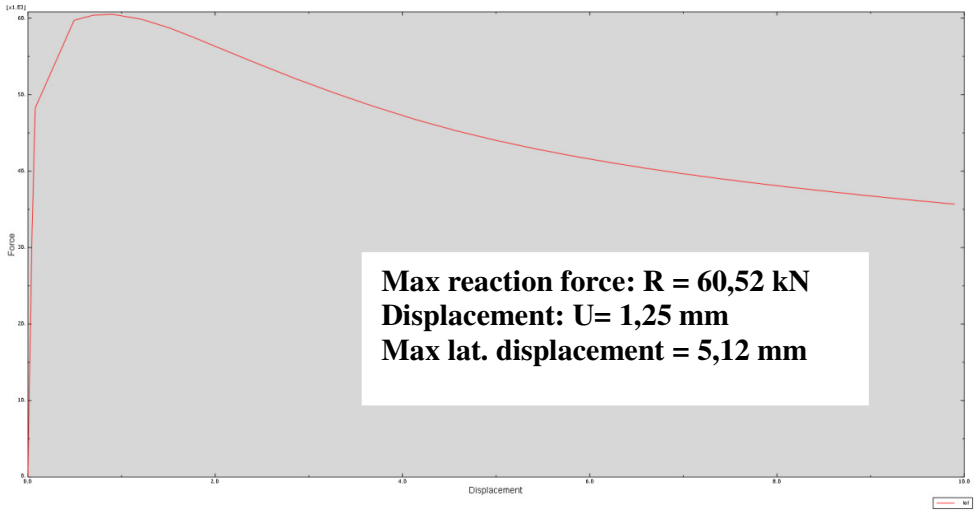

Max reaction force: R = 60,52 kN
Displacement: U= 1,25 mm
Max lat. displacement = 5,12 mm

5.4.Short summary of the results

In the table 5.1 below results from numerical calculations are given and table 5.2 shows the difference between ultimate force gained in laboratory tests and ultimate forced received nonlinear analysis in ABAQUS. From the first one it can be stated that linear buckling analysis provides good results for this problem but after more in-depth analysis of results it is obvious that it is not true. Buckle shape is totally different from this one obtained in reality. Thus, a large convergence of these results should be considered as accidental. But in case of nonlinear buckling these shapes are consistent with the results from the tests. Moreover ultimate reaction forces in each specimen are almost the same. Inaccuracy in results ranged from 0,2% for A5 to 3,56% for A2 specimen.

Analysis type	Ultimate force A1 [kN]	Ultimate force A2 [kN]	Ultimate force A3 [kN]	Ultimate force A4 [kN]	Ultimate force A5 [kN]	Ultimate force A6 [kN]
Lab test	75,37	66,2	43,8	31,0	50,9	35,6
Linear buckling	96,40	68,99	43,71	29,27	47,86	37,64
Nonlinear buckling	75,10	63,82	43,45	30,55	50,8	34,69

Table 5.1 Results obtained from numerical analyses.

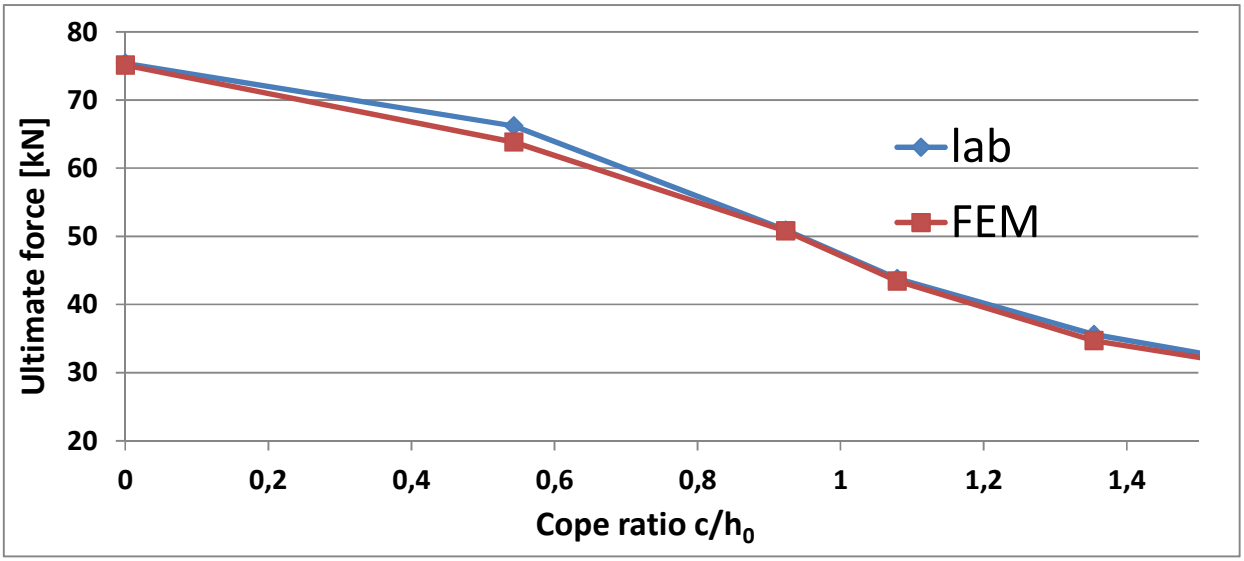

Figure 5.10 Comparison results from FEM and laboratory tests

From the figure 5.10 it can be clearly seen how results are similar. Chart given above is the best endorsement confirms the correctness of the model.

	A1	A2	A3	A4	A5	A6
Cope ratio c/h_0	0,0	0,543	1,079	1,603	0,925	1,354
Inaccuracy [%]	0,36	3,56	0,80	1,45	0,20	2,56

Table 5.2 Inaccuracy of models compared to test results.

5.5. Force-displacement curves, lateral displacement and Mises stresses

To present the results it was decided to show distribution of the mises stresses, deformation in vertical direction to the web surface and reaction force – displacement curve for each specimen. Shapes can be compared with laboratory specimens in 5.5.7.

5.5.1. A1 specimen

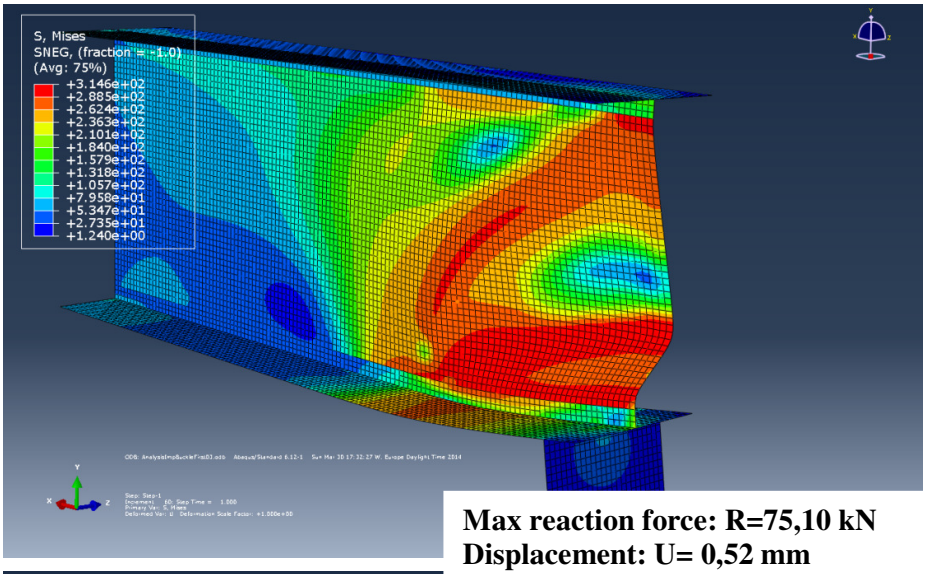

Max reaction force: R=75,10 kN
Displacement: U= 0,52 mm
Max lat. displacement = 3,99 mm

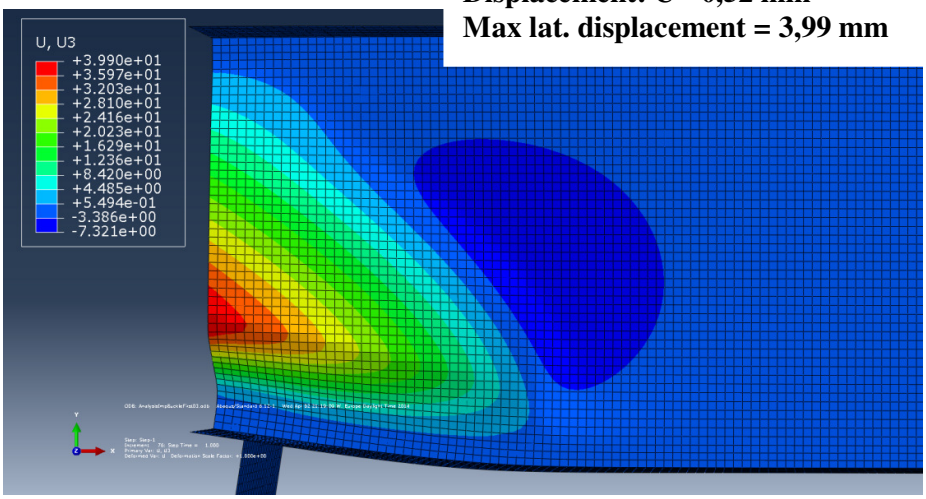

5.5.2. A2 specimen

<

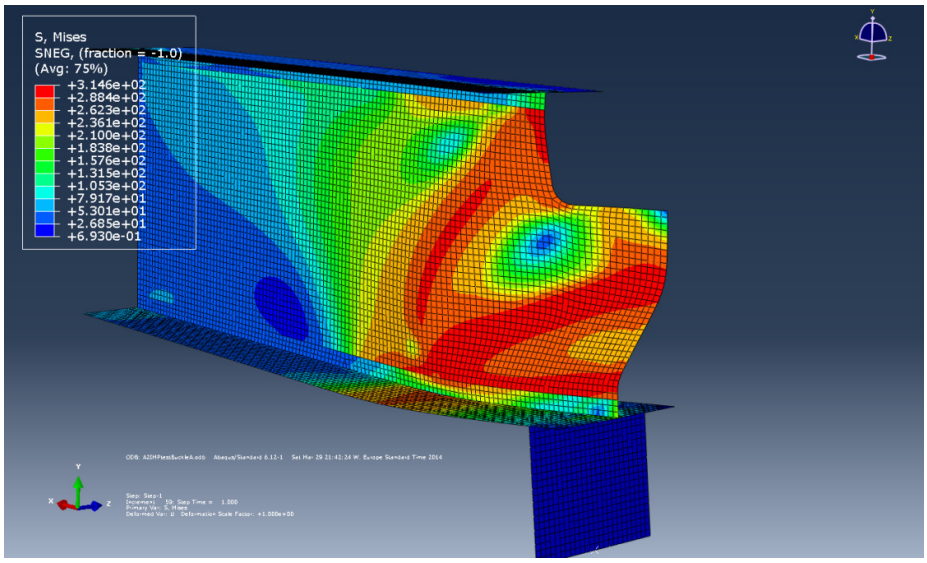

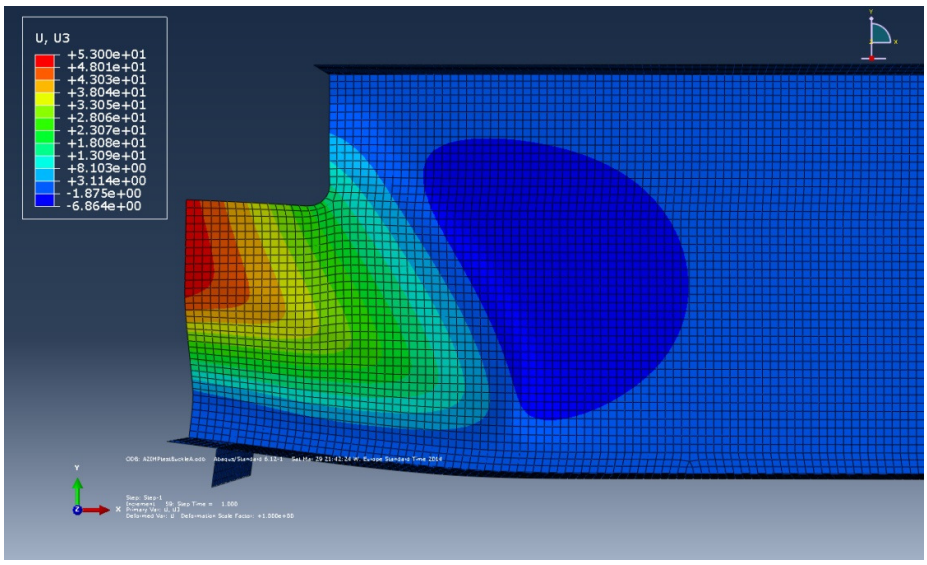

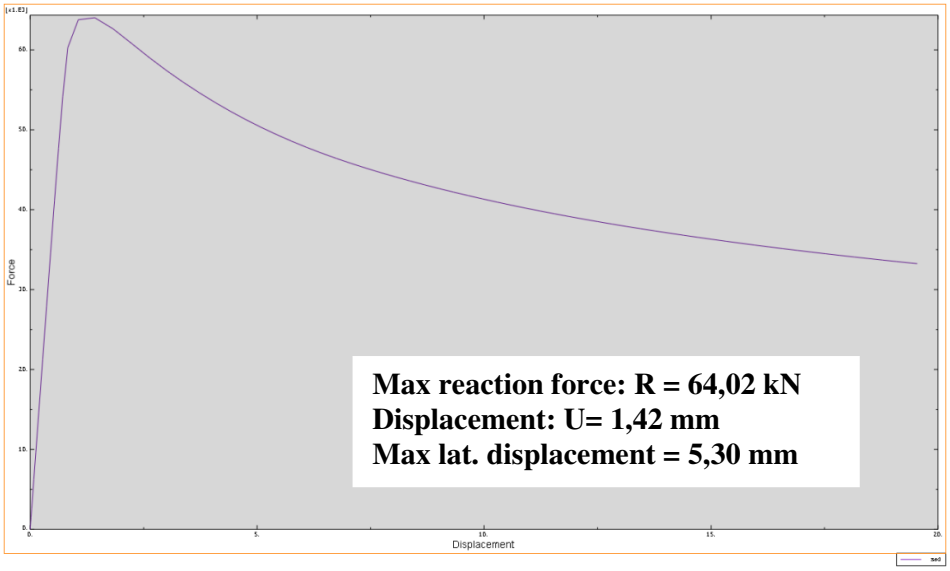

5.5.3. A3 specimen

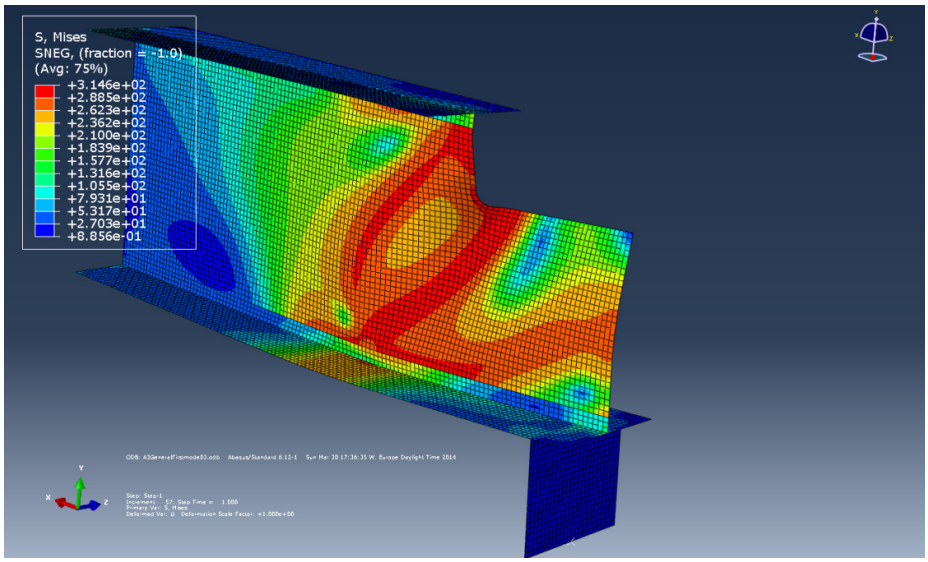

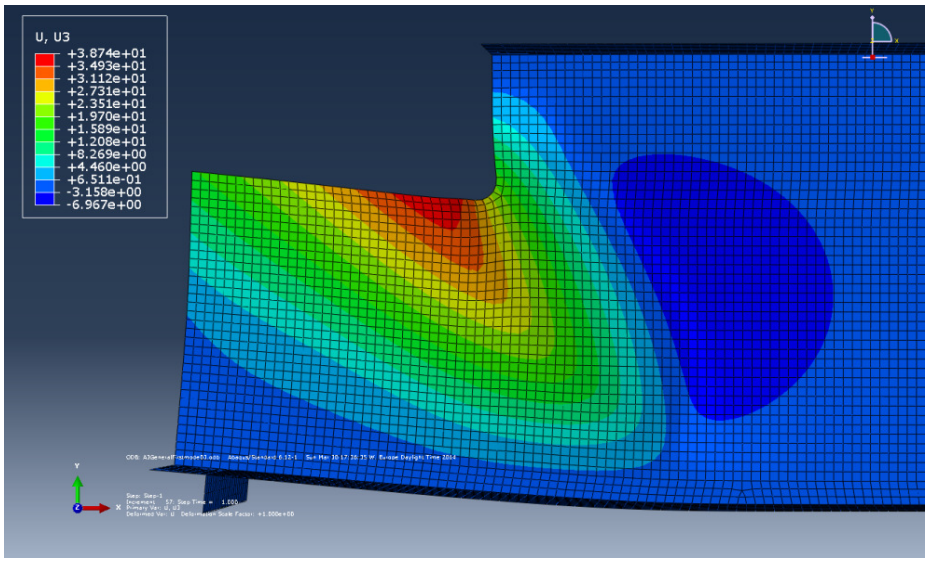

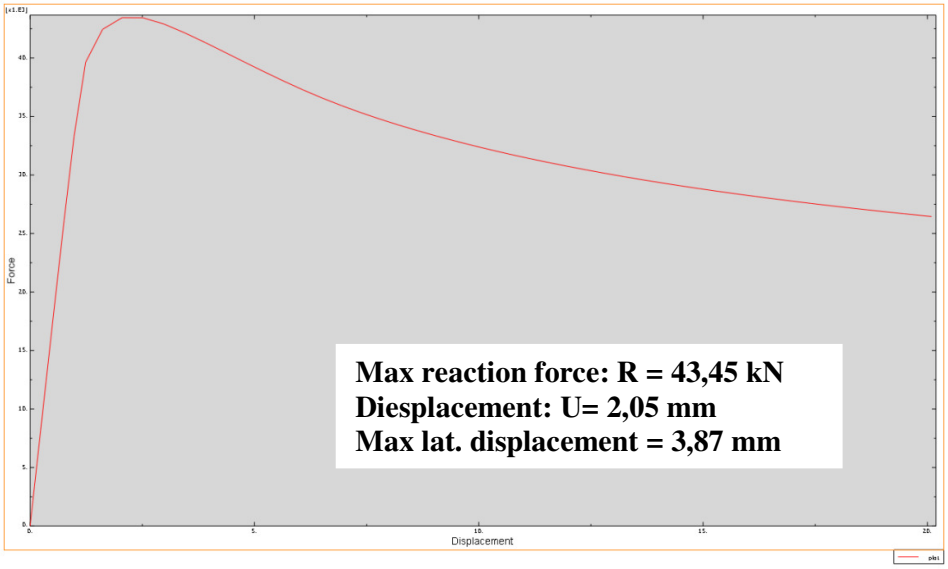

5.5.4. A4 specimen

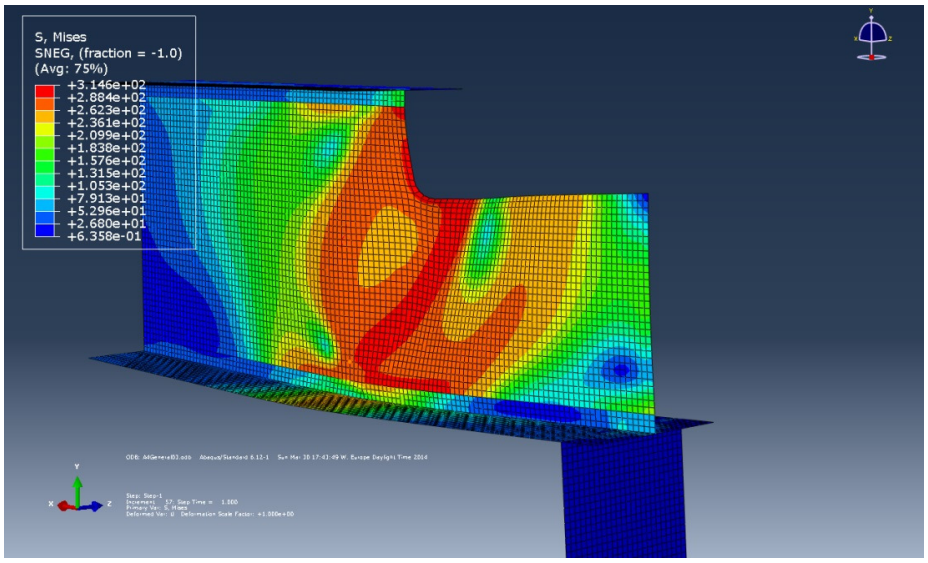

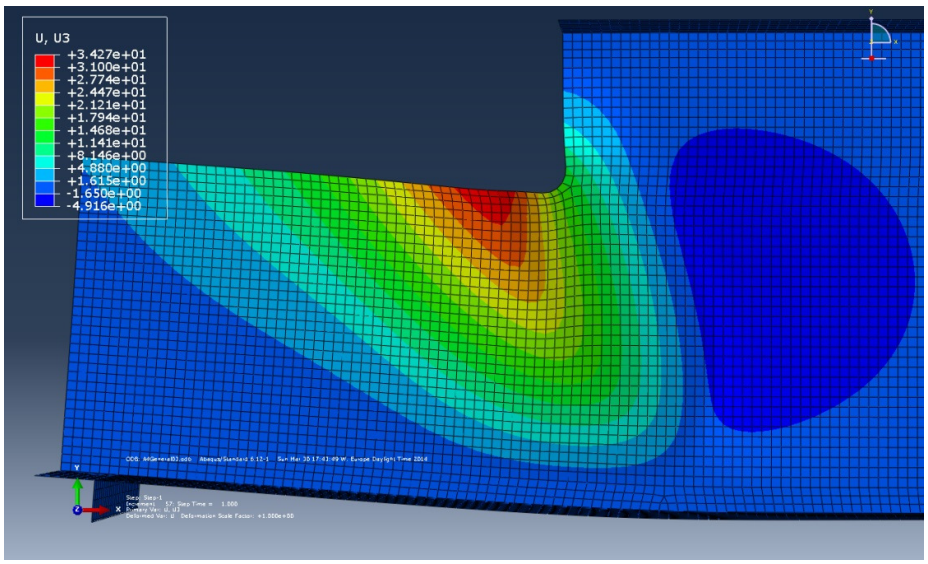

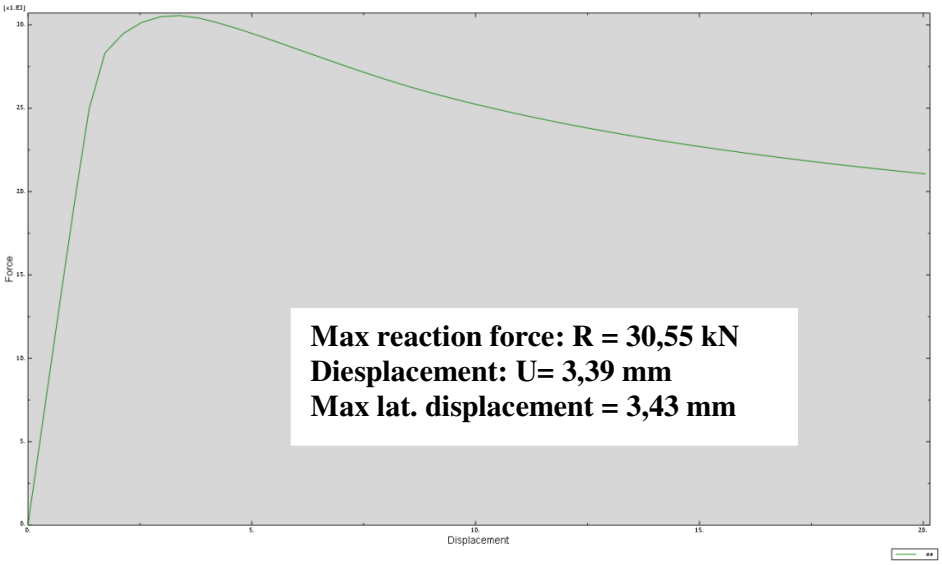

5.5.5. A5 specimen

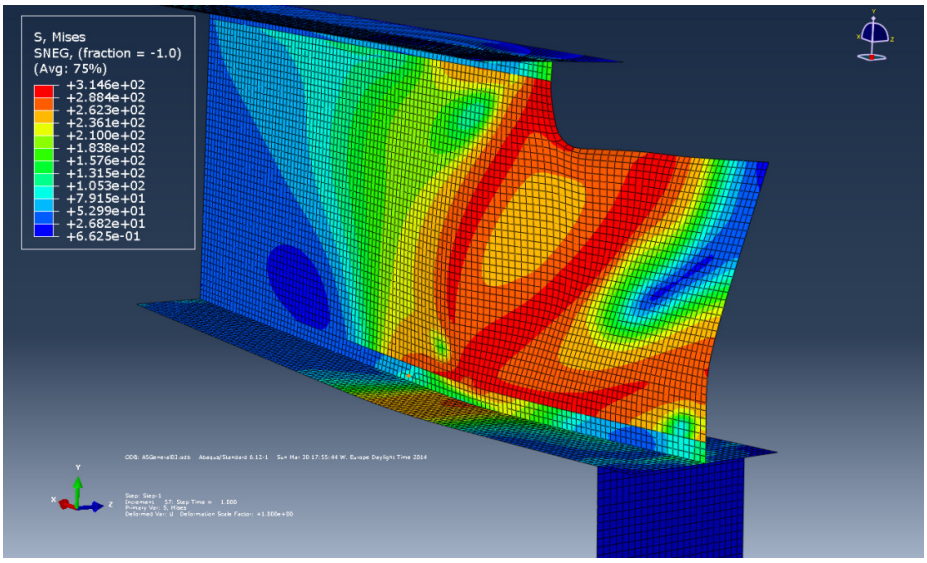

<

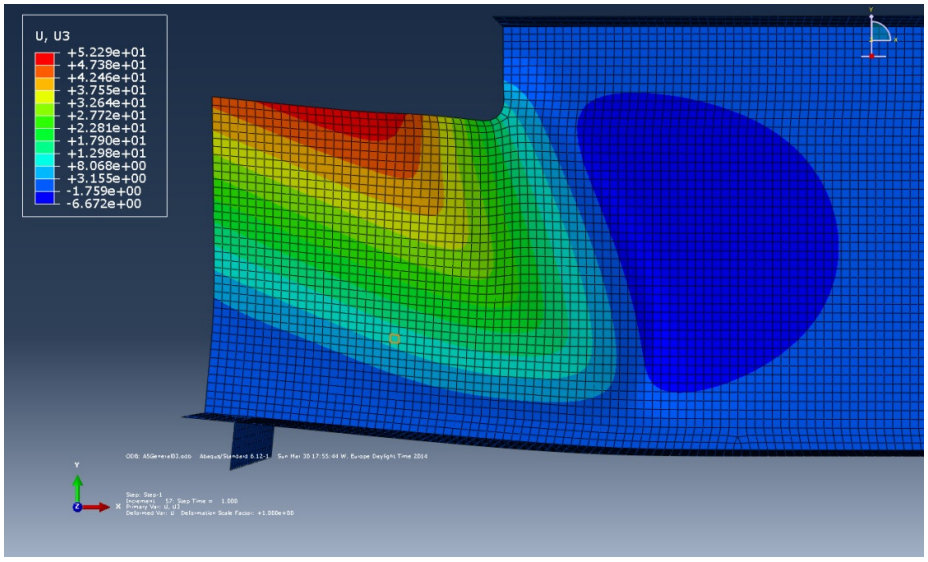

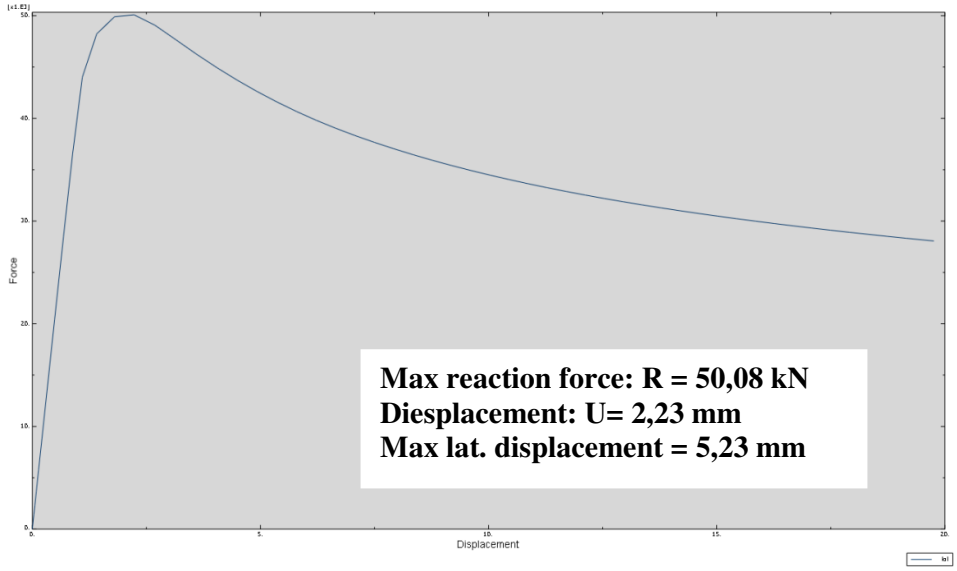

5.5.6. A6 specimen

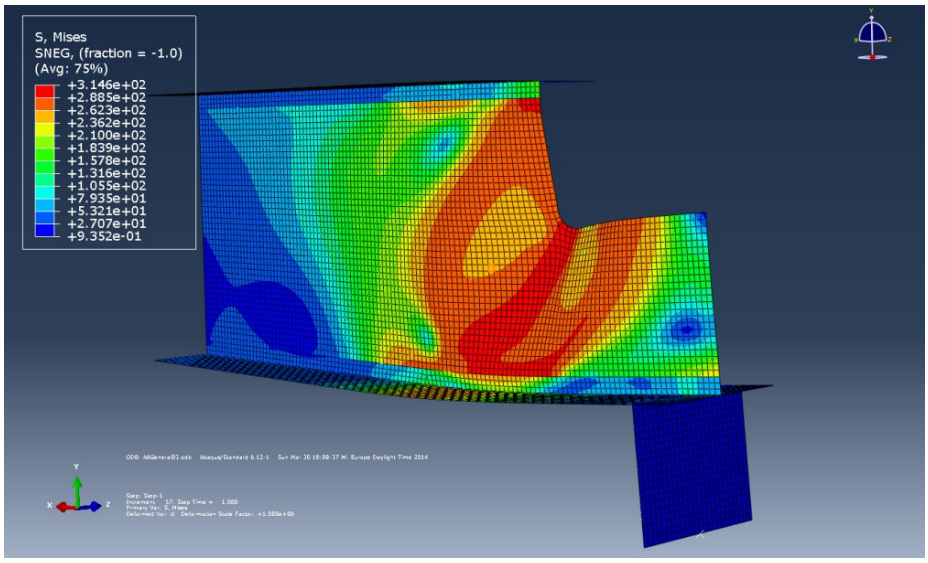

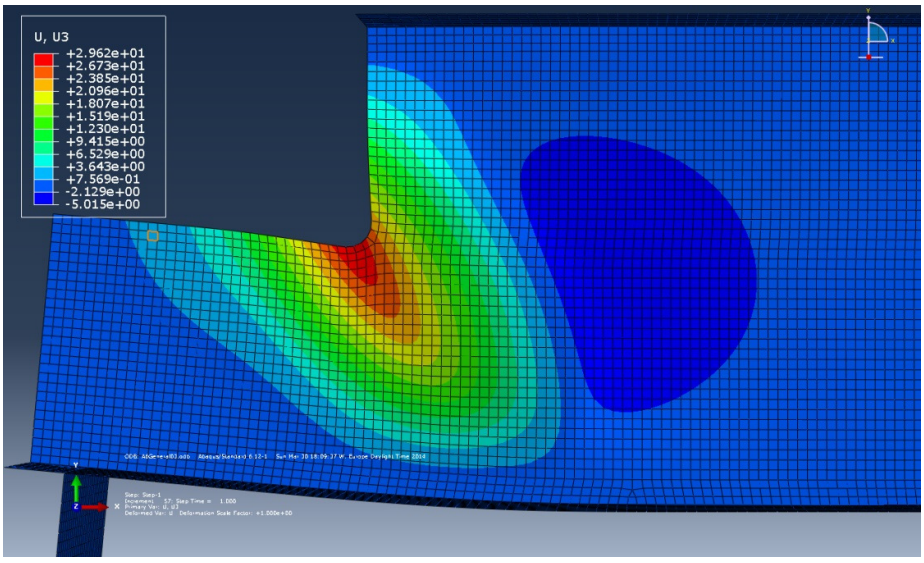

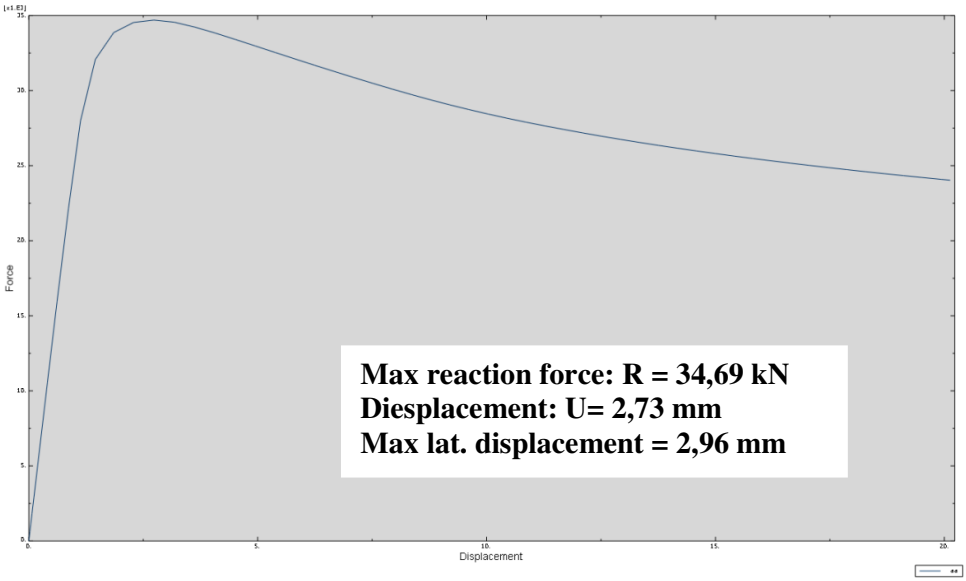

5.5.7. Validation of the buckle shapes

Pictures on the figure below have been showed to be comparable the shapes of buckling obtained from the laboratory tests and from nonlinear analysis in ABAQUS presented in point 5.5 of this work. After comparison it can be concluded that buckle shapes from both different sources (FEM analyses and laboratory tests) are very similar what only approves more the accuracy of the model. Position, when buckle occurs and also extend of buckle fully agreed. This also confirm right selection of imperfection.

(a) Uncoped specimen A1, end view.

(b) Coped specimen A2 (88mm·97mm)

(c) Coped specimen A3 (175mm·97mm)

(d) Coped specimen A4 (260mm·97mm)

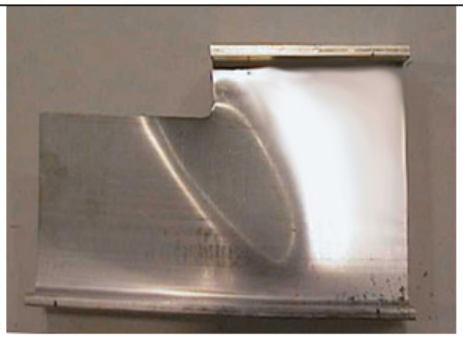

(e) Coped specimen A5 (175mm·70mm)

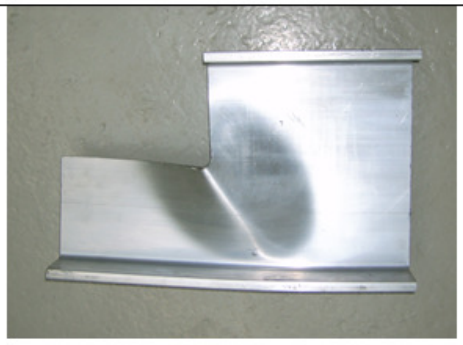

(f) Coped specimen A6 (175mm·130mm)

Figure 5.11 Specimens after tests – buckling shapes.

5.5.8. Validation of the response curves

On the chart below all obtained response curves for each specimen are presented. It can be deducted that not only the values of ultimate forces gives very accurate results, but also force – displacement curves reflect well the character of the process of phenomenon of buckling in time. This fact only increases confidence in the presented model. Results from laboratory tests were given on the figure 3.4 and obtained results can be seen on figure 5.12 (comparison can be found in attachment C).

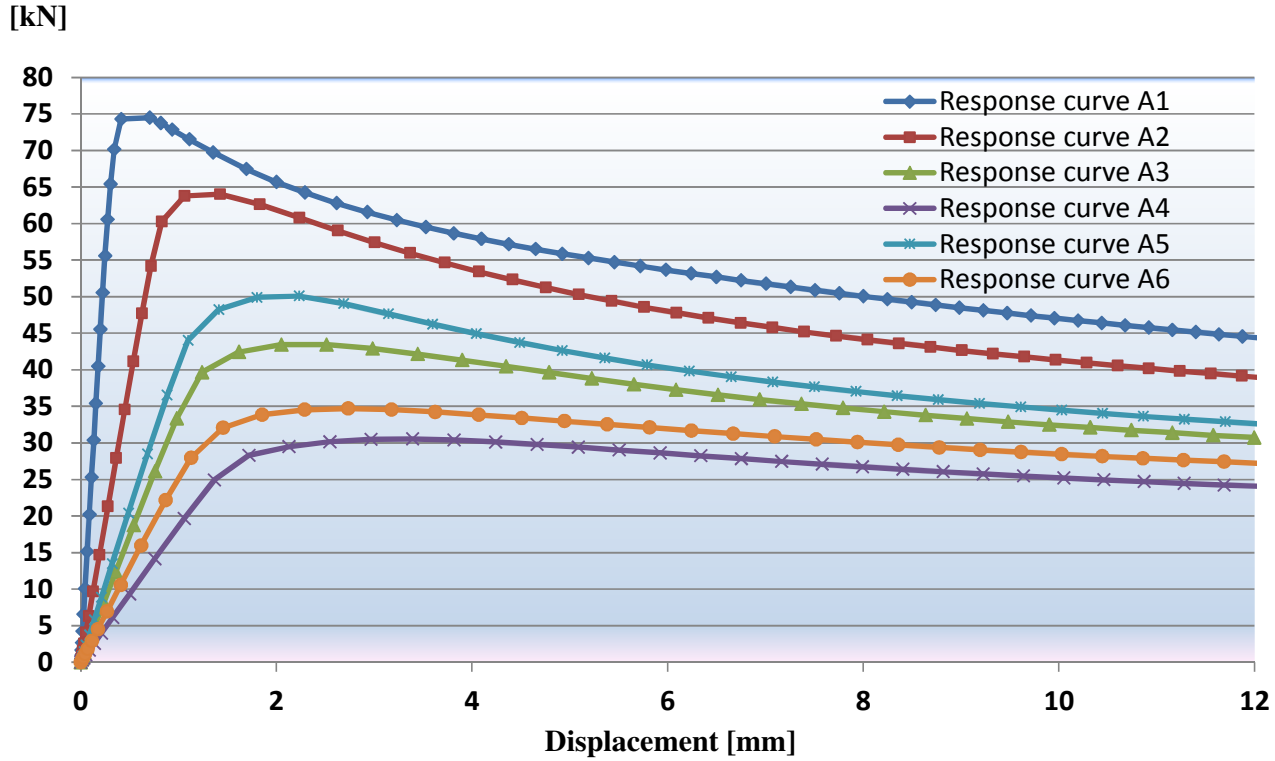

Figure 5.12 Force – displacement curves from nonlinear analysis.

5.6. Summary

The behavior of the coped beams and the ultimate reaction force caused by buckling were investigated both in numerical analyses and laboratory test. Geometry of the problem was simplified to obtain the model dependent on the minimum number of factors. In series of attempts way of support and inputting loading was selected. From another tests material properties were established and introduced to the program. It was stated that S4R shell elements allow to obtain very accurate results and more advanced model with solid element also approved this.

In the next step incrementation and type of analysis were selected. General Static method with maximum increment size 0,02 allows to reflect the behavior of buckling well. Then next tests were run to find the best way of determining imperfections. To this task first buckle shape was used with an amplitude 0,3 mm. Finally mesh size was chosen to provide both very accurate results and the possible lowest time consumption, necessary for calculations. Factors determining the correctness of the model were ultimate reaction force, buckle shape and view on force-displacement curve.

The numerical simulation of the test beam agreed well with the individual test results. The force-displacement curve had approximately the same shape as the curve to the experimental data. Since the results are very close to exact, which were obtained from the tests in the laboratory it can be deducted that prepared model is valid. The model was considered well enough calibrated relative to the experiment and could be used further in the simulation of reinforcing coped beams by stiffeners. The results from analyses underestimate capacity of the cross-section from 0,2% to 3,56% with 1,49% as a middle value. It can be stated then that results are not only accurate but also gives conservative results.

Chapter 6:
Numerical analysis – reinforced coped beams, stiffeners effect

6.1. Assumptions

This investigation can't be compared with any tests, because they were not conducted on NTNU. This is why it was so important to get results in chapter 5 as close as possible to laboratory tests. Thanks this, it can be stated that prepared model is valid and investigation can be extended without need of comparison. But due to lack of researches there was no possibilities to measure many factors influencing on results like the quality of welding, size of the HAZ zone and information about equipment and technique of welding. This data can be found in Eurocode 1999-1-1 but firstly it was necessary to choose some options. Following assumptions were done:

- In the design of aluminium welded structures, the reduction in strength properties that occurs in the vicinity of welds shall be considered
- For design purposes it is assumed that throughout the heat affected zone (HAZ) the strength properties will be reduced on a constant level. The affected region extends immediately around the weld, beyond which strength properties rapidly recover to their full unwelded value.
- It is possible to mitigate the effects of HAZ by artificial ageing applied after welding, but for this work this actions won't be considered.
- Weakening of material can be taken into account by the value of strength $f_{0,haz}$ and $f_{u,haz}$ in the HAZ zones or by reducing the assumed cross-sectional area by factors $\rho_{0,haz}$ and $\rho_{u,haz}$. In this work the first method was used, because it presents the reality better.
- It was assumed that all specimens will be welded same technique, in this case MIG weld laid on unheated material method. It is very important factor in in estimation of extent of the HAZ zone.

6.2.The idea of taking into account the HAZ effect in model

To input HAZ effect to the program, in the model there will be created a separate area of the HAZ zones, close to the stiffeners. These areas will get different material properties, where will be taken into account weakening of the aluminium caused by welding. HAZ zones will be taken from Eurocode 9, point 6.1.6.3 (3) from where can be deducted that b_{haz} (figure 2.1):

b_{haz} = 20 mm for the web of the beam,

b_{haz} = 30 mm for the flange and web near the flange,

b_{haz} for the stiffeners will be equal to the width of the plate.

6.2.1. New material properties

In laboratory test following aluminium alloy was used: EN AW-6082 with chemical symbol EN AW-Al Si1MgMn. Because of the welding to the beam stiffeners around them HAZ zone will be created both on the welded plate and part of the beam. In this zones material will be weakened compared to the other part of the beam. It is difficult to say in advance how much lower the strength of the material will be, because it varies along the distance and highly depend on the welding quality. Simulating this problem properly is not simple without hardness data and simulations of welding or tests, where change in the microstructure of the material can be seen. But as it was mentioned in 2.1.4 it was decided to look on simplified methods, which are presented in Eurocode [1]. It gives conservative approach in the context of capacity, because it provides a weakening of the material equal to the reduction in the weakest point within the heat-affected zone with no change in relation to the distance from the melting zone. The characteristic value of the 0,2% proof strengths $f_{0,haz}$ and the ultimate strength $f_{u,haz}$ should be found.

Eurocode 9 gives the following values for "EN-AW 6082-T6 extruded profiles" for $t \leq 5$ from Table 3.2b, which will be used for beam profile. Because XHP260 profile has 4,65 mm thick web whole section will belong to the group $t \leq 5$mm.

- f_0 = 250 MPa
- f_u = 290 MPa
- $p_{0,haz}$ = 0,50
- $p_{u,haz}$ = 0,64

Eurocode 9 gives the following values for "EN-AW 6082-T6 Sheet, strip and plate" for $t \leq 6$ from Table 3.2a, which will be used for a 5mm thick stiffener.

- f_0 = 260 MPa
- f_u = 305 MPa
- $p_{0,haz}$ = 0,48
- $p_{u,haz}$ = 0,60

Eurocode 9 gives the following values for "EN-AW 6082-T6 extruded profiles" for $6 \leq t \leq 12{,}5$ from Table 3.2a, which will be used for 10mm thick stiffener.

- f_0 = 255 MPa
- f_u = 300 MPa
- $p_{0,haz}$ = 0,49
- $p_{u,haz}$ = 0,62

Because of the tests in the laboratory obtained the exact values of strengths f_0 and f_u there was no sense to use this one presented by Eurocode. Moreover parts of the beams react on the welding only slightly different with $p_{0,haz}$ in range of 0,48 to 0,50 and $p_{0,haz}$ in range of 0,60 to 0,64. Thus, to simplify the model a little bit it was decided to use the middle values which will reduce these strengths. Then new values were calculated from formulas given below and inputted to the program as a curve, which is presented on the figure 6.1.

$$f_{0,haz} = p_{0,haz} \cdot f_0$$

$$f_{u,haz} = p_{u,haz} \cdot f_u$$

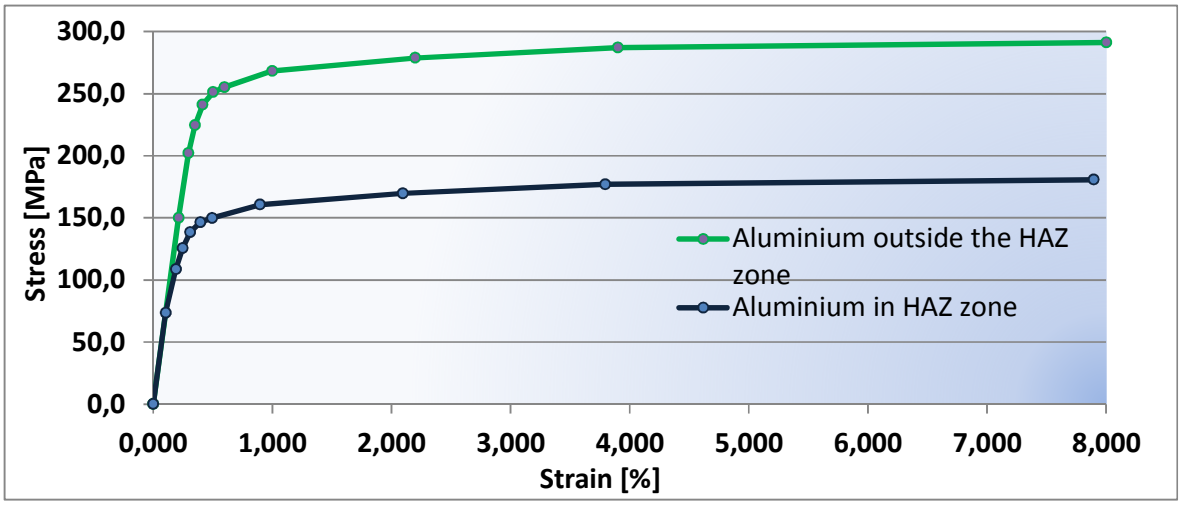

Figure 6.1 Strain – stress curve for aluminium in HAZ zone

6.2.2. Views from ABAQUS

According to HAZ zones sizes b_{haz} from Eurocode [1] created model was divided into several parts. This division caused problems with meshing the whole beam, so different techniques had to be used on different parts of the beam. Final effect can be seen on the figure below.

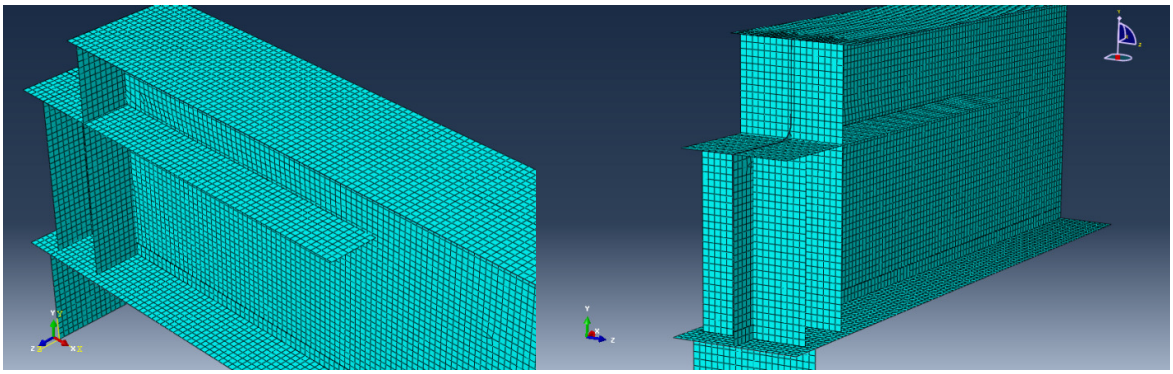

Figure 6.2 View on mesh of the reinforced A2 specimen

On the figure 6.3 below it is showed model, when the HAZ effect is taken into account. Yellow areas are the places, where welding cause the reduciotion in strength of aluminium. Green plates symbolize the full strength material. Picture below show the case when both verticals and longitudinal stiffeners have been used. The size of zones depend on the thickness of the plates and as it can be seen is different it is inreasing near the falnge, where web becomes thicker.

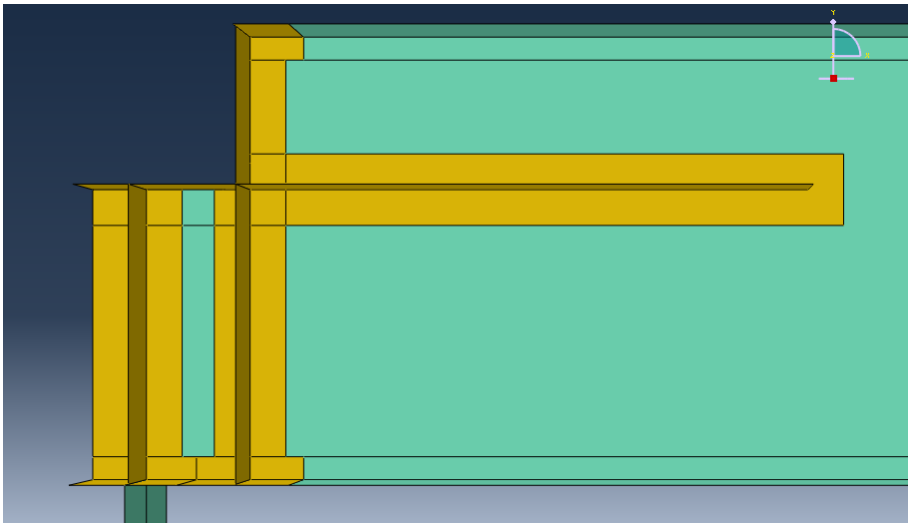

Figure 6.3 A2 specimen with HAZ zones

6.3. Investigated stiffeners

6.3.1. General

It was decided to focus the most in this chapter on influence of the HAZ effect. Because there were investigated done previously by Urseth in his thesis on steel samples it can be possible to connect the current one with them somehow. It can be assumed that additional stiffeners will be increasing the capacity of the beam in the same pattern like in [5] if only HAZ effect will not be taken into the consideration. Thus it appears crucial to investigate how softening of aluminium due to welding will change the improvement in capacity of the beam. A2 and A3 specimens were chosen to check the influence of stiffeners.

6.3.2. Dimensions

Two types of stiffeners will be used for these studies. It was decided to differentiate them in thickness. Because of the reason showed on the figure 2.1 whole part of additional plates will be in range of HAZ effect unless the width of stiffener will be larger than width of the flanges of the beam. But such solution is not applied. Thus 100mm width stiffeners with thickness 5 and 10 mm were used to check the effect of reinforcement. This size was used because on the site stiffeners will be added two the beam in two parts, 50mm wide each. Using shorter stiffener would be very uncomfortable for the welder.

6.4. Effect of longitudinal stiffeners

From Urseth's studies it turned out that long longitudinal stiffeners give almost no improvement in capacity and work only with additional vertical stiffeners. 400mm length can be assumed as a critical value, exceeding which is only the waste of material. It is not the intention of this paper to repeat the results obtained in earlier works. However, to ensure that XHP profile will be reacting similar as IPE 300 for longitudinal stiffeners it was decided to check if the ultimate reaction force will raise with bigger / smaller length. For this task 300 mm and 500 mm length of stiffener was chosen.

Growth in capacity caused by longitudinal stiffeners was observed in Urseth's studies only on specimens with high cope ratio. Thus, to check the influence of using longer longitudinal stiffener A3 specimen was chosen. Results given below showed how

ultimate force from linear and nonlinear analyses is changing. This time studies focused on checking Urseth's model so HAZ effect was not taken into account. Recalling, capacity without stiffener was 43,45 kN

Stiffener's thickness	Max force , 300 mm length [kN]	Max force , 400 mm length [kN]	Max force , 500 mm length [kN]
5 mm	71,65	84,61	96,19
10 mm	82,82	98,27	111,84

Table 6.1 Linear buckling results – longitudinal stiffeners

Stiffener's thickness	Max force , 300 mm length [kN]	Max force , 400 mm length [kN]	Max force , 500 mm length [kN]
5 mm	64,13	73,34	81,20
Increase in capacity [%]	47,6	68,8	86,9
10 mm	68,92	81,35	81,20
Increase in capacity [%]	58,6	87,2	86,9

Table 6.2 Nonlinear buckling results – longitudinal stiffeners

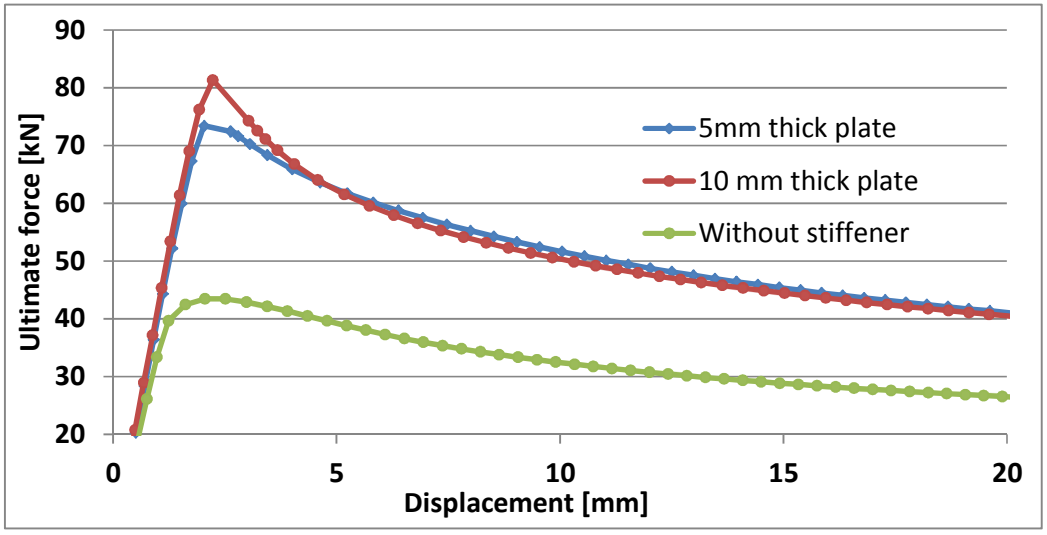

Figure 6.4 Comparison of response curves

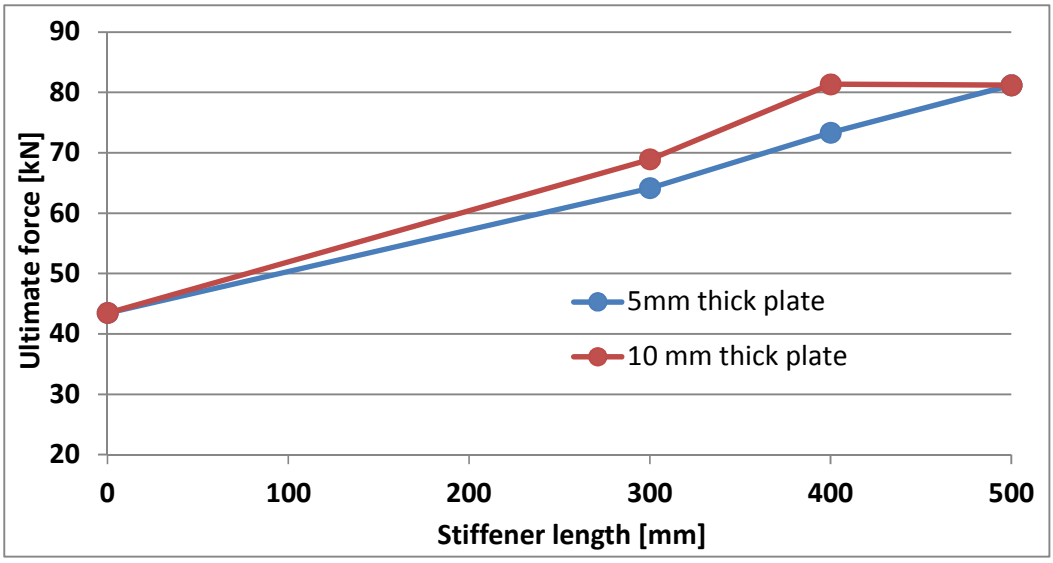

Figure 6.5 Influence of the longitudinal stiffener

For the thick plate results confirmed Urseth's conclusions that increasing the length after 400mm of the stiffeners did not allow obtaining any more improvement in the capacity. It is worth to emphasize that buckle shape remain almost unchanged in all cases so each specimen got very similar initial imperfections. On the other hand for a thick plate this improvement is still visible. It can be stated anyway that generally this size of the stiffener allows improving results in effective way (if only HAZ effect will not be considered). Therefore 400 mm long longitudinal stiffener was chosen for the further investigation of reinforcing coped beams ends. For a better view on the results figure bellows are given. Drawings at the end show mises stresses, and lateral displacement for the 5mm stiffener.

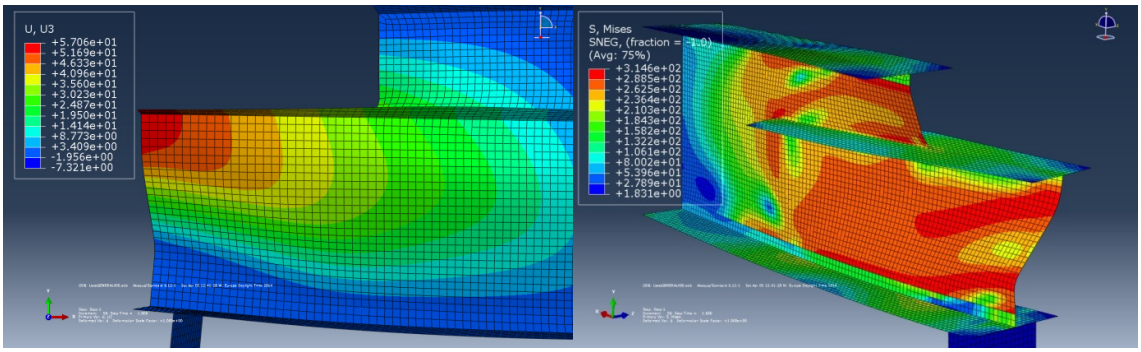

Figure 6.6 Lateral displacement and mises stresses in A3 specimen with 400 longitudinal stiffener without HAZ

6.5. Necessary changes in the model

6.5.1. Imperfection

After linear buckling analyses it turned out, that this time first buckle shape may not necessarily lead to the buckle at the cope in the easiest way. On pictures below there are presented first and fifth (chosen for calculations) buckle shapes for A2 sample with vertical stiffener above the load position. It is clearly visible that this second one better forced appearance of the buckle at the cope. When both stiffeners are used the 8-th buckle shape was used.

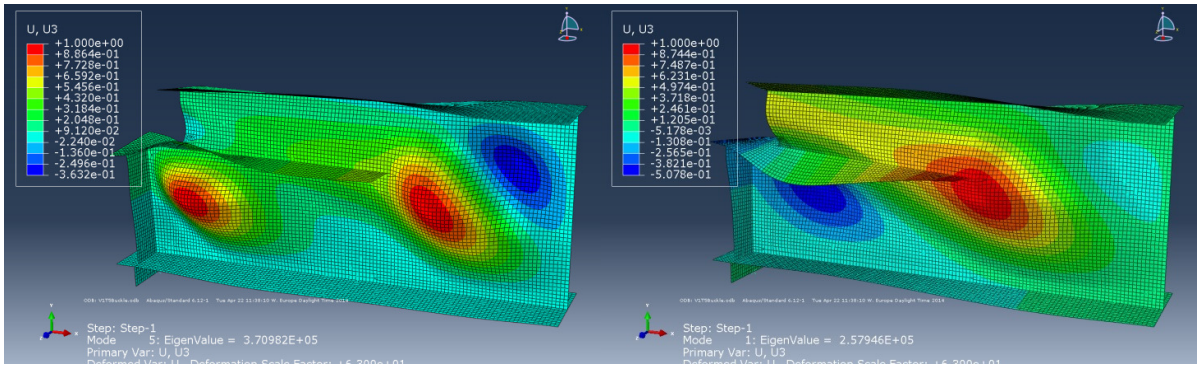

Figure 6.7 First and fifth buckle shape (A2 sample with V1 stiffener)

6.5.2. Load panel

After running non-linear analyses it can observed, that horizontal displacement (along x axis) of the load panel is much higher than in previous calculations. Due to higher forces acting on the beam rotation at the cope end could be larger and this effect causes mentioned displacement. This is particularly evident, when HAZ effect is included in the model, because of the weakening of the bottom flange. This displacement results in increase of arm moment and affects results (makes capacity lower). It was necessary to decrease this displacement, so height of the support panel was decreased from 100 mm to 30 mm. This allows to obtain displacement at the end of panel below 1 mm instead of 7 mm in the worst case.

6.6. Effect of reinforcement

6.6.1. Cases taken into account

In previous point length of longitudinal stiffener was chosen to reinforce the beam. Especially HAZ effect was not considered before to show what will happen if it will

be neglected. It was proved [5] that the best results can be obtained only through a combination of longitudinal and verticals stiffeners. In this point following models will be considered:

- Longitudinal stiffener with vertical above the support (V1)
- Longitudinal stiffener with vertical at the end of the cope (V2)
- Longitudinal stiffener with both verticals (V1V2).

Stiffeners will be varied by thickness and specimens will be investigated with and without influence of HAZ effect. It is believed that together, these 48 cases (24 for each specimen A2 and A3) allow describing the problem properly.

6.6.2. Vertical stiffener above the load – V1

On the pictures below are showed both mises stresses after 20 mm vertical displacement and also deformation, buckling pattern represented by lateral displacement for A2 sample. The results are presented in the following way. Firstly are presented this, which were derived, when stiffeners were 5mm thick without and with taking into account HAZ effect. After them the same was done for 10mm thick stiffeners. Because of large volume of this outcomes it was decided to present them in the appendix A.

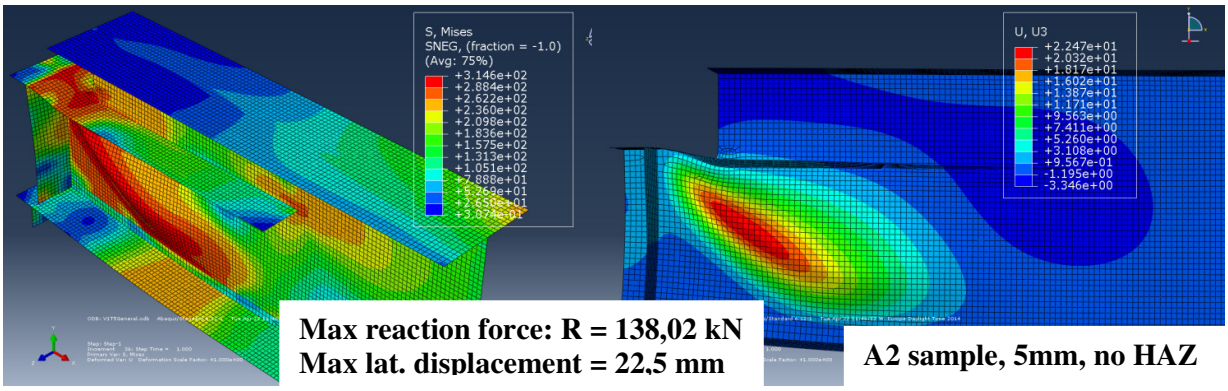

Max reaction force: R = 138,02 kN
Max lat. displacement = 22,5 mm

A2 sample, 5mm, no HAZ

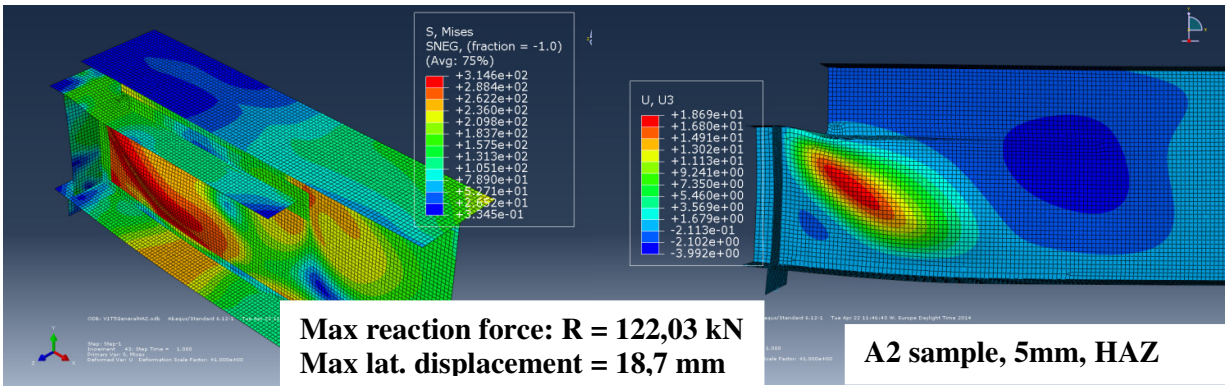

Max reaction force: R = 122,03 kN
Max lat. displacement = 18,7 mm

A2 sample, 5mm, HAZ

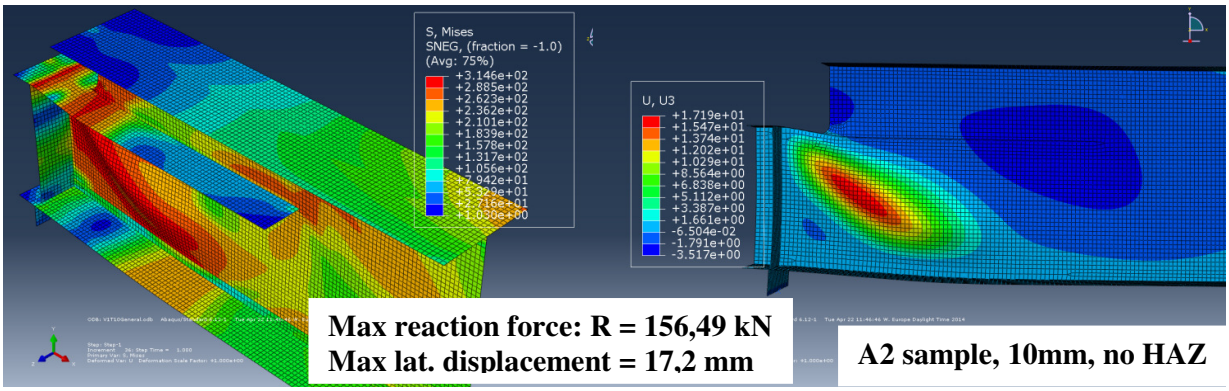

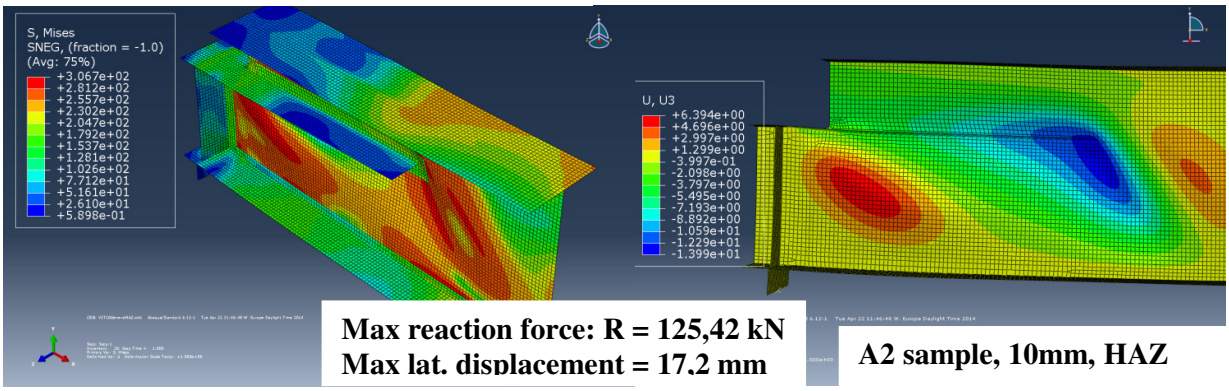

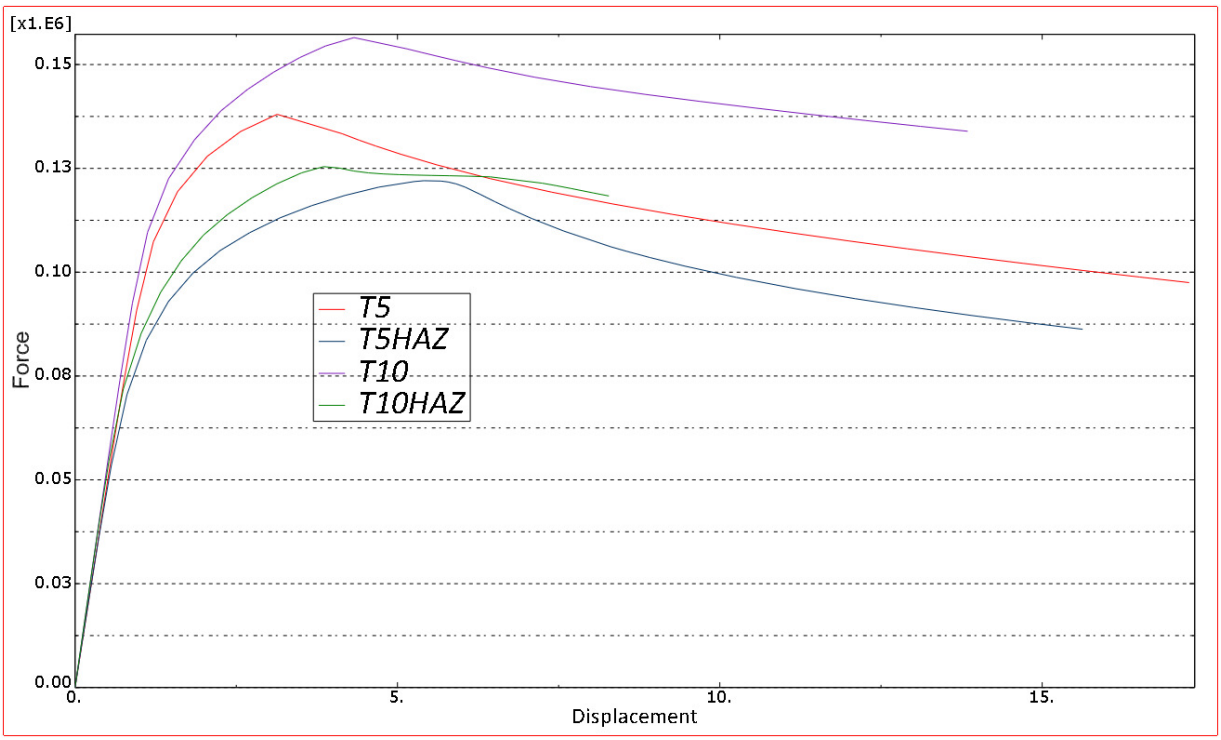

Results from A2 and A3 sample with V stiffeners gave the answer for the question if aluminum beams could be reinforced by welding additional plates to the web, what is the cause of HAZ effect. It can be deducted that increase in capacity is very large (see response curve in 7.6), but is not proportional to the thickness of the stiffeners. In case of

A2 sample with smaller cope this growth in capacity is 90,6% for 5mm thick stiffeners and 95,9% for 10mm stiffeners. For A3 sample these values are 118,6% and 137,7%. This shows that thickness may have influence on the capacity only on beams with larger copes, because only then buckling can move from cope corner to the end of the longitudinal stiffener, what was observed in 10mm plate welded to the A3 sample.

6.6.3. Vertical stiffener near the cope corner – V2

Vertical stiffener welded to the cope corner together with longitudinal stiffener turned out to be the least favorable method of reinforcing the coped beam. In case A2 specimen only 38,7% and 41,8% increase in capacity can be observed for respectively 5mm and 10mm thick plates. For this sample it is very inefficient to use V2 stiffener but in A3 case, where the cope is larger, obtained results are almost the same as the case of application V1 stiffeners – 97% for 5mm plates and 102,5% for 10mm plates. The biggest advantage of usage this type of reinforcement is fact that the reduction due to HAZ effect is here very small for small cope – A2 specimen (13,5 and 17,1%) and almost negligible for larger cope – A3 specimen (3,5 and 3,9%). In all investigated specimens with V2 stiffeners buckling occurred at the end of the cope, above the support. Also here twice thicker stiffeners gave only slightly better results.

6.6.4. Two vertical stiffeners – V1 and V2

As expected connection V1 and V2 stiffeners with longitudinal stiffener provided the highest growth in capacity ranged from 98,4% for A2 specimen with 5mm plates to 173,8% for A3 specimen. From results it can be deducted that reduction in capacity due to HAZ effect becomes smaller with increasing cope size and thickness of the stiffeners. Values of this reduction are from 42,3 % to 26,7%. Buckling occurred in place, where longitudinal stiffener was used and it can be assumed that increasing its length allows obtaining even better results. Even in case of A3 sample the space between stiffeners was not threatened by buckling and the lateral displacement is almost zero in this zone. The ultimate reaction forces are in these case so larger that buckle almost didn't occur after 20mm displacement.

6.7. Summary of the results

All results were gathered to show in the table, how ultimate reaction forces increased due to reinforcement by stiffeners and how big the HAZ effect influence on the capacity is. For each specimen separate table was made.

A2 Sample/ 5mm thick	No stiffeners	V1 stiffener	V2 stiffener	V1V2 stiffeners	V1 stiffener HAZ	V2 stiffener HAZ	V1V2 stiffeners HAZ
Max. reaction force [kN]	64,02	138,02	92,70	173,13	122,03	88,82	127,02
Increase in capacity [%]	-	115,6	44,8	170,4	90,6	38,7	98,4
Reduction due to HAZ effect [%]	-	-	-	-	21,6	13,5	42,3

Table 6.3 Results of reinforcing beam's end by stiffeners – A2, 5 mm sample.

A2 Sample/ 10mm thick	No stiffeners	V1 stiffener	V2 stiffener	V1V2 stiffeners	V1 stiffener HAZ	V2 stiffener HAZ	V1V2 stiffeners HAZ
Max. reaction force [kN]	64,02	156,49	96,33	177,52	125,42	90,79	143,11
Increase in capacity [%]	-	144,4	50,5	177,3	95,9	41,8	123,5
Reduction due to HAZ effect [%]	-	-	-	-	33,6	17,1	30,3

Table 6.4 Results of reinforcing beam's end by stiffeners – A2, 10 mm sample

A3 Sample/ 5mm thick	No stiffeners	V1 stiffener	V2 stiffener	V1V2 stiffeners	V1 stiffener HAZ	V2 stiffener HAZ	V1V2 stiffeners HAZ
Max. reaction force [kN]	43,45	118,73	87,14	138,40	94,99	85,61	110,02
Increase in capacity [%]	-	173,3	100,6	218,5	118,6	97,0	153,2
Reduction due to HAZ effect [%]	-	-	-	-	31,5	3,5	29,9

Table 6.5 Results of reinforcing beam's end by stiffeners – A3, 5 mm sample

A3 Sample/ 10mm thick	No stiffeners	V1 stiffener	V2 stiffener	V1V2 stiffeners	V1 stiffener HAZ	V2 stiffener HAZ	V1V2 stiffeners HAZ
Max. reaction force [kN]	43,45	130,59	89,81	146,40	103,28	87,99	118,95
Increase in capacity [%]	-	200,6	106,7	236,9	137,7	102,5	173,8
Reduction due to HAZ effect [%]	-	-	-	-	31,3	3,9	26,7

Table 6.6 Results of reinforcing beam's end by stiffeners – A3, 10 mm sample

To assess this results it is worth to emphasize that in case of A1 uncoped specimen the ultimate reaction force was 75,1 kN. Both reinforced A2 and A3 sample have larger capacity regardless of the methods V1, V2 or V1V2 used. It can be also observed that specimen with bigger cope got higher increase in ultimate reaction force. When both vertical stiffeners were used – V1 and V2 results shows that cope end is not vulnerable any more for buckling and buckle occurs at the end of longitudinal stiffener. Reduction in capacity due to HAZ effect depends highly on the reinforcement method and ranged from even 3,5% to 42,3% and in general is larger for A2 specimen. So there is no simple way to assess how big reduction could be and FEM calculations should be made each time to obtain reliable results. After investigations these three methods it can be told that even in aluminium beams, where HAZ effect can be met, welding additional stiffeners can significantly increase the capacity. Welding more stiffeners (V1 and V2) allows obtaining the higher capacity and using stiffeners at the cope corner only makes the impact of HAZ effect very low on final result – max 17%.

6.7.1. Choosing best method of reinforcement

To choose the best method of reinforcement charts with responses (force – displacement) for each sample were prepared, where HAZ effect was taken into account. Both samples with 5mm and 10mm thickness were placed on the figure. Additionally also results from clear, without stiffeners A2 and A3 specimens were plotted to show the difference in capacity and behavior of the beam.

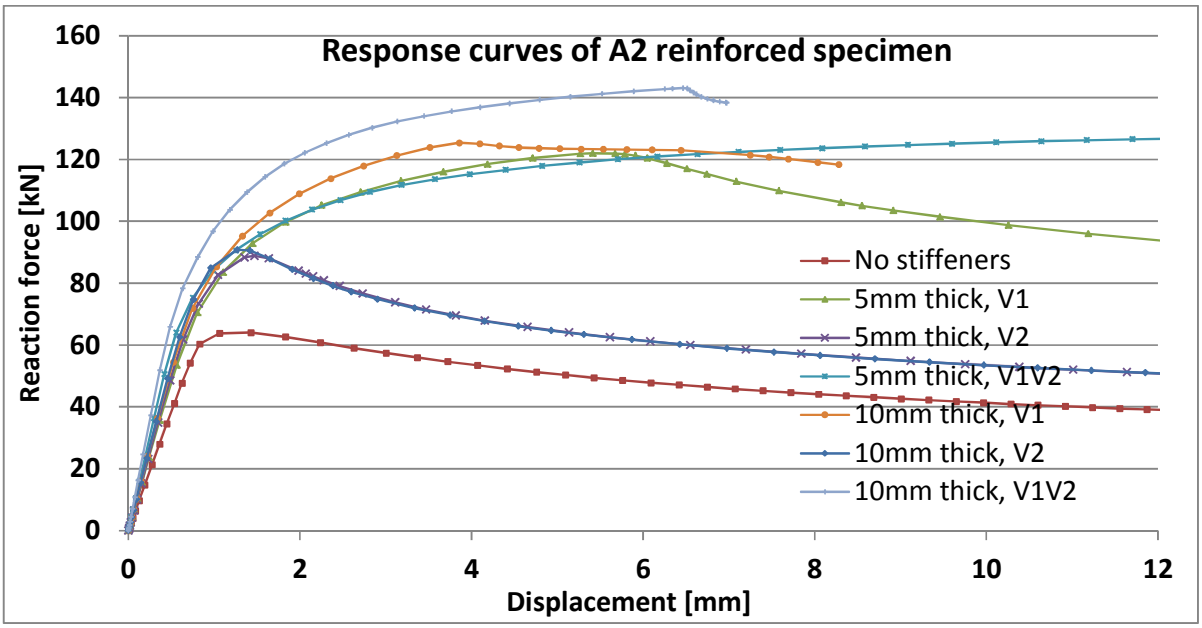

Figure 6.8 Influence of the stiffeners on the A2 specimen.

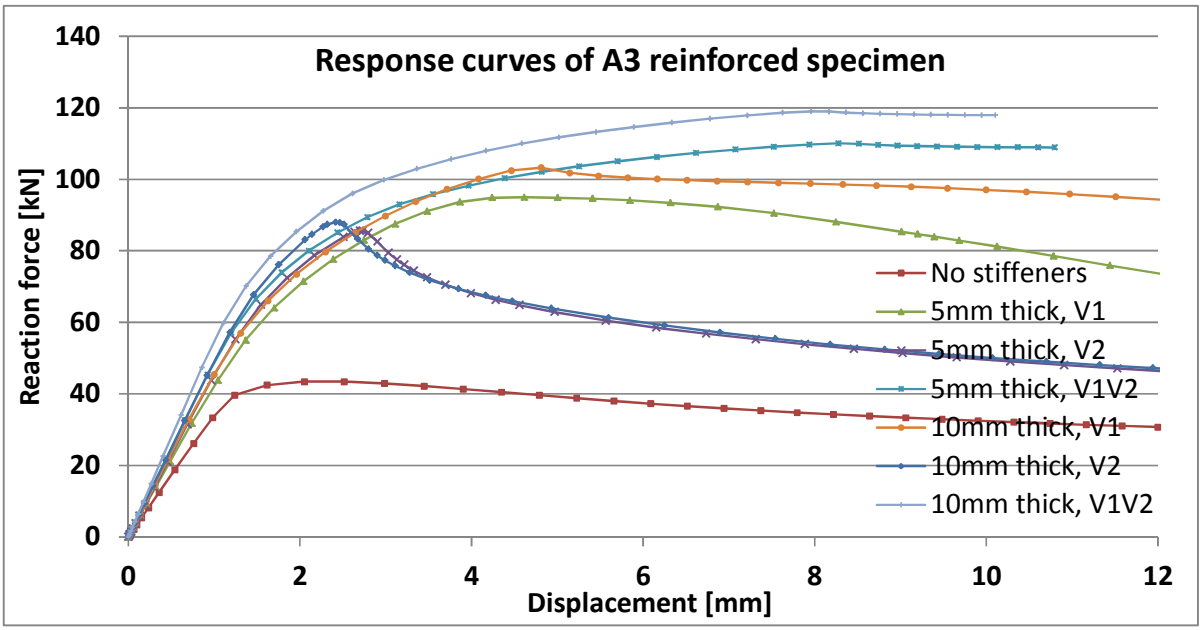

Figure 6.9 Influence of the stiffeners on the A3 specimen.

From charts above it can be deducted that both specimens A2 and A3 behave in very similar way depending on the reinforcement method. Always using more stiffeners or thicker one allows obtaining higher ultimate force. But from these results it can be concluded the best way of improving capacity by welding stiffeners. It is the use of 5mm thick vertical stiffener above the load – V1 in both cases.

There are a lot of reasons why this method recognized as the best:

- It provides 90,6% and 118,6% increase in capacity respectively for A2 (122,03 kN) and A3 (94,99 kN) specimen, what means that the ultimate reaction force was doubled.
- It is the easiest, easiest in execution way of reinforcement. Welding at the end of cope is relatively comfortable for the worker. Also length of weld is the shortest from the investigated methods of reinforcement.
- Is the less material consuming method.
- Doubling of material (10 mm thick stiffeners) increase capacity only about 2,8% for A2 sample and 8,7% for A3, what allows to claim that it is not worth to use thicker stiffeners.
- V2 method always gives worse results and moreover welding at the cope end is more complicated what makes it not recommended to use.
- To obtain better results it is necessary to welded two vertical stiffeners but increase in capacity compared with results from V1 is not significant also: 4,1% for A2, 15,8% for A3 if 5 mm thickness of stiffeners would be used and 17,3% for A2, 25% for A3 if 10 mm thickness of stiffeners would be used.

Chapter 7: Final conclusion

In this paper main objective was to develop the numerical model which will give accurate results in comparison with this performed in laboratory tests and extend it to investigate the behavior of reinforced by stiffeners coped beams. Laboratory tests were widely discussed in point 4. In point 5 there are described all necessary steps to create numerical models, which gave results showed in 6. The reaction of the ultimate loads predicted by the FEM analyses to the real values obtained in the laboratory ranges from 0,964 to 0,998 which can be considered as a very accurate. It means that the results from analyses underestimate capacity of the cross-section from 0,2% to 3,56% with 1,49% as a middle value for all six specimens. Comparison of the response curve can be found in the attachment C in this thesis. Different size of the cope (c x d_c) was checked but in general developed model is valid for all of them.

Accurate results encouraged to investigate more advanced cases, where longitudinal and vertical stiffeners were used to increase the ultimate capacity of the beams. In point 6 two specimens with different cope ratio –A2 and A3 were investigated to find the most effective way of reinforcement. It was necessary to provide some detail to the model due to HAZ effect. Longitudinal stiffener was putted along the cope and two different placed vertical stiffeners were checked. First one was in the cope corner and the second directly above the load. Buckling results for whole specimens can be found in the attachment A. All calculations were done both for clear aluminium beam and affected by the HAZ effect to find an clear answer how HAZ effect influence on the ultimate capacity of the beam and if is even worth to weld plates to beam. It turned out that although HAZ effect decrease dramatically properties of the material, zone of the HAZ is not large and welding additional stiffeners can actually be very good solution for reinforcement of the beam. HAZ effect have different influence on the capacity of the beam and it can decreased it from 3,5% to even 42,3%. But still when it will be taken into account that the ultimate forced can be more than twice larger these numbers are not big.

The best stiffeners set was easy to found. It can be distinguished by very good results, low material consumption and simplicity of implementation. More about choice of V1(vertical stiffener at the cope corner and 400 mm long longitudinal) solution with 5mm and 100 mm width stiffeners can be found in 6.7.1.

A. FEM results of reinforced beams

8.1. A3 sample with V1 stiffener

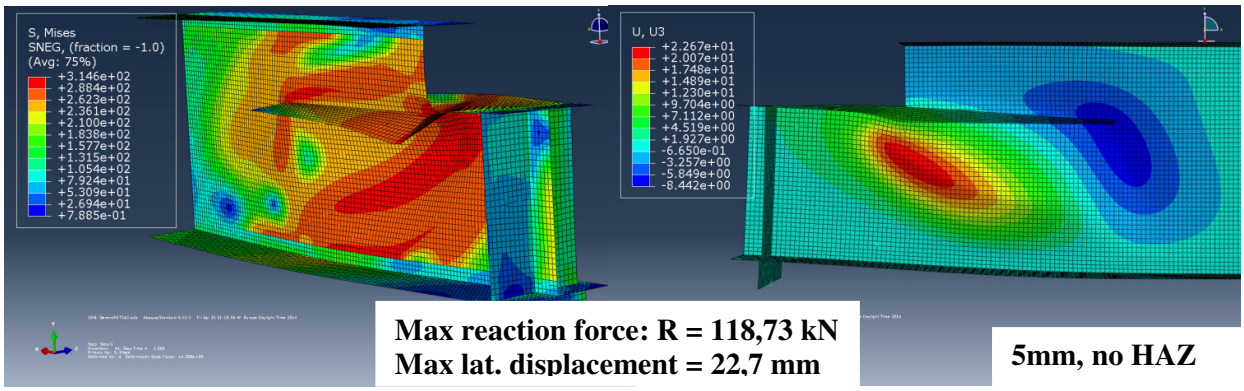

Max reaction force: R = 118,73 kN
Max lat. displacement = 22,7 mm

5mm, no HAZ

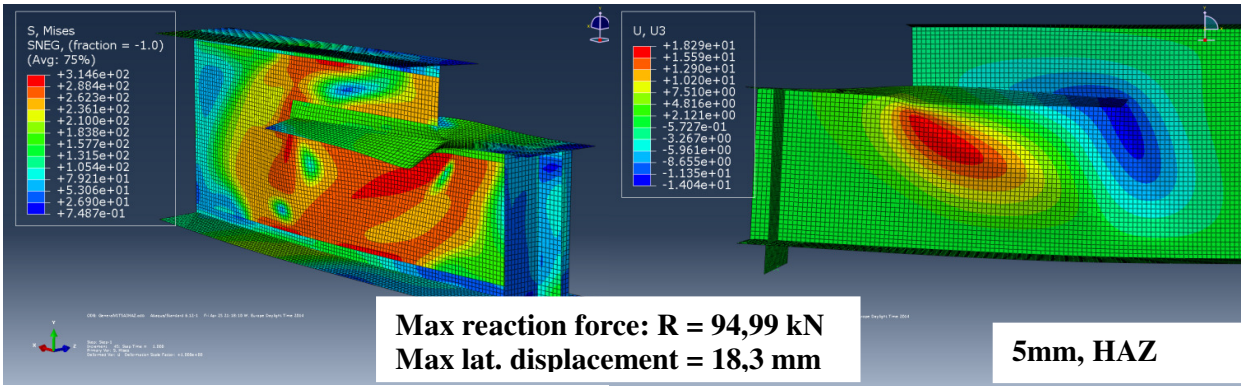

Max reaction force: R = 94,99 kN
Max lat. displacement = 18,3 mm

5mm, HAZ

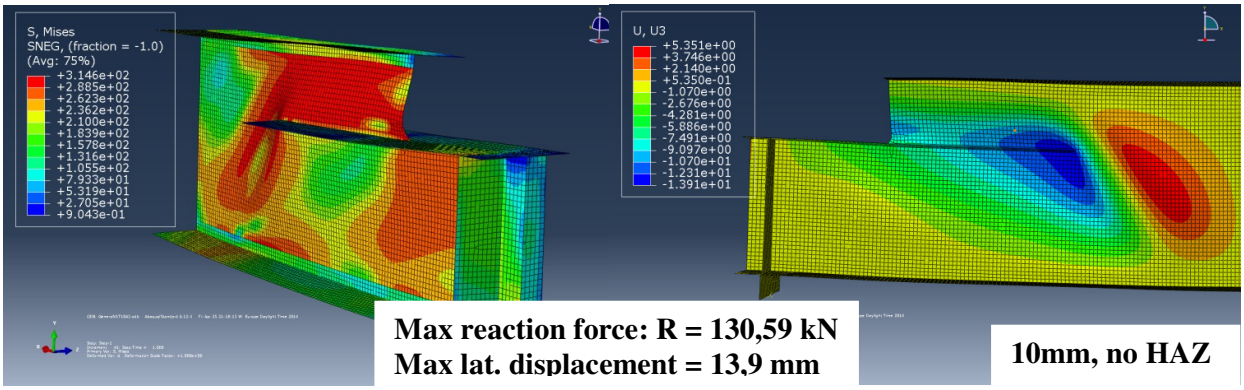

Max reaction force: R = 130,59 kN
Max lat. displacement = 13,9 mm

10mm, no HAZ

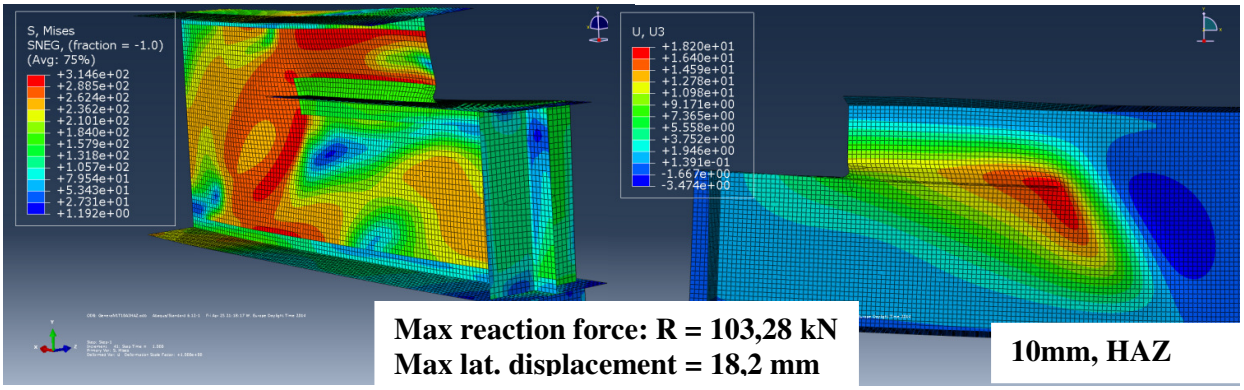

Max reaction force: R = 103,28 kN
Max lat. displacement = 18,2 mm

10mm, HAZ

8.2. A2 sample with V2 stiffener

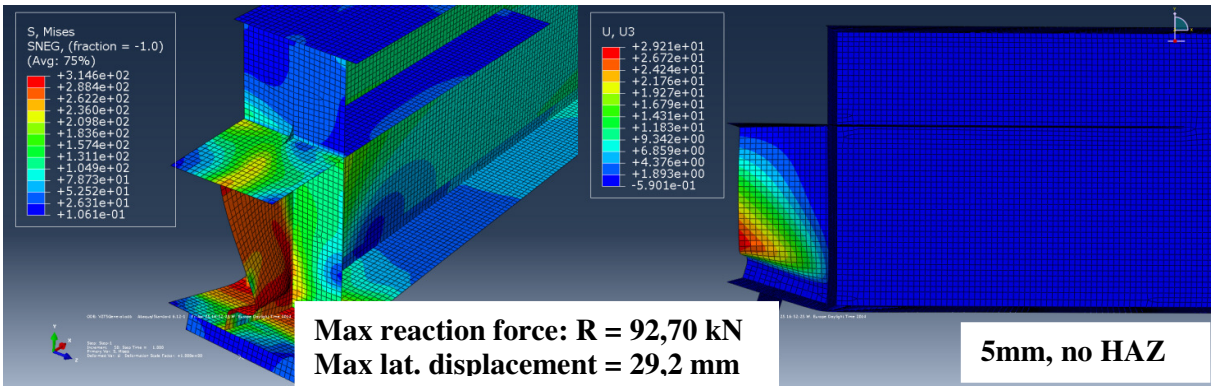

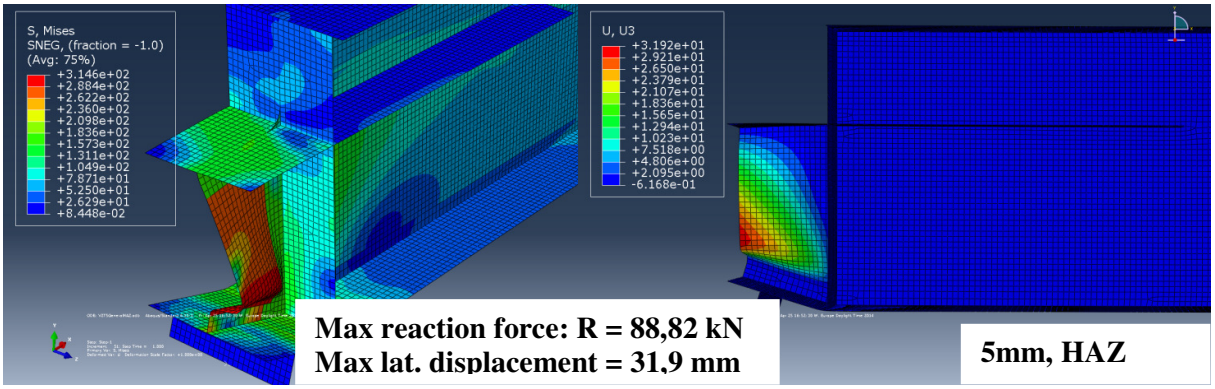

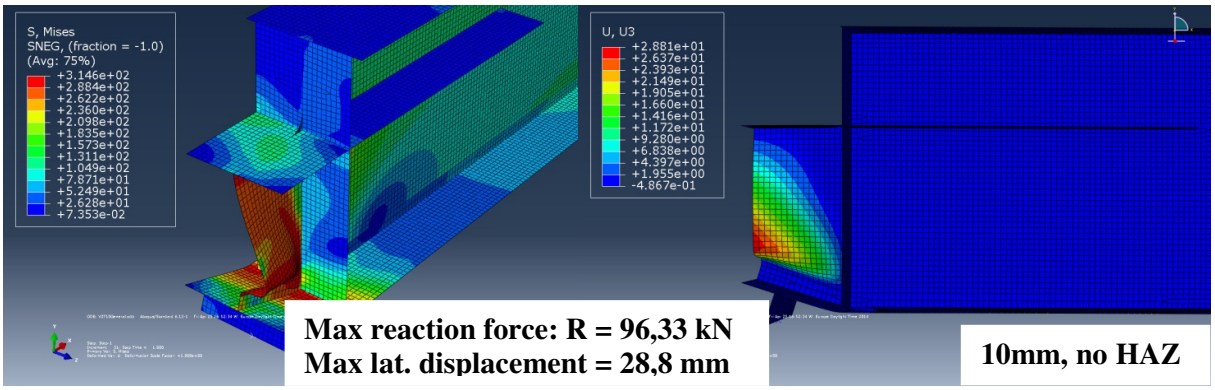

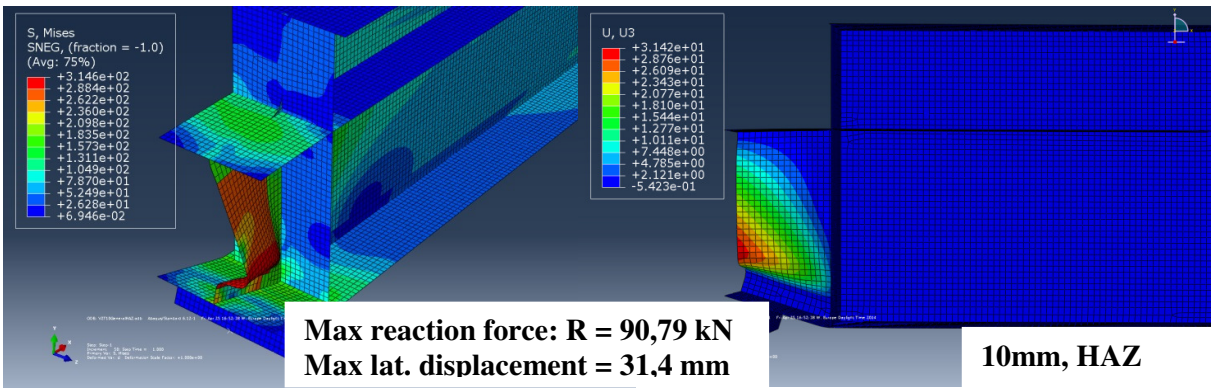

8.3. A3 sample with V2 stiffener

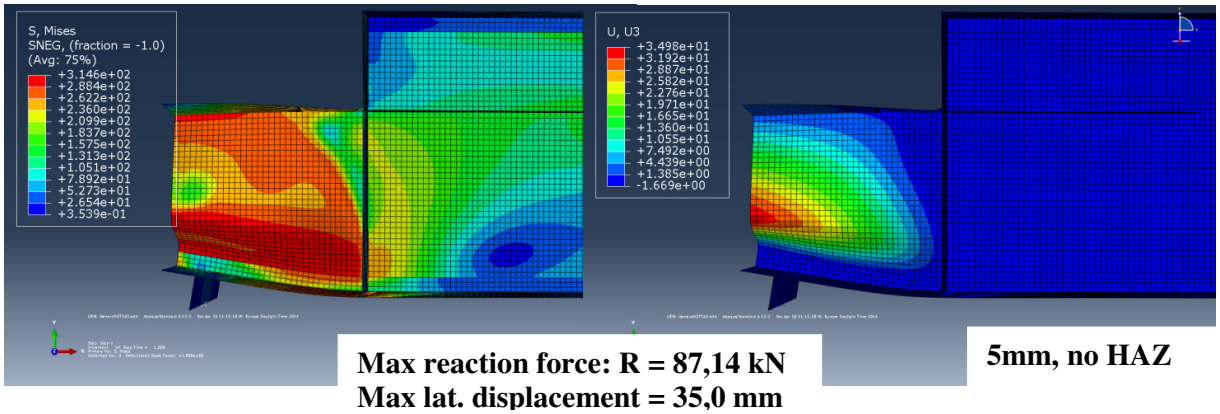

Max reaction force: R = 87,14 kN
Max lat. displacement = 35,0 mm

5mm, no HAZ

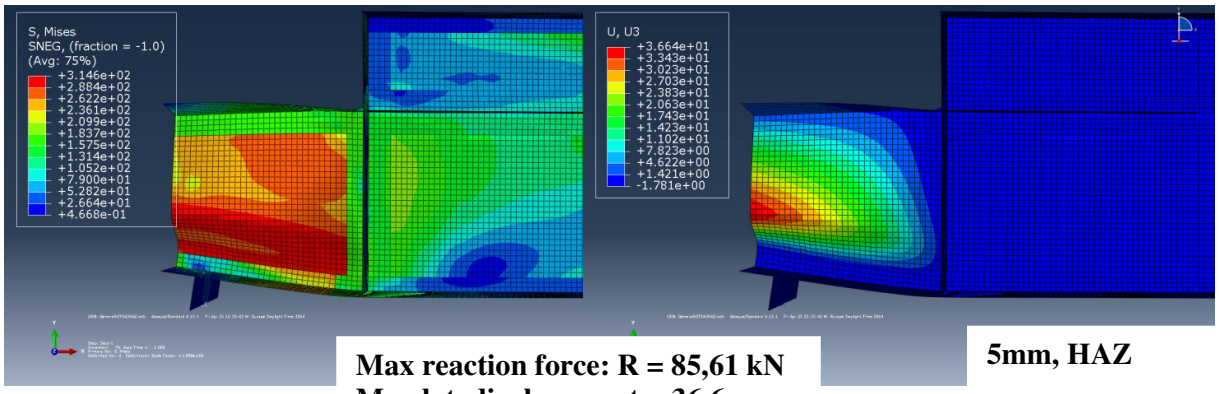

Max reaction force: R = 85,61 kN
Max lat. displacement = 36,6 mm

5mm, HAZ

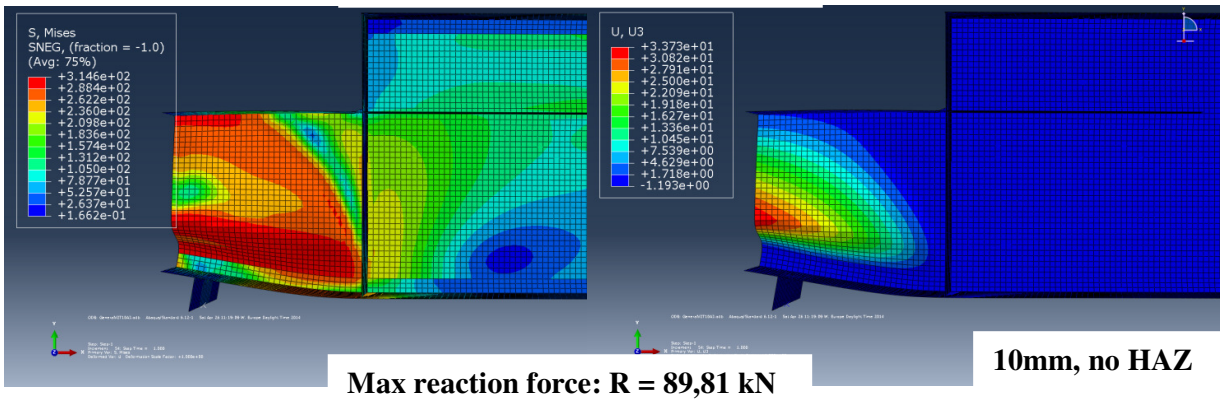

Max reaction force: R = 89,81 kN
Max lat. displacement = 33,7 mm

10mm, no HAZ

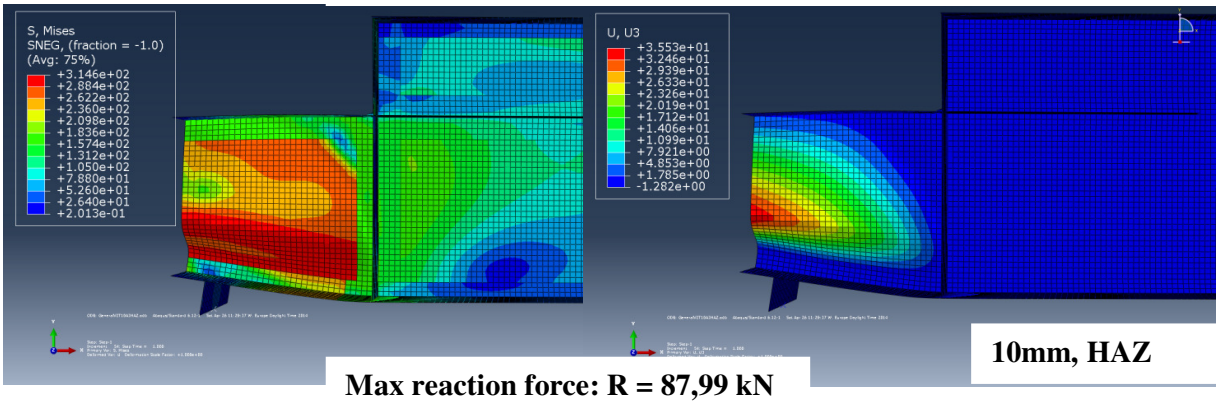

Max reaction force: R = 87,99 kN
Max lat. displacement = 35,5 mm

10mm, HAZ

8.4. A2 sample with V1 and V2 stiffeners

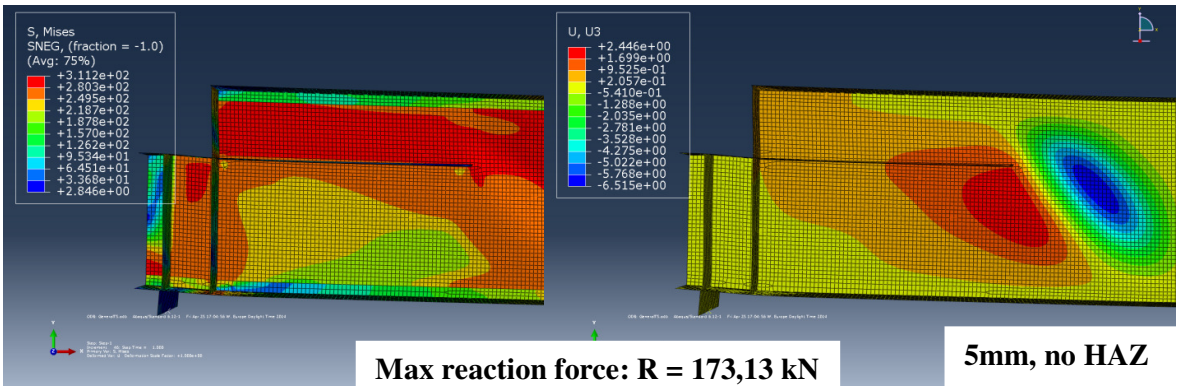

Max reaction force: R = 173,13 kN
Max lat. displacement = 2,45 mm

5mm, no HAZ

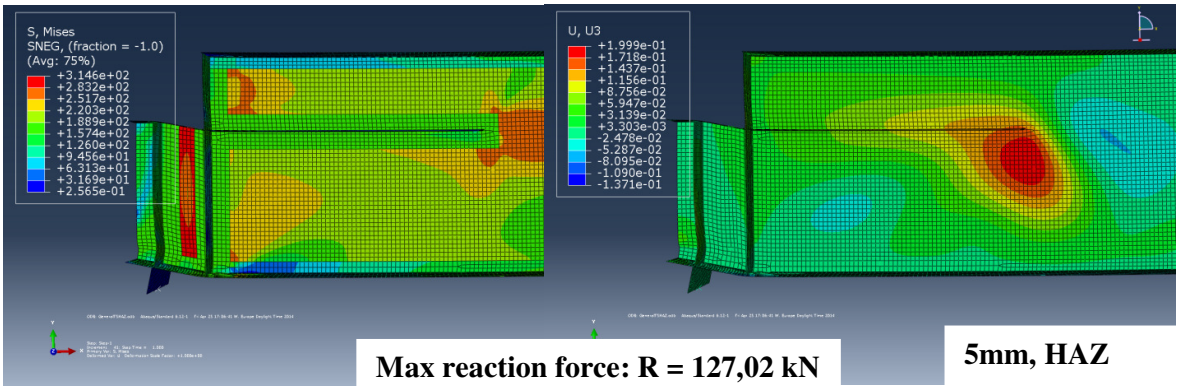

Max reaction force: R = 127,02 kN
Max lat. displacement = 0,20 mm

5mm, HAZ

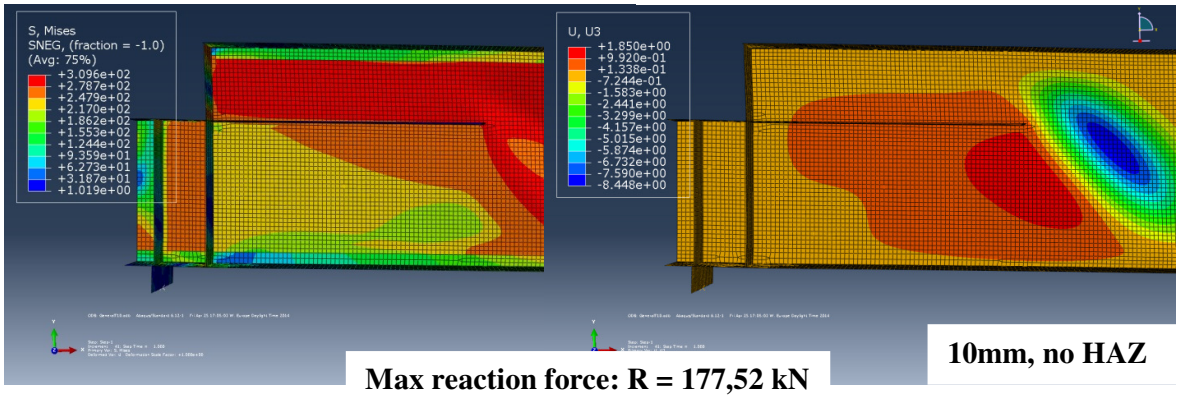

Max reaction force: R = 177,52 kN
Max lat. displacement = 1,85 mm

10mm, no HAZ

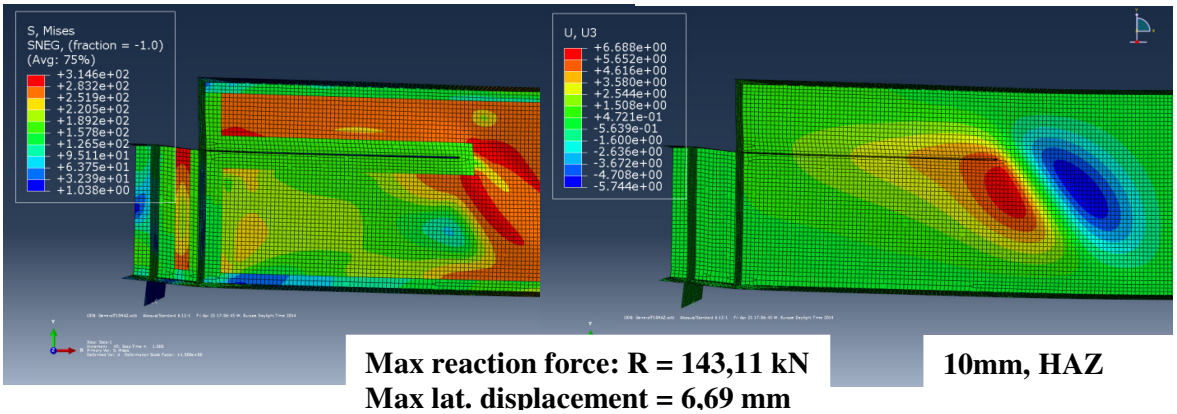

Max reaction force: R = 143,11 kN
Max lat. displacement = 6,69 mm

10mm, HAZ

8.5. A3 sample with V1 and V2 stiffeners

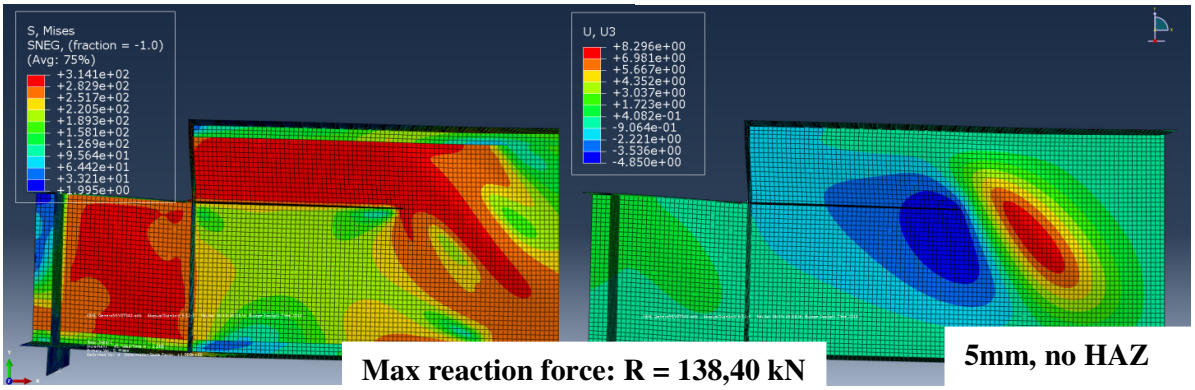

Max reaction force: R = 138,40 kN
Max lat. displacement = 8,30 mm

5mm, no HAZ

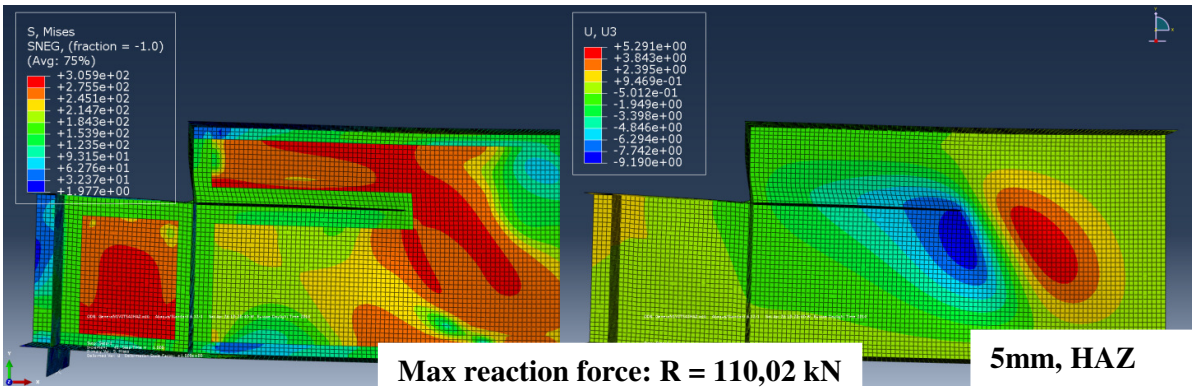

Max reaction force: R = 110,02 kN
Max lat. displacement = 9,20 mm

5mm, HAZ

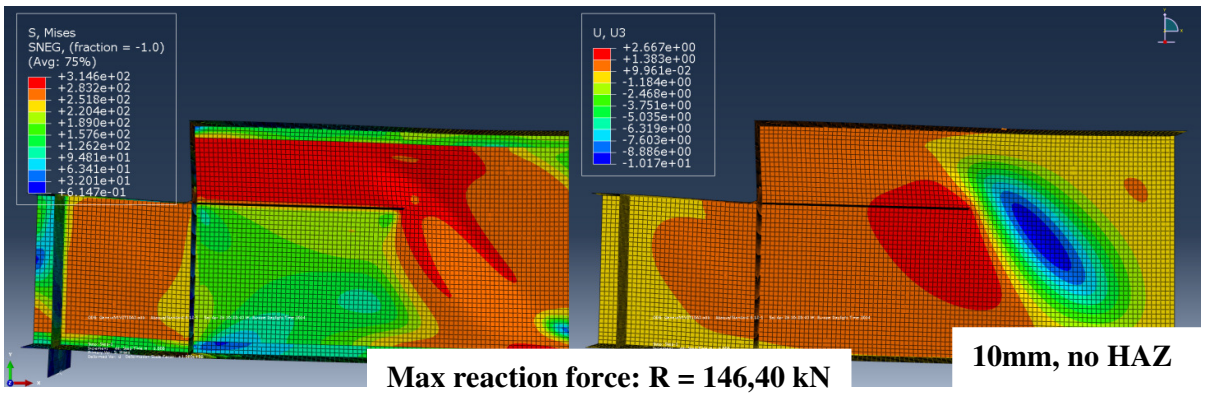

Max reaction force: R = 146,40 kN
Max lat. displacement = 2,67 mm

10mm, no HAZ

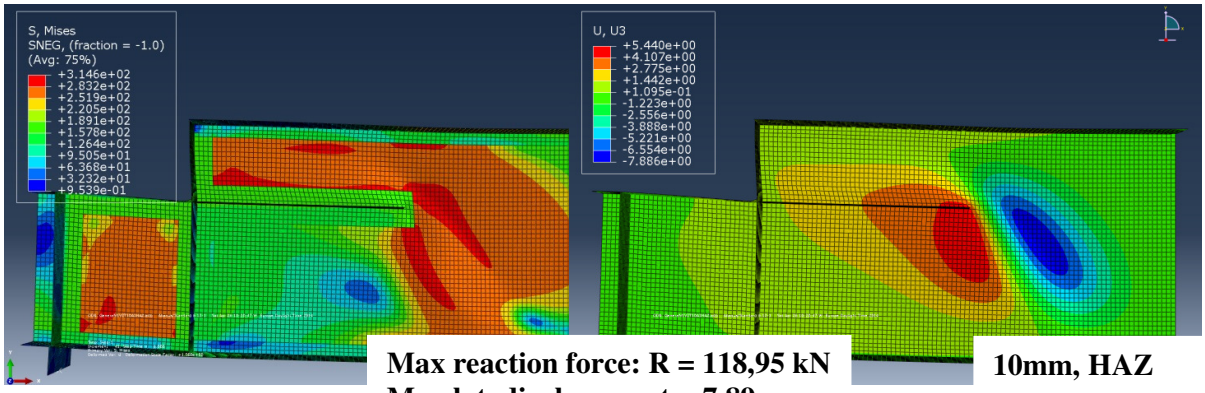

Max reaction force: R = 118,95 kN
Max lat. displacement = 7,89 mm

10mm, HAZ

8.6. Response curves

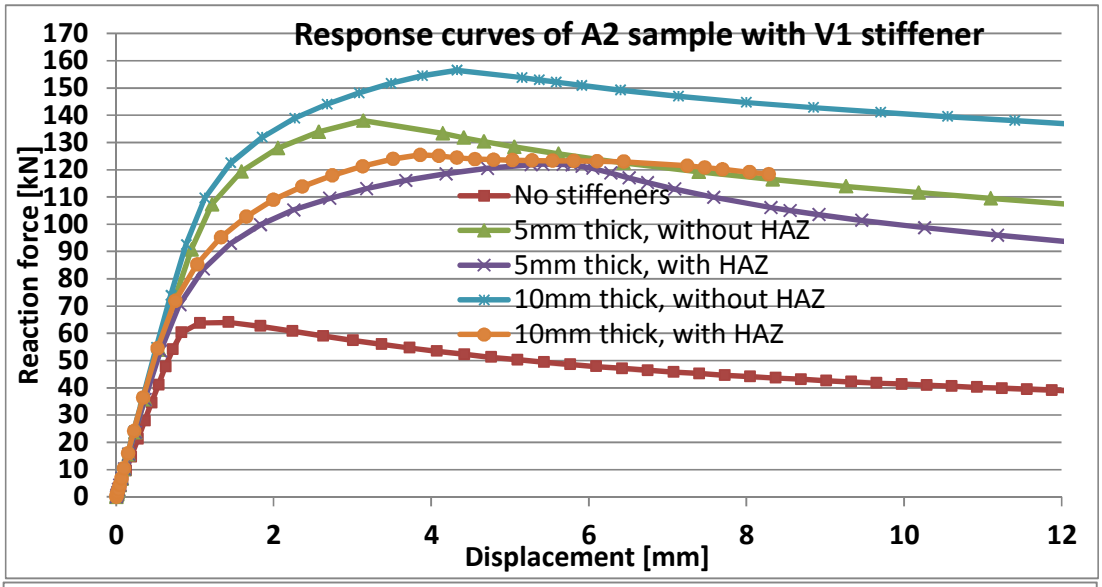

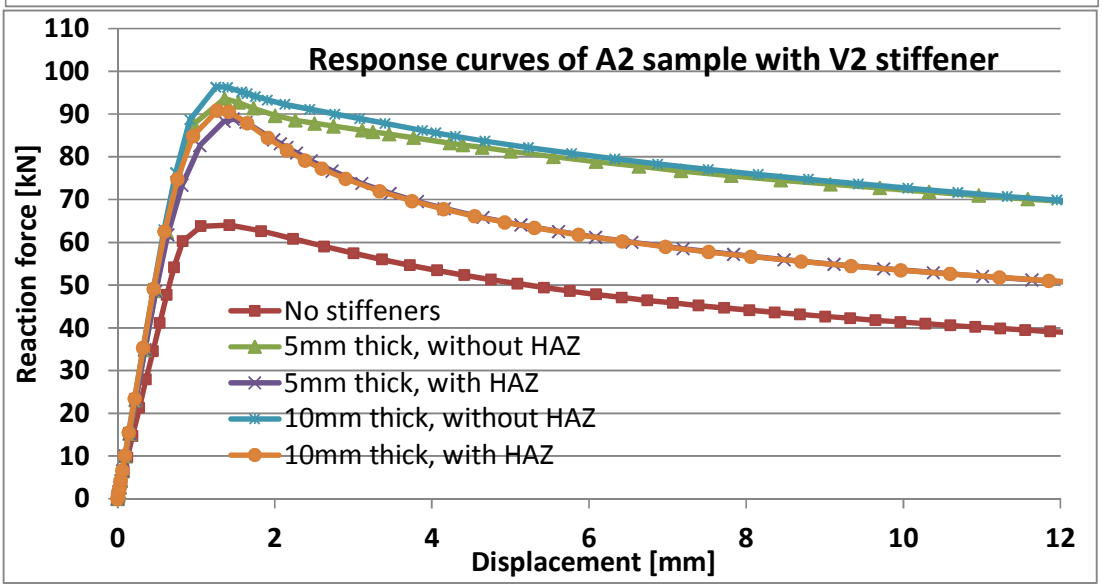

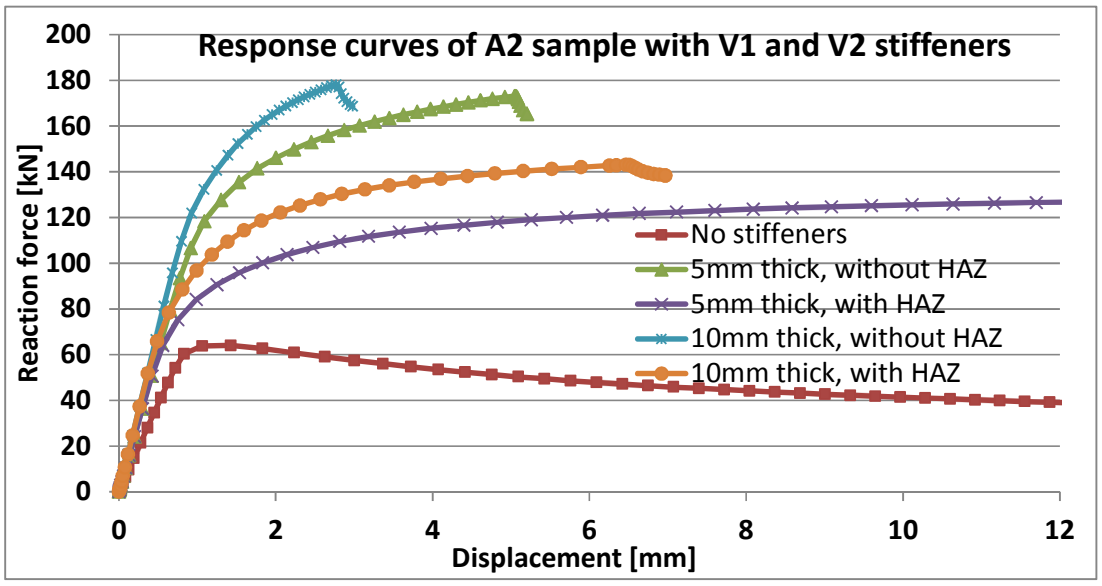

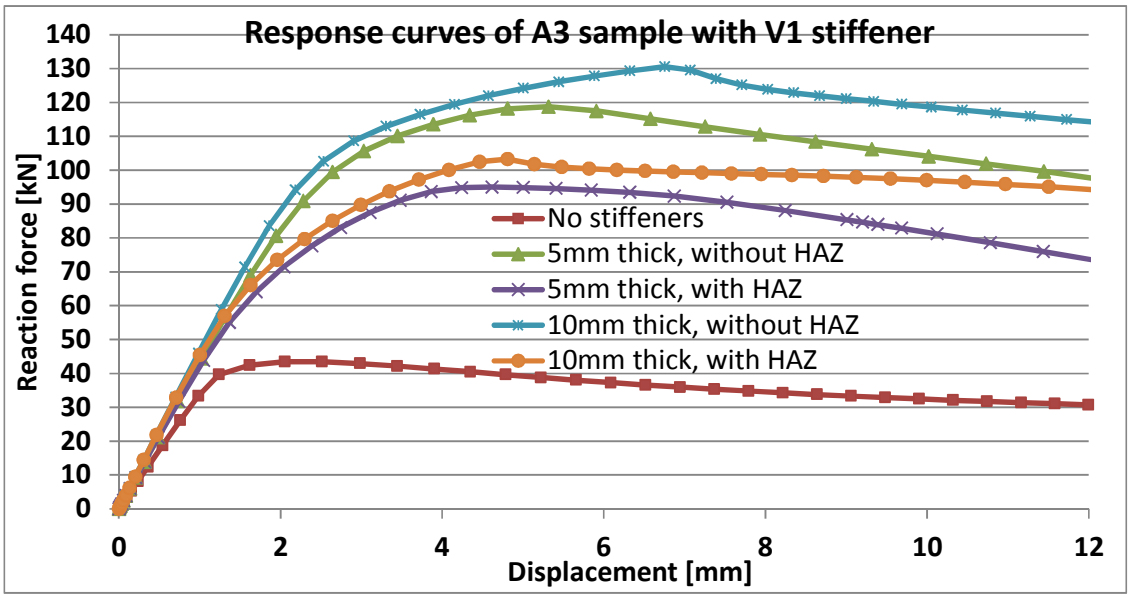
Response curves of A3 sample with V1 stiffener
Reaction force [kN]
Displacement [mm]
No stiffeners
5mm thick, without HAZ
5mm thick, with HAZ
10mm thick, without HAZ
10mm thick, with HAZ

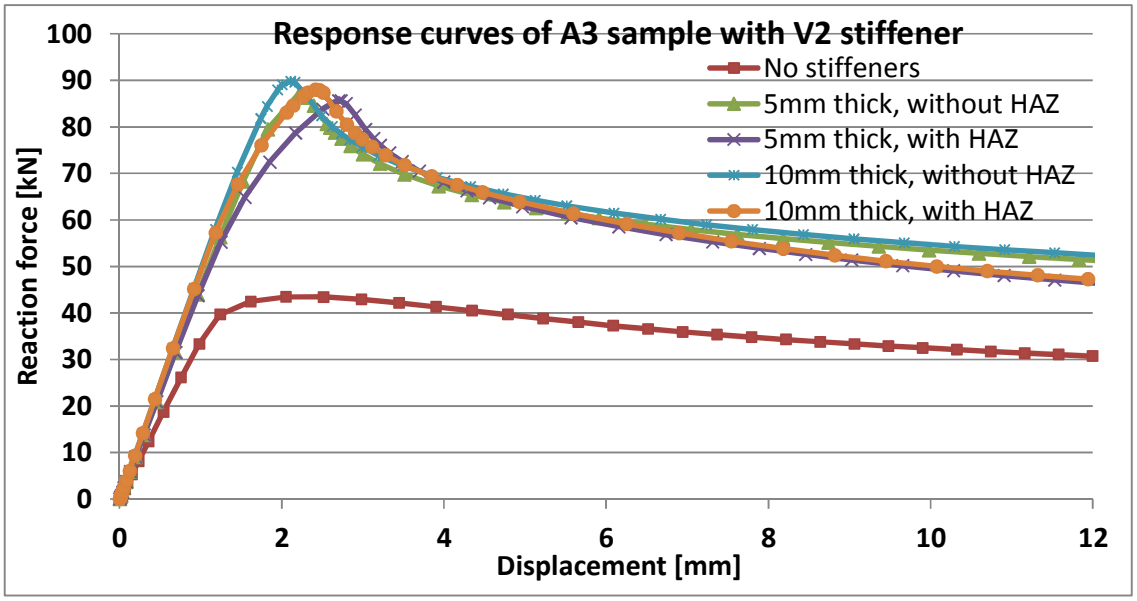
Response curves of A3 sample with V2 stiffener
Reaction force [kN]
Displacement [mm]
No stiffeners
5mm thick, without HAZ
5mm thick, with HAZ
10mm thick, without HAZ
10mm thick, with HAZ

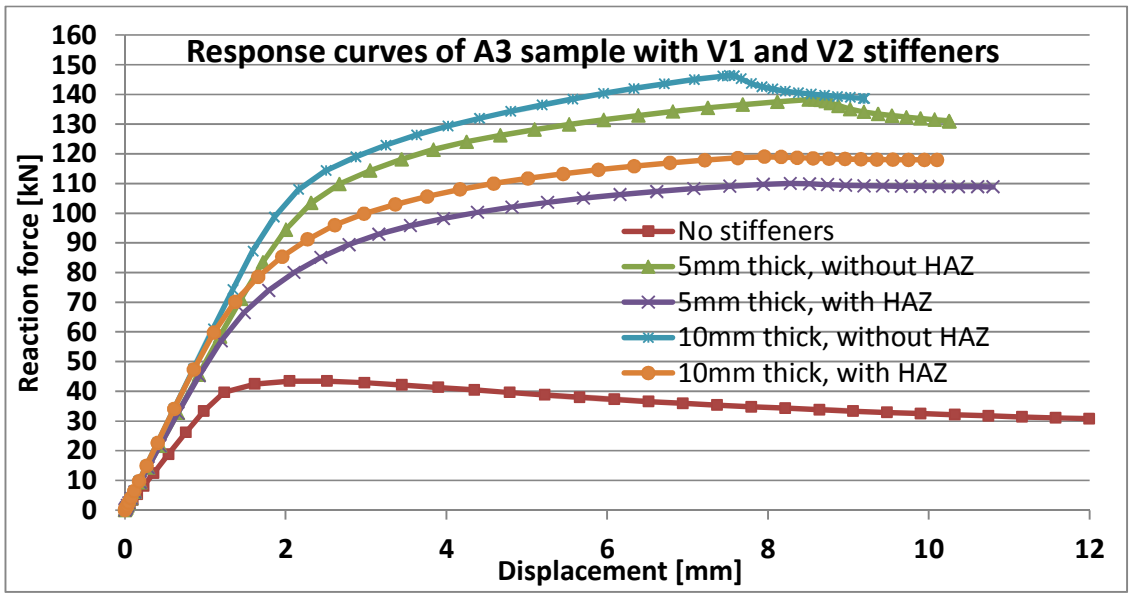
Response curves of A3 sample with V1 and V2 stiffeners
Reaction force [kN]
Displacement [mm]
No stiffeners
5mm thick, without HAZ
5mm thick, with HAZ
10mm thick, without HAZ
10mm thick, with HAZ

B. Effect of the imperfection choice

9.1. Buckle A

D [mm]	F [kN]	D [mm]	F [kN]	D [mm]	F [kN]	D [mm]	F [kN]
0,00	0,00	2,24	60,80	8,69	43,12	14,71	36,55
0,01	0,44	2,63	59,02	9,01	42,65	15,02	36,29
0,01	0,89	3,00	57,42	9,33	42,20	15,33	36,05
0,02	1,55	3,37	55,97	9,65	41,77	15,65	35,81
0,03	2,55	3,72	54,65	9,97	41,35	15,96	35,58
0,05	4,04	4,07	53,43	10,28	40,95	16,27	35,35
0,08	6,28	4,41	52,30	10,60	40,57	16,59	35,12
0,12	9,64	4,76	51,26	10,92	40,19	16,90	34,91
0,19	14,68	5,09	50,30	11,24	39,83	17,21	34,69
0,28	21,31	5,43	49,41	11,55	39,49	17,53	34,49
0,36	27,93	5,76	48,58	11,87	39,15	17,84	34,28
0,45	34,55	6,09	47,80	12,19	38,83	18,15	34,08
0,54	41,15	6,42	47,09	12,50	38,51	18,46	33,89
0,63	47,71	6,75	46,42	12,82	38,20	18,78	33,70
0,72	54,18	7,07	45,79	13,13	37,91	19,09	
0,83	60,27	7,40	45,20	13,45	37,62	19,40	
1,06	63,78	7,72	44,64	13,76	37,34	19,54	
1,42	64,02	8,04	44,11	14,08	37,07		
1,83	62,62	8,37	43,60	14,39	36,80		

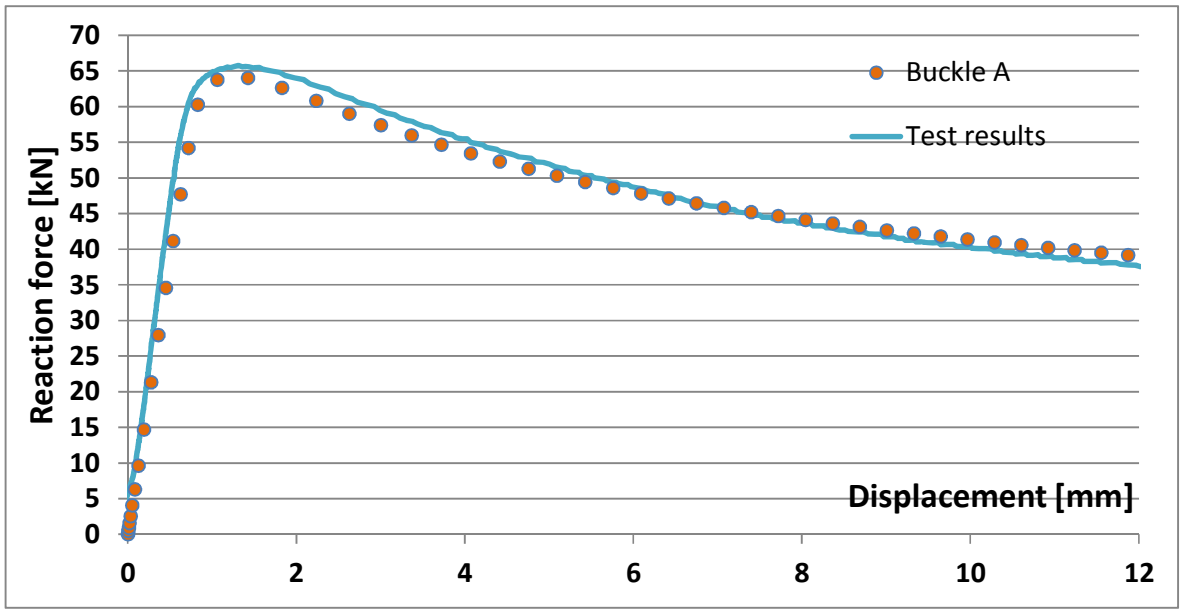

9.2. Buckle B

D [mm]	F [kN]	D [mm]	F [kN]	D [mm]	F [kN]	D [mm]	F [kN]
0,00	0,00	0,72	54,72	5,50	48,76	15,69	35,67
0,01	0,44	0,83	60,92	6,38	46,78	16,52	35,07
0,01	0,89	1,25	64,22	7,25	45,14	17,36	34,50
0,02	1,55	1,39	64,06	8,11	43,73	18,19	33,97
0,03	2,55	1,54	63,63	8,96	42,47	19,02	33,47
0,05	4,04	1,76	62,70	9,81	41,34	19,46	33,21
0,08	6,28	2,10	61,14	10,66	40,31	0,00	0,00
0,12	9,64	2,59	58,72	11,50	39,38	0,00	0,00
0,19	14,68	3,06	56,65	12,34	38,52	0,00	0,00
0,29	22,23	3,52	54,86	13,18	37,73	0,00	0,00
0,44	33,54	3,96	53,28	14,02	36,99	0,00	0,00
0,66	50,41	4,61	51,20	14,85	36,31	0,00	0,00

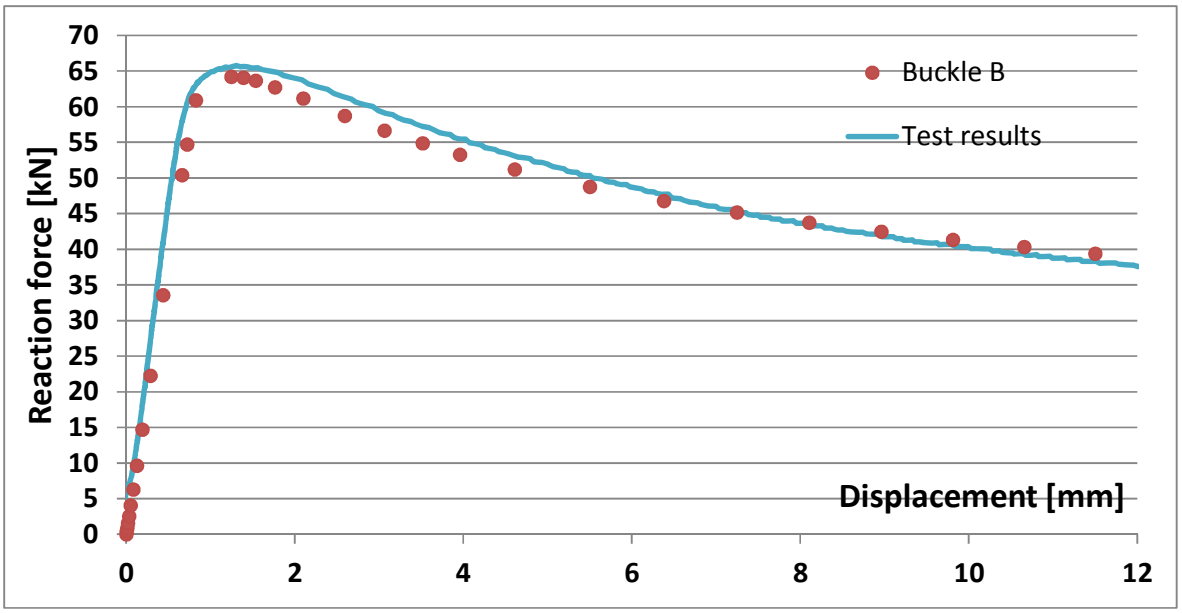

9.3. Buckle C

D [mm]	F [kN]	D [mm]	F [kN]	D [mm]	F [kN]	D [mm]	F [kN]
0,00	0,00	1,19	66,04	8,73	42,77	16,70	34,96
0,01	0,44	1,36	65,57	9,16	42,18	17,12	34,67
0,01	0,89	1,63	64,25	9,58	41,62	17,53	34,40
0,02	1,55	2,02	62,03	10,00	41,08	17,95	34,14
0,03	2,55	2,40	59,92	10,43	40,57	18,36	33,88
0,05	4,04	2,76	58,06	10,85	40,09	18,78	33,63
0,08	6,28	3,11	56,46	11,27	39,62	19,19	33,38
0,12	9,64	3,45	55,05	11,69	39,18	19,41	33,26
0,19	14,68	3,91	53,30	12,11	38,75	0,00	0,00
0,29	22,23	4,38	51,78	12,53	38,34	0,00	0,00
0,40	31,06	4,83	50,43	12,95	37,95	0,00	0,00
0,52	39,88	5,27	49,23	13,37	37,57	0,00	0,00
0,64	48,65	5,71	48,15	13,78	37,20	0,00	0,00
0,76	57,32	6,15	47,18	14,20	36,85	0,00	0,00
0,79	59,46	6,59	46,30	14,62	36,51		
0,84	62,65	7,02	45,50	15,04	36,18		
0,85	63,83	7,45	44,75	15,45	35,86		
0,88	65,57	7,88	44,05	15,87	35,55		
1,02	66,26	8,31	43,39	16,29	35,25		

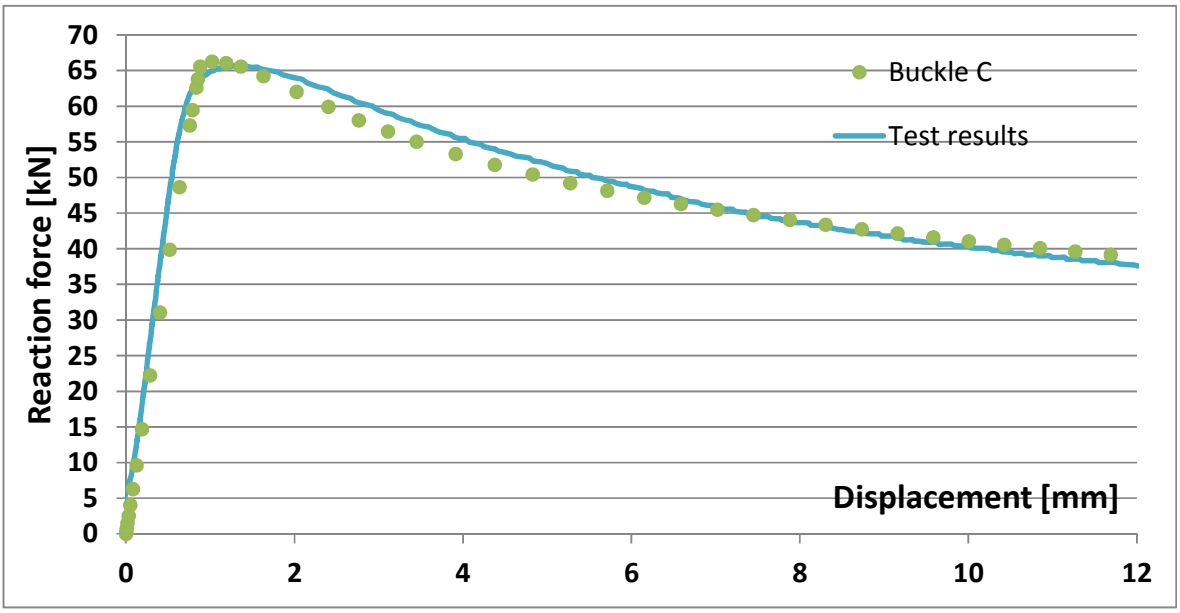

9.4. Buckle D

D [mm]	F [kN]	D [mm]	F [kN]	D [mm]	F [kN]	D [mm]	F [kN]
0,00	0,00	0,72	54,75	5,49	48,74	15,66	35,69
0,01	0,44	0,82	61,11	6,36	46,76	16,50	35,08
0,01	0,89	1,23	64,63	7,23	45,14	17,33	34,52
0,02	1,55	1,37	64,40	8,09	43,73	18,16	33,99
0,03	2,55	1,52	63,90	8,94	42,48	18,99	33,49
0,05	4,04	1,75	62,91	9,79	41,35	19,43	33,23
0,08	6,28	2,09	61,27	10,64	40,33	0,00	0,00
0,12	9,64	2,58	58,76	11,48	39,39	0,00	0,00
0,19	14,68	3,05	56,64	12,32	38,54	0,00	0,00
0,29	22,23	3,50	54,83	13,16	37,75	0,00	0,00
0,44	33,55	3,95	53,24	13,99	37,01	0,00	0,00
0,66	50,42	4,60	51,17	14,83	36,33	0,00	0,00

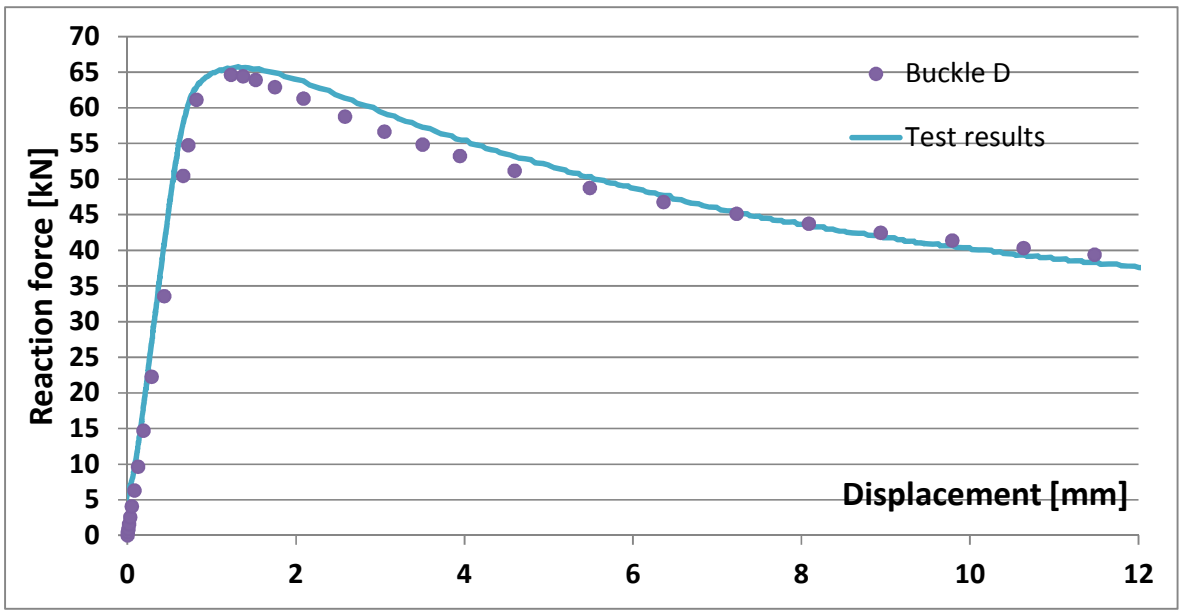

9.5. Load

D [mm]	F [kN]	D [mm]	F [kN]	D [mm]	F [kN]	D [mm]	F [kN]
0,00	0,00	0,05	4,04	2,33	60,21	10,87	40,13
0,00	0,00	0,08	6,28	2,82	58,02	11,71	39,20
0,00	0,00	0,12	9,64	3,28	56,11	12,56	38,35
0,00	0,00	0,19	14,68	3,73	54,43	13,40	37,57
0,00	0,00	0,29	22,23	4,17	52,91	14,23	36,85
0,00	0,00	0,44	33,54	4,82	50,89	15,07	36,17
0,00	0,00	0,66	50,39	5,71	48,49	15,91	35,54
0,00	0,00	0,72	54,69	6,59	46,54	16,74	34,94
0,01	0,44	0,84	60,78	7,46	44,93	17,58	34,38
0,01	0,89	1,26	64,09	8,32	43,52	18,41	33,86
0,02	1,55	1,48	63,85	9,17	42,27	19,24	33,36
0,03	2,55	1,82	62,56	10,02	41,15	19,52	33,20

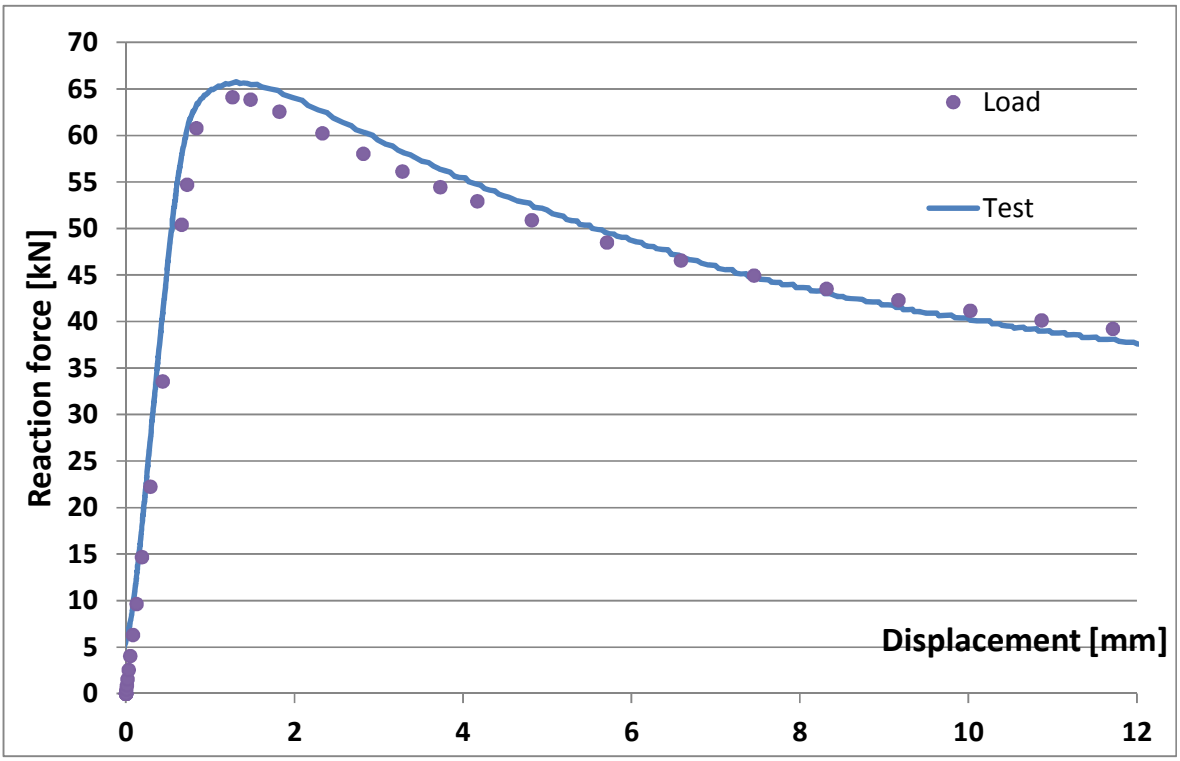

9.6. SIN 1

D [mm]	F [kN]	D [mm]	F [kN]	D [mm]	F [kN]	D [mm]	F [kN]
0,00	0,00	0,72	54,76	5,56	49,19	15,77	35,67
0,01	0,44	0,82	61,11	6,44	47,10	16,60	35,07
0,01	0,89	1,24	64,80	7,31	45,38	17,44	34,50
0,02	1,55	1,39	64,69	8,17	43,91	18,27	33,97
0,03	2,55	1,54	64,35	9,03	42,60	19,10	33,46
0,05	4,04	1,77	63,44	9,88	41,44	19,55	33,20
0,08	6,28	2,13	61,83	10,73	40,38	0,00	0,00
0,12	9,64	2,63	59,46	11,57	39,43	0,00	0,00
0,19	14,68	3,11	57,40	12,42	38,55	0,00	0,00
0,29	22,23	3,57	55,58	13,26	37,75	0,00	0,00
0,44	33,55	4,01	53,95	14,10	37,01	0,00	0,00
0,66	50,43	4,66	51,76	14,93	36,32	0,00	0,00

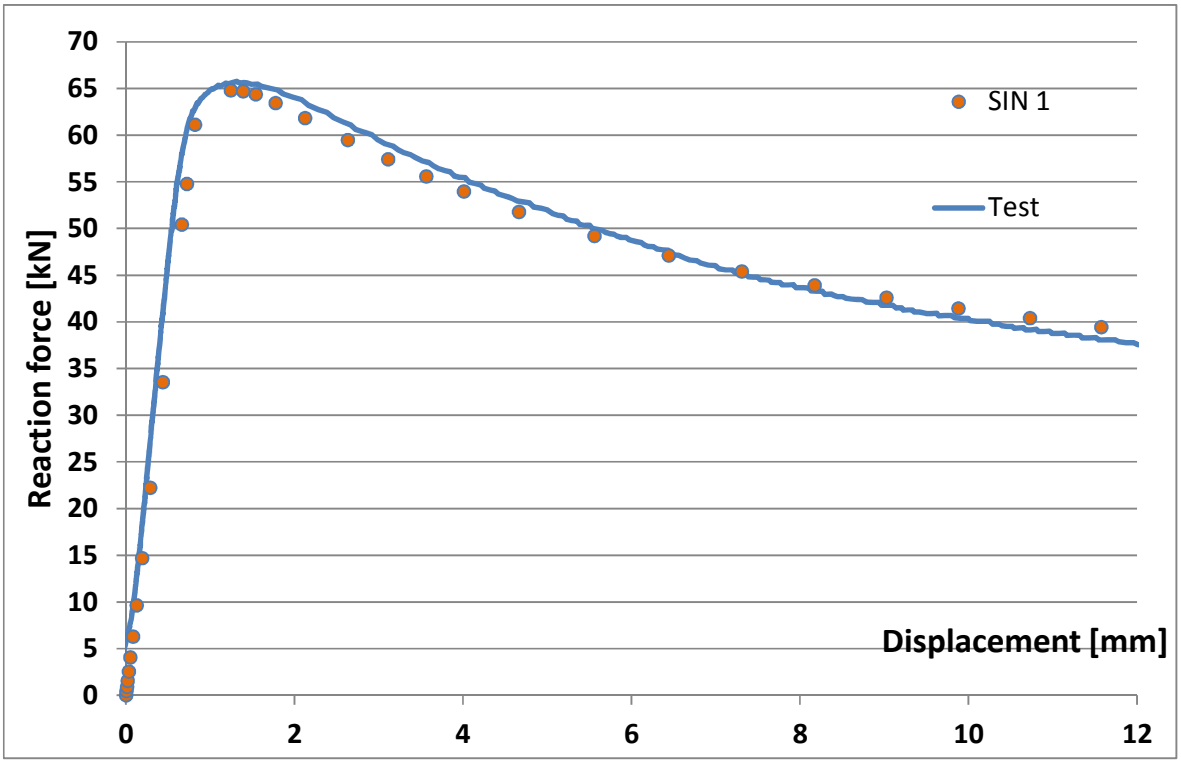

9.7. SIN 2

D [mm]	F [kN]	D [mm]	F [kN]	D [mm]	F [kN]	D [mm]	F [kN]
0,00	0,00	0,76	56,54	7,02	46,18	0,00	0,00
0,01	0,44	1,01	63,43	7,91	44,55	0,00	0,00
0,01	0,89	1,55	63,68	8,79	43,13	0,00	0,00
0,02	1,55	1,70	63,29	10,10	41,28	0,00	0,00
0,03	2,55	1,93	62,47	11,41	39,71	0,00	0,00
0,05	4,04	2,26	61,09	12,71	38,34	0,00	0,00
0,08	6,28	2,75	59,06	14,00	37,15	0,00	0,00
0,12	9,64	3,20	57,25	15,29	36,09	0,00	0,00
0,19	14,68	3,64	55,61	16,58	35,13	0,00	0,00
0,29	22,23	4,28	53,37	17,86	34,26	0,00	0,00
0,44	33,54	5,21	50,47	19,15	33,47	0,00	0,00
0,66	50,38	6,12	48,12	19,61	33,20	0,00	0,00

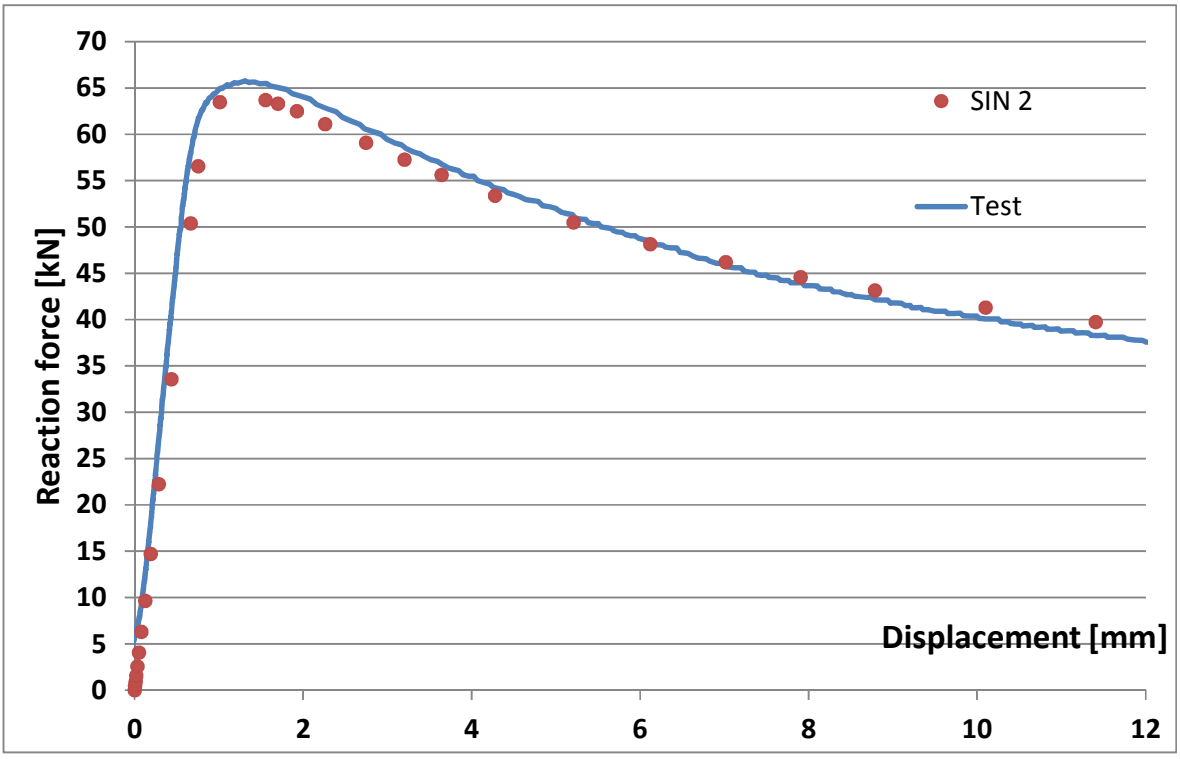

9.8. SIN3

D [mm]	F [kN]	D [mm]	F [kN]	D [mm]	F [kN]	D [mm]	F [kN]
0,00	0,00	0,83	59,06	6,97	46,17	14,62	36,66
0,01	0,44	1,43	63,02	7,62	44,97	15,25	36,16
0,01	0,89	1,62	62,70	8,27	43,90	15,88	35,68
0,02	1,55	1,83	62,06	8,91	42,91	16,51	35,22
0,03	2,55	2,13	60,88	9,55	42,00	17,13	34,78
0,05	4,04	2,58	59,06	10,19	41,16	17,76	34,37
0,08	6,28	3,22	56,60	10,83	40,39	18,39	33,97
0,12	9,64	3,82	54,47	11,46	39,66	19,01	33,59
0,19	14,67	4,41	52,57	12,10	38,98	19,63	33,23
0,29	22,22	4,98	50,87	12,73	38,35	0,00	0,00
0,44	33,52	5,65	49,09	13,36	37,75	0,00	0,00
0,61	46,66	6,31	47,53	13,99	37,19	0,00	0,00

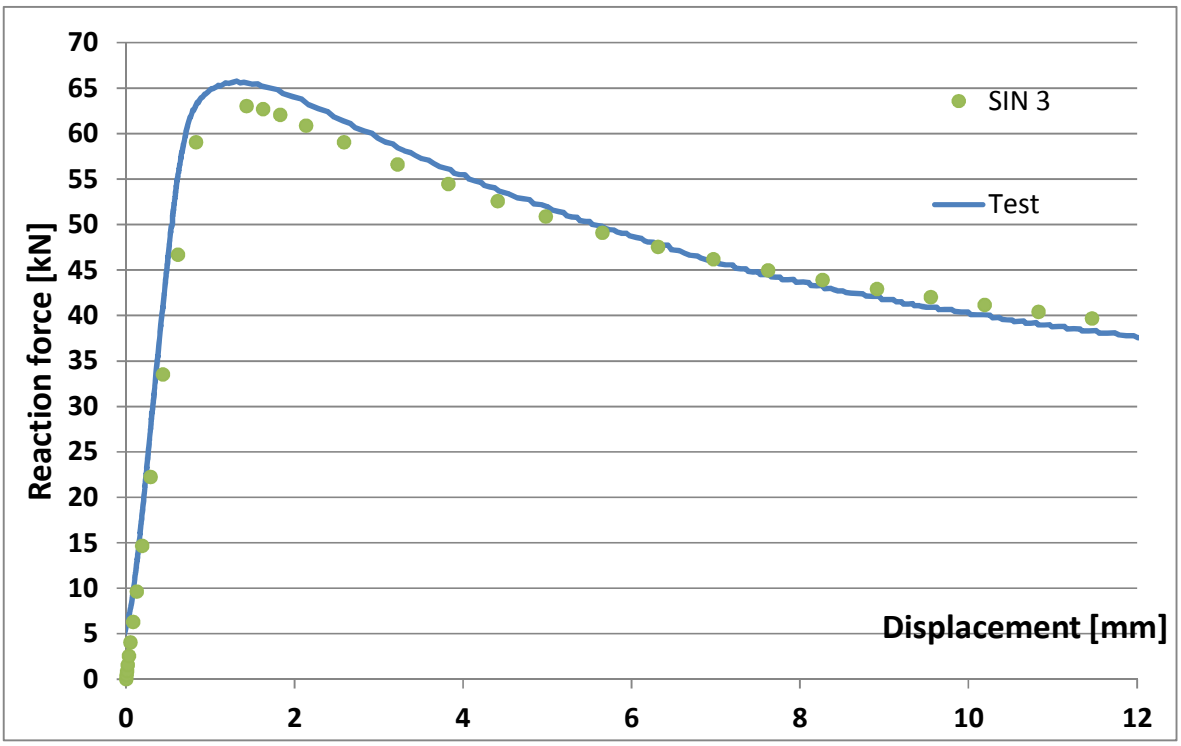

C Test and FEM results - comparison

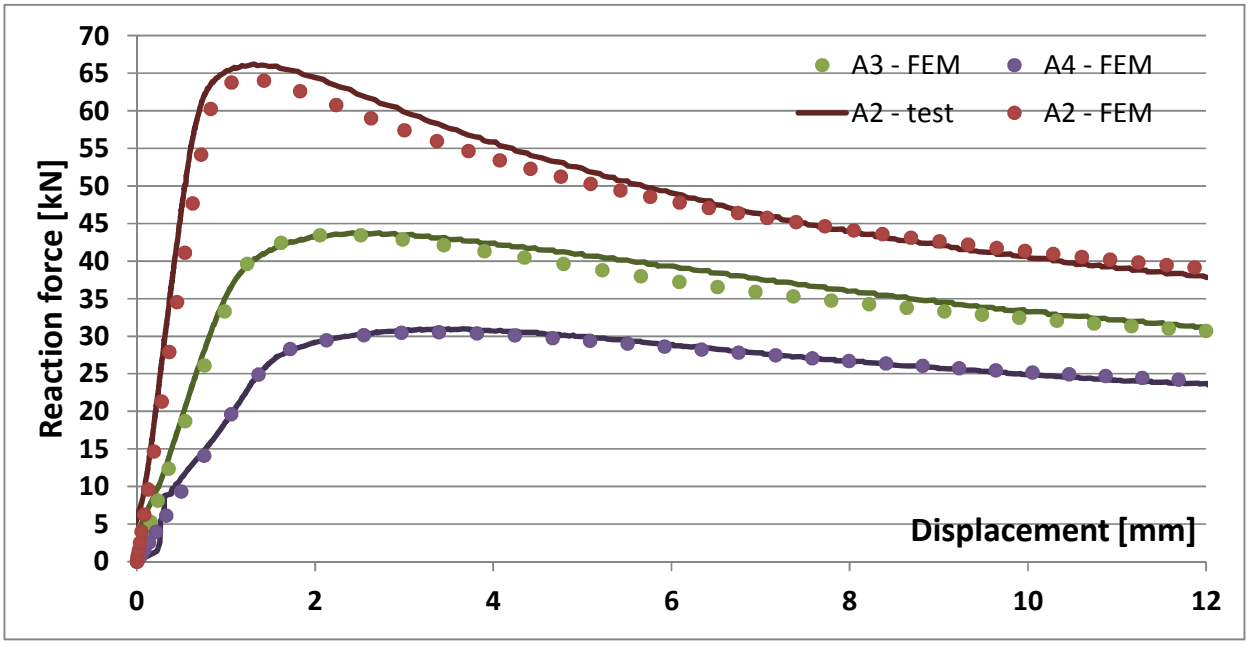

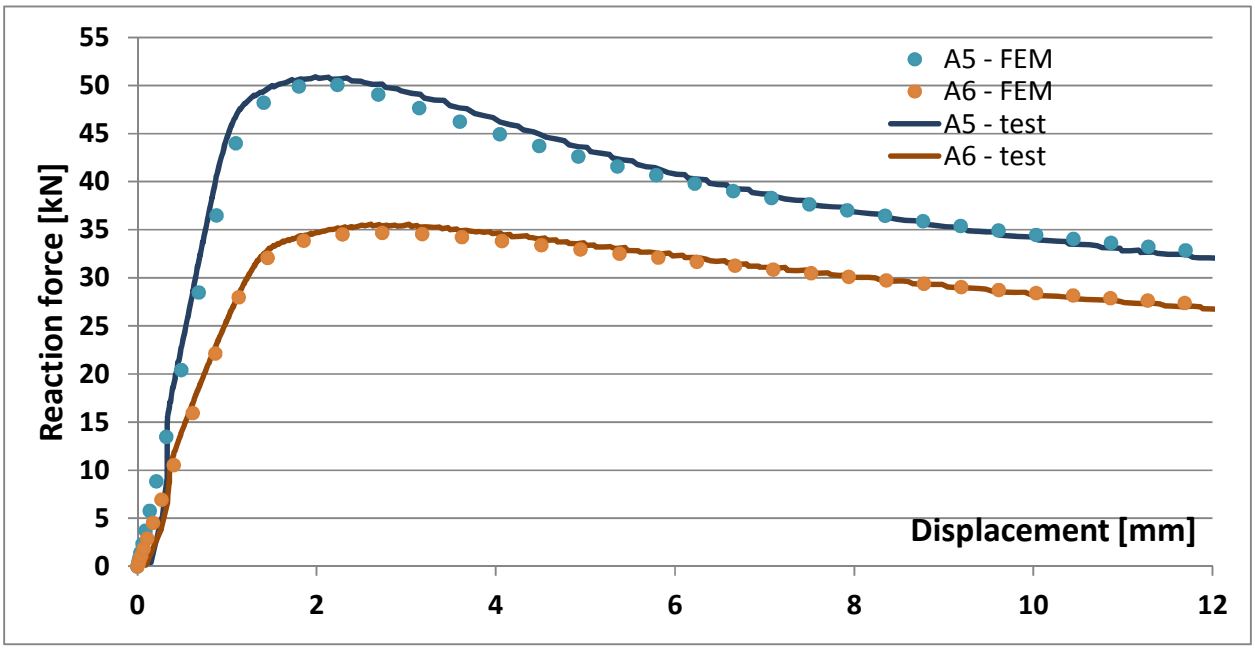

D Hand calculations

In this attachment reduced XHP profile will be investigated. When the cope is done and longitudinal stiffener is added it can be said that new aluminium profile was created. The purpose of this point is to check if moment capacity was not exceeded on the cope area and longer than a cope's depth longitudinal stiffener is not necessary.

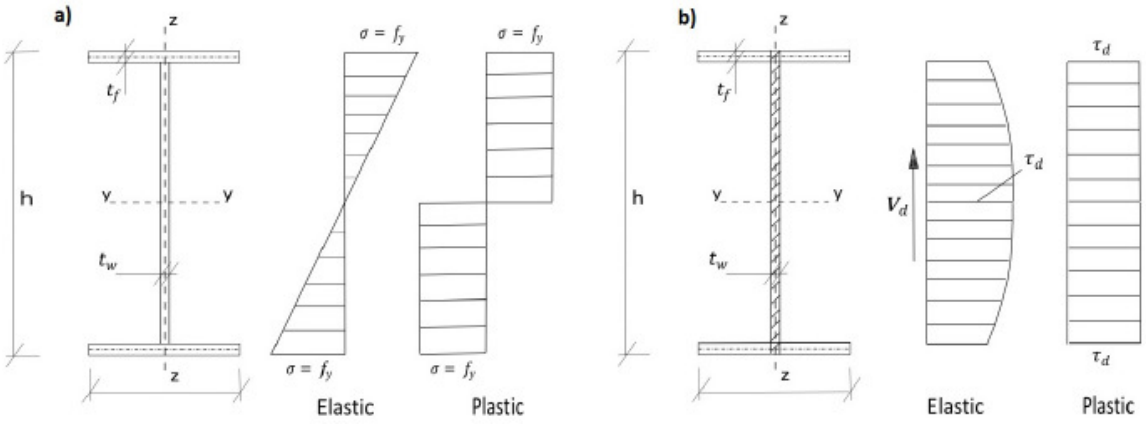

For a not reduced profile real dimensions are: h =259,2mm, b =119,4mm, t_f = 11,7mm, t_w = 4,65mm and r = 7mm, but in calculations the curved part of the profile will be neglected. For A2 specimen cope was 88x97, where 97mm was the height of the cope. Reduced profile will have h = 162,2mm and also changed size of the upper flange. Longitudinal stiffener is 100mm width and 5 mm thick.

Firstly class part of the profile were found:

parameter $\varepsilon = \sqrt{\frac{257,3}{235}} = 1,04$

web: $\frac{c}{t} = \frac{h - 2t_f - 2r}{t_w} = \frac{162,2 - 2 \cdot 11,7 - 2 \cdot 7}{4,65} = 26,8 < 74,9 = 72\varepsilon$

flange: $\frac{c}{t} = \frac{b - t_w - 2r}{2t_f} = \frac{119,4 - 4,65 - 2 \cdot 7}{2 \cdot 11,7} = 4,3 < 9,4 = 9\varepsilon$

Both parts are class first. Whole profile belongs to the first class.

To find $W_{el,HAZ}$ and $W_{pl,HAZ}$ according to the Eurocode [1] it is necessary to reduce the thickness of the parts of the profile, where HAZ effect occurs. Reduction factor $p_{0,HAZ}$ belonged to the range from 0,48 to 0,50 and in simplification could be stated as 0,49.

In this case thickness of the upper flange is 2,45mm, bottom flange 5,73mm and part of the web (20mm from flanges - area of the HAZ) is 2,28. This small reduction of the web will not be taken into account in hand calculations as a simplification and due to neglecting rounded part of the section.

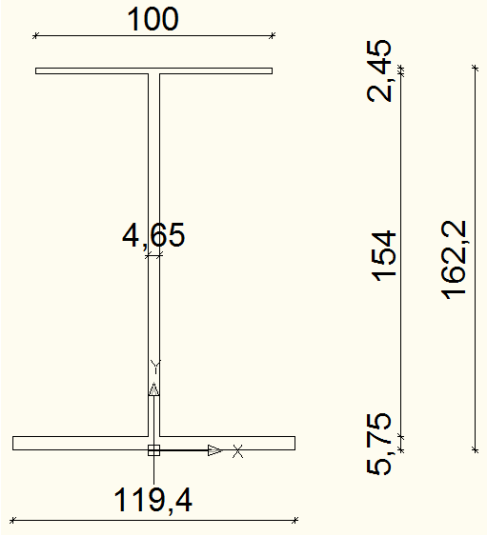

Figure 11.1 Reduced XHP profile

Finding mass center:

$$S_x = 5{,}75 \cdot \frac{5{,}75}{2} \cdot 119{,}4 + 4{,}65 \cdot 154{,}02 \cdot \left(5{,}75 + \frac{154{,}02}{2}\right) + 2{,}45 \cdot 100 \cdot \left(154{,}02 + 5{,}75 + \frac{2{,}45}{2}\right) = 1973{,}8 + 59272{,}1 + 39443{,}8 = 100689{,}7\ mm^3$$

$$y_{x,el} = \frac{Sx}{A} = \frac{100689{,}7}{5{,}75 \cdot 119{,}4 + 4{,}65 \cdot 154{,}02 + 2{,}45 \cdot 100} = \frac{100689{,}7\ mm^3}{1647{,}74\ mm^2} = 61{,}11mm$$

$y_{x,pl}$: $119{,}4 \cdot 5{,}75 + (y_{x,pl} - 5{,}75) \cdot 4{,}65 = 100 \cdot 2{,}45 + (154 + 5{,}75 - y_{x,pl}) \cdot 4{,}65$

From the equation above it was calculated that $y_{x,pl} = 35{,}27$mm

Moment of inertia and static moment according to the elastic/plastic center point:

$$S_{xc,pl} = 2 \cdot ((35{,}27 - 5{,}75) \cdot 4{,}65 \cdot \frac{(35{,}27 - 5{,}75)}{2} + 5{,}75 \cdot 119{,}4 \cdot (35{,}27 + 5{,}75/2)) = 2 \cdot 28214{,}5\ mm^3 = 56{,}43\ cm^3$$

$$I_{xc,el} = \frac{(61{,}11 - 5{,}75)^3}{3} \cdot 4{,}65 + \frac{(154{,}02 + 5{,}75 - 61{,}11)^3}{3} \cdot 4{,}65 + \frac{5{,}75^3}{12} \cdot 119{,}4 + 5{,}75 \cdot 119{,}4 \cdot (61{,}11 - 5{,}75/2)^2 + \frac{2{,}45^3}{12} \cdot 100 + 2{,}45 \cdot 100 \cdot (154{,}02 + 5{,}75 - 61{,}11 + 2{,}45/2)^2 = 652{,}6\ cm^4$$

Following results were checked in Autocad:

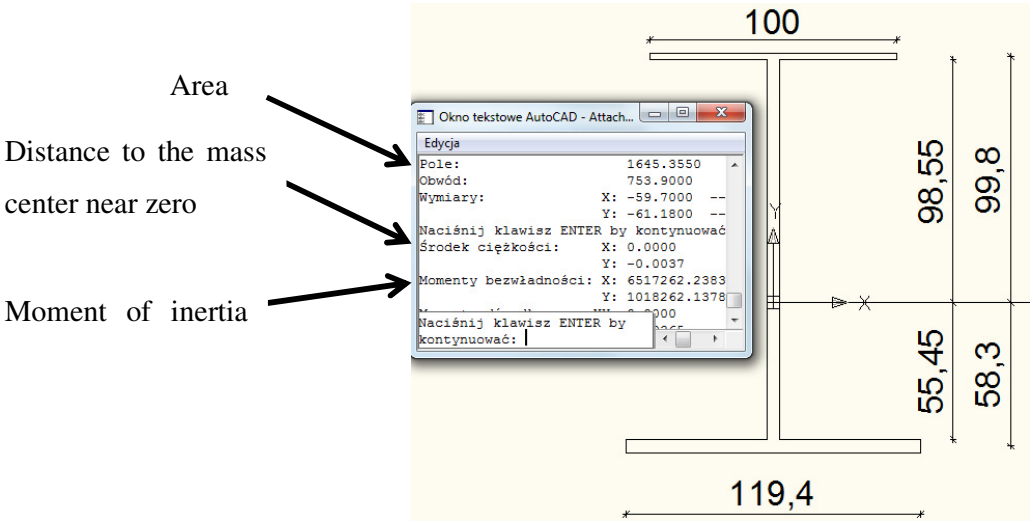

Figure 11.2 Autocad results

$W_{el,HAZ} = I_{xc,el} / z_{max}$ $W_{pl,HAZ} = 2\ S_{xc,pl}$

$W_{el,HAZ} = 652{,}6\ cm^4 / 9{,}98cm = 65{,}4\ cm^3$ $W_{pl,HAZ} = 2 \cdot 56{,}43 = 112{,}9\ cm^3$

$$M_{el,HAZ} = W_{el,HAZ} \cdot f_y = 65{,}4cm^3 \cdot 257{,}3\ MPa = 16{,}83\ kNm$$

$$M_{pl,HAZ} = W_{pl,HAZ} \cdot f_y = 112{,}9cm^3 \cdot 257{,}3\ MPa = 29{,}04\ kNm$$

$$R_{el,HAZ} = M_{el,HAZ} / (c\text{-}30) = 16{,}83 / 0{,}58 = 29{,}02\ kN$$

$$R_{pl,HAZ} = M_{pl,HAZ} / (c\text{-}30) = 26{,}27 / 0{,}58 = 50{,}07\ kN$$

It is clear from results that the part of the beam which is coped can't be treated as a beam and determining the capacity by maximum moment gives wrong results. It is because coped part is very short and ratio height/length is much larger than in the elements where bending is the most important inner force. It was decided to calculate additional shear capacity.

$$V_d = \frac{f_{02}}{\sqrt{3}} \cdot t_w \cdot h_w = \frac{257{,}3}{\sqrt{3}} \cdot 4{,}65 \cdot 154 = 106{,}38\ kN$$

In this very simplified way it was obtained much closer result according to FEM model.

Bibliography:

[1] *EN 1999-1-1:2007, Design of aluminium structures, Part 1-1 General structural rules.*

[2] Getting Started with Abaqus: Interactive Edition: http://www.tu-chemnitz.de/projekt/abq_hilfe/docs/v6.12/books/gsa/default.htm

[3] Abaqus/CAE User's Manual

[4] Abaqus Analysis User's Manual

[5] Hågen Urseth. *Design of Beam Ends with Copes*. Master Thesis. NTNU, Department of Structural Engineering,

[6] KH Holthe. *Lecture notes: TKT4192: Finite Elements Methods in Strength Analysis*. NTNU, Deapartment of Structural Engineering, 2011.

[7] Hanne Gundersen. *Beekningar for bjelkeendar og sveiste plater.* Masteroppgåve 2008, NTNU, Institutt for konstruksjonsteknikk, Fakultet for ingeniørvitskap og teknologi.

[8] Abaqus Users Forum

[9] Hydro Aluminium Vekst. *Aluminium in the marine environment.*

[10] Nilssen, G. *Kapasitet av bjelkeender med utkapp*, hovudoppgåve ved Institutt for Konstruksjonsteknikk, NTNU, hausten 2001.

[11] Hydro Aluminium Profiler a. "*XHP – I-Beams*", http://hap.hydal.com/wp-content/uploads/2013/10/xhp.pdf, latest update, 13.mai 2008.

[12] Bonkerud, P.Ø.: "Kapasitet til bjelkeender med utkapp", masteroppgåve ved Institutt for Konstruksjonsteknikk, NTNU, 2007.

[13] *NS-EN 1993-1-5. Eurocode 3: Prosjektering av stålkonstruksjoner. Del 1-5:Plater påkjenti plateplanet*. Standard Norge, 2012.

[14] Jerzy Pamin i Marek Słonski. *Analiza płyt i powłok MES. Zagadnienie wyboczenia.*

[15] Ove Lagerqvist. *Patch Loading: Resistance of Steel Girders Subjected to Concentrated Forces*. PhD thesis, 1994.

[16] Salmon CG, Johnson JE. *Steel structures, design and behavior, 3rd edition*, 1990, Harper & Row publishers, New York.

[17] Martin LH, *Methods for the limit state design of triangular steel gusset plates.* Building and Environment, Pergamon Press, G.B., 1979, Vol. 14:147:155.

[18] Lauren Kougias *A Study of the Effect of Imperfections on Buckling Capability in Thin Cylindrical Shells Under Axial Loading.* An Engineering Project Submitted to the Graduate Faculty of Rensselaer Polytechnic Institute, December, 2009.

[19] Memon Bashir-Ahmed, Su Xiao-zu, *Arc-length technique for nonlinear finite element analysis.* Department of Structural Engineering, Tongji University, Shanghai 2004, China.

[20] Adam Wosatko, *Analiza statyczna MES dla ustrojów powierzchniowych*. Wykład, mechanika materiałów i konstrukcji budowlanych, Wydział Inżynierii Lądowej, Politechnika Krakowska.

[21] M. Fafard and B. Massicotte, *Geometriacl Interpretation of the Arc-length method.* Department of Civil Engineering, Lava1 University, 1991, Canada.

[22] J. Cheng and J. Yura. *Local web buckling of coped beams*. Journal of Structural Engineering, 112(10):2314-2331, 1986.

[23] M. Yam, A. Lam, V. Iu, and J. Cheng. *Local web buckling strength of coped steel I beams*. Journal of Structural Engineering, 129(1):3-11, 2003.

[24] Cheng, J.J. Roger. *Design of Steel Beams with End Copes*. Journal of Constructional Steel Research 25 (1993) 3-22, 1993.

[25] R.R. Ambriz and V. Mayagoitia. *Welding of Aluminum Alloys*. Instituto Politécnico Nacional CIITEC-IPN, México.

[26] P.K. Tryland T., Aalberg A., Larsen. *Design of coped beam ends for concentrated load*. 1999.